FACHHOCHSCHUL-STUDIENGÄNGE OÖ
Automatisierte
Anlagen- und Prozesstechnik

Wels

Experimental Investigation of Proton Induced Thermal Shocks and Magnetohydrodynamic Effects in Molten Metal Pion Production Targets for a Neutrino Factory

Diploma thesis

Submitted for the acquisition of the academic degree

Diplom - Ingenieur (FH)

by

Daniel Schaffarzick

September 2001

Examiner:

Dr. DI Daniel Heim

Herewith, I, Daniel Schaffarzick, declare, that I have completed the diploma thesis submitted independently and without forbidden other assistance. I have indicated each of the aids and sources I have used.

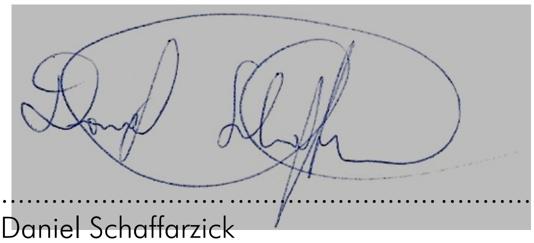

……………………………………………………………

Daniel Schaffarzick

Elsbethen, 10.09.2001

Dear Jacques,

Thank you for your excellent supervision and help during my time at CERN!

Daniel

Für Adrian

Vielen Dank für Deine Unterstützung und Hilfe während meiner Zeit am CERN

Daniel

Abstract

Neutrinos are one of the basic subatomic particles among electrons, protons and many more, which build all matter. Neutrinos appear in three different types. Sources of neutrinos are the sun and nuclear power plants. But the type of neutrinos created there is not exactly known and the type changes between their creation to their detection, so only assumptions can be made. This change of type is called "neutrino oscillation". In order to enable the nuclear physisists to find out more about the neutrinos and the neutrino oscillation, a neutrino factory will be built which will produce a high intensity neutrino beam with exactly known parameters like number of particles and type of neutrinos. This neutrino beam can then be used to investigate the properties of the neutrinos at near and far detectors.

In cooperation with other laboratories CERN has started a study of some of the many technological challenges of a neutrino factory. A major issue of the facility is the pion production target where pions are produced by shooting a proton beam onto matter (target). These pions then decay into neutrinos. At CERN the choice was made to concentrate on the development and investigation of a liquid metal target, particularly mercury. Experiments were fixed to show the feasibility of a liquid metal target. The experiments should cover ejection and capture of the jet, hydrodynamics, distortion of the jet by proton beam interaction, behaviour of the mercury jet in high magnetic fields and handling liquid metals.

In this dissertation theoretical studies have been collected and analysed as well as experimental studies have been performed. The main part consists of the preperation and performance of the experimental studies. To use a liquid metal target is a completely new technology and there exists no experience in this field. The experiments are an important part of the whole project as they should verify the validity of the theoretical studies and consequently confirm the definitive feasibility of a liquid metal target station.

The first part of this dissertation explains the motivation for and the goal of the project, an overview of the theoretical background of nuclear physics and a description of the future neutrino factory.

The next part describes some theoretical studies concerning the evaluation of models for the target and their behaviour at intense proton beam impact, located in high magnetic fields. Theoretical models should show the understanding of the liquid metal target, especially concerning the hydrodynamics including cavitation on proton impact.

After that the main part describes the experiments which will provide benchmarks for theoretical models of the behaviour of liquid metal under the given circumstances and gives details about their realization. The experiments consist of setups which are used to place mercury inside very strong magnetic fields and in the line of proton beams. The reaction of the mercury to these inducements is observed optically by recording high speed videos of the events. These videos are used to evaluate some key parameters like the velocity and direction of escaping droplets when the mercury is disrupted due to the impacts.

The concluding parts eventually include the results of the experiments and the extrapolated consequences for the final neutrino factory target design. The experiments show that the simulations are not very far from the reality. The effects on the mercury correspond widely to the simulations and they are considerable. Nevertheless the effects are within a range that a neutrino factory based on a mercury jet target seems to be feasible.

Abstrakt

Neutrinos sind neben den Elektronen, Protonen und anderen Teilchen die grundlegendsten subatomaren Teilchen, die unsere gesamte Materie bilden. Trotzdem sind sie erst wenig erforscht. Neutrinos kommen in drei verschiedenen Arten vor. Einige der Quellen von Neutrinos sind die Sonne und Kernkraftwerke. Jedoch ist nicht bekannt, welche Typen von Neutrinos dort entstehen, es können nur Annahmen getroffen werden. Es ist bekannt, dass Neutrinos ihre Art von ihrem Entstehungsort bis zu ihrer Detektion ändern. Dieses Phänomen nennt sich „neutrino oscillation". Um den Physikern eine weitere Erforschung der Neutrinos und der neutrino oscillation zu ermöglichen, soll eine Neutrino Factory gebaut werden. Dies ist eine Einrichtung, um einen intensiven Neutrinostrahl zu erzeugen, bei dem die Art der Neutrinos bekannt ist. Dieser Neutrinostrahl kann dann genutzt werden, um die Eigenschaften der Neutrinos in nahen und fernen Detektoren zu erforschen.

In Zusammenarbeit mit anderen Forschungszentren hat CERN eine Studie über die technologischen Herausforderungen einer Neutrino Factory ins Leben gerufen. Eine der Hauptaufgaben einer solchen „Anlage" ist das Pion Production Target. Hier werden Pionen durch Beschuss von Materie mit einem Protonenstrahl erzeugt. Diese Pionen zerfallen darauf in Neutrinos. Am CERN einigte man sich darauf, bei den weiteren Studien sich auf die Entwicklung eines Flüssig-Metall Targets, insbesondere auf Quecksilber zu konzentrieren. Es wurden Experimente festgelegt, um die Umsetzbarkeit eines Flüssigmetall Targets zu zeigen. Diese Experimente sollen die Erzeugung und das Auffangen des Flüssig-Metall Strahles, Hydrodynamik, Verzerrung des Strahles durch Proton Strahl Interaktion, Verhalten von Quecksilber in starken magnetischen Feldern und die Handhabung von Flüssig-Metallen beinhalten.

Im Rahmen dieser Arbeit wurden sowohl theoretische Studien gesammelt und diskutiert als auch experimentelle Studien durchgeführt. Der Hauptanteil besteht aus der Durchführung der experimentellen Studien. Die Verwendung eines Flüssigmetall Targets ist eine völlig neue Technologie und es besteht praktisch keine Erfahrung auf diesem Gebiet. Die Experimente bilden einen wichtigen Teil des Gesamtprojektes, um die Gültigkeit der theoretischen Studien zu überprüfen und somit die endgültige Umsetzbarkeit einer derartigen Target Station zu bestätigen.

Der erste Teil der vorliegenden Diplomarbeit stellt eine Einführung dar, welche die Motivation und die Aufgabenstellung für das Projekt, eine Übersicht über theoretische Grundlagen der Teilchenphysik und eine Beschreibung der zukünftigen Neutrino Factory beinhaltet.

Der folgende Teil widmet sich einigen Simulationen die sich mit Modellen von Flüssig-Metall Strahlen und deren Verhalten unter Einfluss eines Protonenstrahls sowie in starken Magnetfeldern. Diese theoretischen Modelle sollen das Verständnis von Flüssig-Metallen in den gegebenen Umfeldern insbesondere deren Hydrodynamik inklusive Kavitation zeigen.

Im Anschluss werden die Experimente, welche die Gültigkeit der Simulationen bestätigen sollen, aufgelistet und detailliert auf deren Umsetzung eingegangen. Die Experimente bestehen aus Aufbauten, um ruhendes Quecksilber und einen Quecksilberstrahl in einen Protonenstrahl zu platzieren und einen Quecksilberstrahl in ein Magnetfeld zu schießen. Die Reaktion des Quecksilbers auf diese Einwirkungen wird optisch mit einer digitalen Hochgeschwindigkeitskamera beobachtet. Die gewonnenen Videos können dann ausgewertet

werden um Parameter wie Geschwindigkeiten und Richtungen der Tröpfchen zu bestimmen, wenn das Quecksilber durch den Protonenstrahl zerrissen wird.

Die beiden abschließenden Kapitel beinhalten die Ergebnisse der Experimente und eine Diskussion der aus den Ergebnissen abgeleiteten Konsequenzen für das endgültige Neutrino Factory Target Design. Die Ergebnisse haben gezeigt, dass die vorangegangenen Simulationen nicht allzu weit von der Realität abweichen. Die Effekte entsprechen weitgehend den Erwartungen und beeinflussen das Verhalten des Quecksilbers zum Teil erheblich. Jedoch bewegen sich die Effekte in einem Bereich, der die Realisierung einer Neutrino Factory basierend auf einer Flüssigmetall Target Station aufgrund der Experimentergebnisse nicht ausschließt.

Acknowledgments

I wish to express my gratitude to all professors and staff at the FH. Primarily my gratitude is addressed to Daniel Heim, my supervisor at the FH, for his support and consultation and to Peter Stanley Orgill for his help in English questions.

I thank Burkhard Stadlman who kindly agreed to be coexaminer.

I owe special thanks to Jacques Lettry, who helped me in all concerns. He was my supervisor at CERN and he made possible my stay in the unique environment at CERN.

I am grateful to all my colleagues at CERN, especially to Adrian Fabich, for their excellent support and helpful advice.

Finally, I am indebted to my family for their help during my whole time of study.

Curriculum vitae

Personal Data	*Name*	**Daniel Schaffarzick**
	Address	A-5061 Elsbethen, St.Peterstr. 15
	Place and date of birth	Salzburg, 2.8.1976
	Nationality	Austrian
	Telephone	+43 662 630063 mobile: +43 664 4762102
	E-Mail	daniel.schaffarzick@gmx.net
	Martial status	single
School Education	*1983 – 1987*	• Primary School in Elsbethen (Salzburg)
	1987 – 1992	• Secondary School in Nonntal (Salzburg)
	1992 – 1996	• Vocational School in Gmunden (passed with commendation)
Apprenticeship	*1992 – 1996*	• Electrician and process control technician at Halvic / Solvay, Hallein (Salzburg)
	11.9.1996	• Completion of apprenticeship Electrician, Salzburg
	18.7.1996	• Completion of apprenticeship process control technician, passed with distinction, Linz
Vocational Experience	*1996 – 1997*	• Company electrician and process control technician at Solvay, Hallein
	1997	• PC-hard- and software technician at M&T, Salzburg
	1999	• Service technician at Bernecker & Rainer Industrial-Electronics, Eggelsberg
	2000 - 2001	• Practical training and diploma thesis at CERN, Geneva (Switzerland)
Secondary Education	*1996 – 1997*	• Preparatory Course for Technicians, Wels
	1997 - 2001	• Student at Advanced Technology College on the course Automated Plant- and Process Technology
Qualifications	*30.6.2000*	• Junior Project Manager (awarded by Project Management Austria)
	21.5.2001	• Quality Management Commissary (awarded by TÜV Austria)
	14.9.2001	• Value Analyst (VDI)
Other Skills	*Languages*	• German • English • French
	Driving Licence	• Classes A, B

Contents

List of Figures

List of Tables

0.1 Symbols and Abbreviations

0.1.1 Symbols

Symbol	Unit		Explanation
c	m/s	c=3·10^8m/s (constant)	speed of light (in vacuum)
c_s	m/s		speed of sound
c_V	J/Kg·K		specific heat
B	T	$1T=1\frac{V\cdot s}{m^2} = 104gauss$	magnetic flux density
E	eV	1eV=1,6·10^{-19}J	energy
f	Hz		frequency
I	A		electrical current
l	m		length, distance
m	eV/c^2	$1eV/c^2 = 1,8 \cdot 10^{-36}kg$	mass
P	W		power
p	bar	1bar=1N/cm^2	pressure
t	s		time
T	$^\circ C$, K		temperature
Z	g/mole		atomic mass
v	m/s		velocity
α_V	K^{-1}		volume thermal expansion coefficient
ε	$[\Omega m]^{-1}$		electrical conductivity
ρ	kg/m^3		density
κ	m^2/N		compressibility
ν			Neutrino
$\overline{\nu}$			Anti-Neutrino
ν_e			Electron-Neutrino
ν_μ			Muon-Neutrino
ν_τ			Tau-Neutrino

0.1.2 Abbreviations and Terms

Abbreviation	**Explanation**
AGS	Alternating Gradient Synchrotron
BNL	Brookhaven National Laboratory (USA)
ESS	European Spallation Source
FFAG	Fix Field Alternating Gradient
FNAL	Fermi National Accelerator Laboratory
LHC	Large Hadron Collider
LEP	Large Electron Positron Collider
Linac	Linear Accelerator
MARS	Simulation code for calculating decay products
NUMI	Neutrinos a the Main Injector (Fermilab)
ppb	protons per bunch
ppp	protons per puls
rf cavity	part of an accelerator
Spallation	high-energy nuclear reaction
SPL	Superconducting Proton Linac

Chapter 1

Introduction

1.1 Motivation

Almost every day, fresh results steadily fuel the progress of science. Less frequently, major breakthroughs in experimental techniques revolutionize the way in which this research is done. Examples of such breakthroughs in particle physics include the development of accelerators in the 1950s, and of colliding rings in the late 1960s, finally culminating with CERN's proton-antiproton collider, using beam-cooling techniques and opening up a new energy regime.

Although there is still a long research and development road to be negotiated, the first major breakthrough in particle physics experimental techniques for the 21st century looks to be the advent of a new type of machine - the muon storage ring - and using it to provide neutrino beams.

Making accelerators with muons seems crazy at first. Machine builders so far have had the wisdom to store and accelerate particles that are abundant - like the protons and electrons naturally found in matter - or, if not abundant, that at least have the good taste to be stable, like positrons and antiprotons.

It takes at least 30 min to fill CERN's LEP collider and accelerate its beams of electrons and positrons. How could one do such a thing with unstable muons, with their combined inconveniences of being rare and having a lifetime of only 2.2 ms?

Progress in accelerator techniques has made this challenge at least conceivable, to the extent that there has been discussion of muon collider rings as a serious future option in the US and at CERN.

When, following the inspiration of the US muon collider collaboration, European physicists started looking at this new route, the obstacles appeared overwhelming, with many new problems to solve simultaneously.

A breakthrough came with the realization that muon decay could be turned into an advantage - muon storage rings would be an abundant source of neutrinos. Coming at the same time as the new awareness of neutrino oscillations, this step forward met with a thunderclap of enthusiasm.

The muon storage ring as neutrino source, nicknamed ”neutrino factory”, requires a much lower density of particles and should thus be easier to build than a muon collider. The decay of muons into electrons provides the only known source of high-energy electron-type neutrinos - a unique and powerful new physics tool.

The key requirement is a very intense proton accelerator, delivering several megawatts of beam power. These protons will be used to create pions, which will be magnetically collected. Designing a target to withstand so much power more than once is beyond what has been achieved so far and will require either a liquid jet target or an other system (e.g. a moving solid target) to dissipate the heat. As a liquid jet target seems to be the most promising solution and there has never been a similar target before, big effort will be taken to realize a target system using a liquid metal jet. The first step towards a liquid jet target is to work out a basic knowledge about the behaviour of liquid metals under conditions when particles are collided onto it or in a high magnetic field for further development.

The main goal of the present project is to estimate the state of the target after the interaction with the proton pulses. In particular, the main issues are the distortion of the jet due to eddy currents as it propagates into the magnetic field, the deformation of the jet surface due to strong pressure waves caused by the proton pulses, the possibility of the jet to break up into droplets and the pressure field evolution.

1.2 Task

The tasks to be coped within the framework of this diploma thesis and the preceding practice placement at CERN extend over

- working out a basic knowledge and a theoretical background about nuclear physics in order to understand the context of the project,
- working out procedures for a safe handling of mercury and a safe operation of the experiment setups,
- studying existing simulations for later comparison with the experiment results,
- developing a concept for performing the proposed experiments,
- making plans and sketches for producing the required parts for the experiment setups at the workshop,
- selecting the required equipment and evaluating the best supplier,

- attending some of the experiments,
- collecting the experiment results, valuating and summarizing them,
- assessing the validity of the simulations and the consequences of the results for the final target design

1.2.1 Practice Placement - Diploma Work

During the six month lasting practice placement a part of the theoretical background was gained, the concept and safety instructions for the experiments were worked out and the setups were built. After the setups were tested one experiment was also performed within this time.

The consequent diploma work covers a literature study about the remaining basic knowledge about nuclear physics and a analysis of the existing simulations. The evaluation of the collected data as well of the first experiment at CERN as of the experiments performed in Grenoble and at the BNL in the USA, the comparison with the simulations and the discussion of the results and consequences are also part of the diploma work.

1.3 CERN

CERN[1,2] [1] is the European Laboratory for Particle Physics or European Organization for Nuclear Research. The Laboratory was founded in 1951 and was a great example of successful international collaboration as on of the first Europe's joint ventures. At present there are 20 Member States of the CERN convention. Geographically the CERN site is located at the Franco-Swiss border west of Geneva, Switzerland. About 6.500 scientists, representing 500 universities and over 80 nationalities use CERN's facilities.

The business of CERN is to find answers to nature's most fundamental questions. What is matter? Where does it come from? How does it form such complex objects like human beings, stars and planets? But as more or less "spin-off" the Laboratory plays also an important role in developing future technologies. The accelerators and detectors used at CERN have always been challenging projects for industry. The huge amount of data collected by the detectors caused a need of developing always higher computing power. But this is just one field where

[1]CERN stands for "Conseil Européen pour la Recherche Nucléaire"

[2]the preferred spelling of the word "Organization" in British English is with a "z"; it is an exception to the rule that "-isation" is spelled with an "s". Recently both forms have become acceptable. This spelling was not influenced by US practice: see The Oxford English Dictionary, 1936 and 1961, Vol.VII, p.195; The Oxford English Dictionary, 2nd edition, 1989, Vol.X, p.923. But all this is perhaps irrelevant: the legal name is with a "z" because that is what is written in the Convention.

CERN pushed the level of performance higher and higher. From materials- and surface technology over computing to quality assurance, particle physics demands the ultimate in performance.

Due to this high-tech environment present at CERN, it contributes also an important part to advanced technical education. There is a wide range of training schemes and fellowships.

In order to get more familiar with the framework of the nuclear research especially faced to the research of neutrinos and to understand the purpose of this diploma work, the following part of the introduction describes briefly the composition of the matter.

1.4 Matter

All matter exists of molecules, which exist of atoms, which further exist of the protons and neutrons in the nucleus and the electrons surrounding the nucleus. But these particles are not the smallest components which make up the matter. There are even smaller parts, the protons and neutrons exist of. There was and there still is a great effort in the research of the very smallest particles at research centres all over the world. Here just an overview about the development of the picture we have today about the composition of matter [3] will be given. Until the end of the 19. century scientists believed that the atoms are elementary (what means that they are the smallest parts and are not further divisible). In 1911 Rutherford proved with his -Streuexperiment- that atoms have nuclei. Chadwick discovered in 1932 the neutron. In the following 30th until the 50th a lot more particles were found. After the first euphoria about the discovered particles there followed a disillusionment because of the now existing "particle zoo" which got more mysterious with increasing complexity. Like in chemistry where the periodic table of the elements brought some order in the elements, the scientists tried to find a system to order the particles in a similar elegant way. Murray Gell-Mann introduced in 1964 the quarks after he introduced in 1961 the "Achtfachen Weg" as the first step towards a order in the particle zoo. He did not want to give the quarks a the fundamental status describing name, so he chose an artificial name. Actual the name "quark" descends from the roman "Finneganes Wake" from James Joyce. Initially Gell-Mann gave the quarks three "flavours", after him, in 1974, 1977 and 1995, three further flavours were discovered. Today all information about the particles discovered so far builds the "standard model".

1.4.1 Standard Model

[4],[5]

"The standard model is working too well" said Richard P. Feynman and he emphasized symbolic with this sentence the power of the standard model. All the experimental confirmed predictions showed that it really works very well. Most of the particle physicists believe that the standard model could be supplemented but never completely rejected how it happened to some atom models. The standard model describes the composition of matter with only a few fundamental particles.

The standard model consists of only 12 fundamental particles, six quarks and six leptons and the four fundamental interactions.

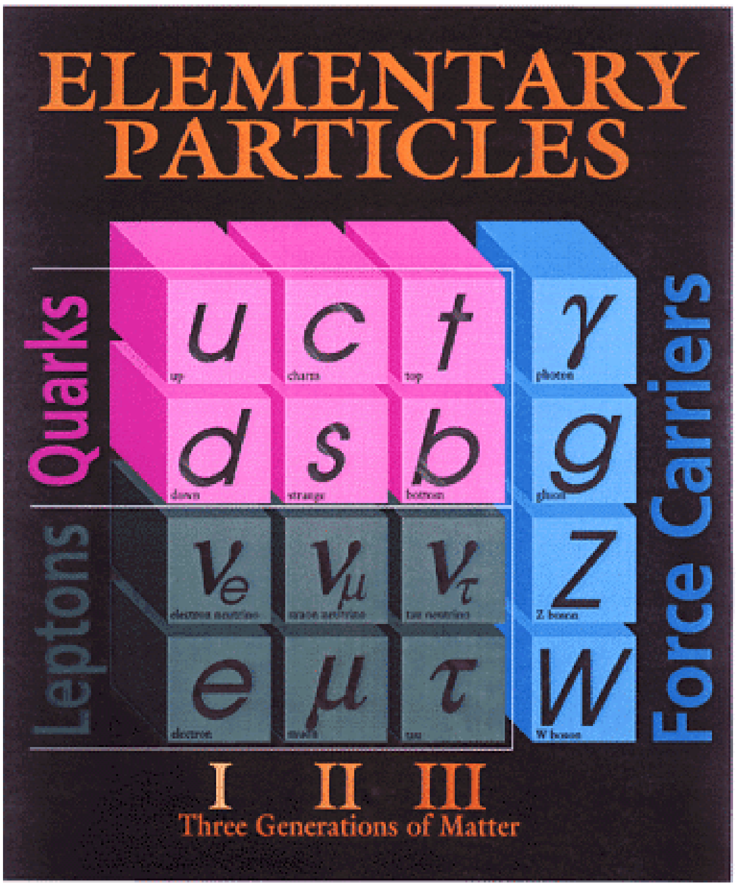

Figure 1.1: Elementary Particle Chart

Before starting a brief description of the particles of the standard model, here are some definitions:

Energy - given in eV.

$$1eV = 1,6 \cdot 10^{-19} J \tag{1.1}$$

It is the energy gained by one electron in crossing a potential difference of one Volt.

Mass - given in eV/c^2.

$$1eV/c^2 = 1,8 \cdot 10^{-36} kg \tag{1.2}$$

For example the mass of a proton is $0,938 GeV/c^2 = 1,67 \cdot 10^{-27} kg$.

Electric charge - given in units of the charge of a proton. In SI units the proton's electric charge is $1,6 \cdot 10^{-19}$ Coulombs.

Spin - the angular momentum of the particles. The unit of the spin is given in h-bar (quantum unit of angular momentum).

$$h - bar = h/2pi = 6,58 \cdot 10^{-25} GeVs = 1,05 \cdot 10^{-34} Js \tag{1.3}$$

In a more abstract level the fundamental particles and forces of the standard model can be divided into two groups: the Fermions and the Bosons. The Fermions can be further divided into the Leptons and the Quarks. Both have the spin 0,5. The Leptons are lightweights (greek. leptos = light). The Electron is a Lepton. There are two more negative charged Leptons, the Muon and the Tau. The Neutrinos, three further Leptons which come in three flavours, corresponding to the Electron, Muon and Tau, have no electric charge and a very little mass. Much more information about Neutrinos follows in an other chapter. The Quarks only exist in groups. Their distinguish mark is the flavour. The "up", "charm" and "top" Quarks have positive charge, while the "down", "strange" and "bottom" Quarks are negatively charged.

FERMIONS matter constituents spin = 1/2, 3/2, 5/2,...

Leptons spin = 1/2			Quarks spin = 1/2		
Flavor	Mass GeV/c²	Electric charge	Flavor	Approx. Mass GeV/c²	Electric charge
ν_e electron neutrino	$< 7 \times 10^{-9}$	0	u up	0.005	2/3
e electron	0.000511	-1	d down	0.01	-1/3
ν_μ muon neutrino	< 0.0003	0	c charm	1.5	2/3
μ muon	0.106	-1	s strange	0.2	-1/3
ν_τ tau neutrino	< 0.03	0	t top (initial evidence)	170	2/3
τ tau	1.7771	-1	b bottom	4.7	-1/3

Figure 1.2: Fermions

Groups of Quarks are called Hadrons. Groups of two Quarks are the Mesons and groups of three Quarks are the Baryons (greek. baryos = heavy). Mesons consists of a Quark and a Antiquark, because the electrical charge has to be a whole number. These Mesons are instable and decay rapidly. The Baryons can further be divided into the Nucleons and the Hyperions. Protons and Neutrons are Nucleons. Hyperions are heavier than the Nucleons and are instable.

Mesons $q\bar{q}$					
Symbol	Name	Quark content	Electric charge	Mass GeV/c^2	Spin
π^+	pion	$u\bar{d}$	+1	0.140	0
K^-	kaon	$s\bar{u}$	−1	0.494	0
ρ^+	rho	$u\bar{d}$	+1	0.770	1
D^+	D^+	$c\bar{d}$	+1	1.869	0
η_c	eta-c	$c\bar{c}$	0	2.979	0

Figure 1.3: Mesons

Baryons qqq and Antibaryons $\bar{q}\bar{q}\bar{q}$					
Symbol	Name	Quark content	Electric charge	Mass GeV/c^2	Spin
p	proton	uud	1	0.938	1/2
$\bar{p}$	anti-proton	$\bar{u}\bar{u}\bar{d}$	−1	0.938	1/2
n	neutron	udd	0	0.940	1/2
Λ	lambda	uds	0	1.116	1/2
Ω^-	omega	sss	−1	1.672	3/2

Figure 1.4: Baryons and Antibaryons

There exist a lot (hundreds) of different Hadrons, which are also called the "particle zoo"

The Bosons are the carriers of the four fundamental forces. There are four interactions (gravitation, electromagnetic, weak and strong force), therefore there are four associated types of Bosons.

BOSONS force carriers spin = 0, 1, 2,...

Unified Electroweak spin = 1	Mass GeV/c²	Electric charge
γ photon	0	0
W^-	80.22	−1
W^+	80.22	+1
Z^0	91.187	0

Strong or color spin = 1	Mass GeV/c²	Electric charge
g gluon	0	0

Figure 1.5: Bosons

The Boson associated to the gravity is the Graviton which has not yet been observed. The Bosons associated to the electromagnetic force is the Photon. As the Photon has no mass, it is the ultimate in stability. Hence the range of the electromagnetic force is infinite because the Photon does not decay. Gravity is also of infinite range, so the Graviton would also be massless.

The Gluon (carrier of the strong force, which comes in eight types) and the W and Z (weak force) are very short range Bosons. Their range is only 10^{-15} and 10^{-18} m. They only exist in the nuclei.

1.4.2 Matter-Antimatter

Antimatter has exact opposite properties as the related matter except from mass. Thus for example the Electron has an antiparticle called Positron. This Positron has exactly the same quantity of charge but positive. The masses are identical. But mass and charge are not the only properties of particles, there are others such as the spin. So also neutral particles with no charge can have an antimatter partner.

When a particle collides with its antiparticle, the two particles are completely converted into energy (according to Einstein's equation $e=m \cdot c^2$). This is, what happened for over ten years now in CERN's giant LEP (Large Electron Positron Collider) ring. Bunches of electrons and positrons were accelerated in opposite directions. When the kinetic energy of the particles reached a certain level, collisions have been made happen inside four particle detectors around the ring. The energy created by these collisions then converted itself into many other particles which were observed in the detectors.

Now the LEP has been closed to make place for the new LHC (Large Hadron Collider) which will begin to operate in 2005.

1.5 Neutrinos

[6]

The first Neutrino was initially, like many other particles, "invented" to close a gap before it was really observed years later. In 1930 Wolfgang Pauli introduced an electrical uncharged particle, which carries an energy to close the "energy gap" at the beta-minus decay. Enrico Fermi gave this particle in 1933 the Name Neutrino ("little neutral particle"). Today it is known, that it is the electron anti-neutrino at the beta-minus decay. It took until 1959 when Cowan and Reines proved the existence of the neutrinos in an experiment. In the late fifties and early sixties lead the apparent violation of the maintenance of the number of leptons at a particle reaction to the division of the neutrinos into two kinds: the electron- and the myon-neutrino. The heaviest lepton, the tauon and his tauon-neutrino were discovered just end of the seventies.

1.5.1 What are Neutrinos ?

[7]

It's nothing, almost nothing. As would say F. Reines: it is "the most tiny quantity of reality ever imagined by a human being".

Within the standard model, the neutrino has a zero mass, a zero charge and a spin $\frac{1}{2}$.

The neutrinos, existing in the three types electron-, muon- and tau-neutrino have kept since 1956 many mysteries. The neutrinos are only affected by the weak interaction out of the four fundamental forces. This is why they can pass through the earth without any deviation. They interact only one time over one billion in any matter. This fact is why it is very difficult to detect the neutrinos.

Since the discovery of the neutrino there has been a great effort to find answers to the questions about their properties.

Although today the three main questions about neutrinos are still opened:

- What is their exact mass?
- Has it a magnetic spin?
- Is it identical to its anti-particle?

In addition the neutrino seems to have a remarkable property: its spin is always orientated in the direction opposite to its velocity (left helicity). The anti-neutrino is always of right helicity (spin in the same direction as the velocity). This hypothesis was imagined in 1956 by T.D. Lee and C.N. Yang and was confirmed in the following year by Ambler, Hayward, Hoppes, Hudson and Wu, observing an asymmetry of the electrons coming from beta decay of Cobalt 60 nuclei [8].

If the neutrinos are massive or if neutrinos are identical to anti-neutrinos, then they will not always respect the following observed rule: A neutrino is always left and an antineutrino is always right.

1.5.2 Some Orders of Magnitude

Neutrinos from Stars

Our sun emits around $2{\cdot}10^{38}$ neutrinos per second !...

and the earth receives more than 40 billions neutrinos per second and cm^2.

This huge raining is undetected by the five senses of the homo sapiens.

Number of neutrinos in the universe

Big-Bang

about 330 neutrinos per cm^3

Stars

about 0.000006 neutrinos per cm^3

Explosions of supernovae

about 0.0002 neutrinos per cm^3

Energies of the neutrinos

The Big-Bang neutrinos

the most numerous, are also the less energetic:

0.0004 eV

(they have still a speed of 2000 km/s if their mass is 10 eV/c^2).

Neutrinos from the sun

until about 20 MeV depending of their origin.

Neutrinos from nuclear reactors

a mean energy of 4.0 MeV (between 1 MeV and 10 MeV).

Neutrinos from accelerators today

very various: a mean energy from 30 MeV to 30 GeV.

Cross section for interactions with nucleons

10^{-38} cm^2 at 1 GeV and increasing with energy.

Some surprising numbers

The human body contains about 20 milligrams of Potassium 40, which is beta radioactive. As a consequence, the body emits about 340 millions neutrinos per day. Neutrinos interact very few, there are thus 340 millions neutrinos per day, which run from our body at the speed of light until the end of the universe!...

Neutrino detectors today detect about one neutrino every 10 seconds. For all the duration of the experiment, neutrinos will have deposited a little more than 0.03 Joules in the detector

The human body receives per second about 400.000 billions neutrinos from the sun, but also 50 billions neutrinos (but this number is not well known) from the natural radioactivity of the earth, and 10 to 100 billions neutrinos from nuclear plants all over the world.

Chapter 2

Neutrino Factory

There is a strong interest from the physics community for high-quality, high-intensity neutrino beams as produced by a neutrino factory. With the help of other European laboratories, CERN has started a study on some of the many technological challenges of such a facility.

The production of neutrinos with accelerators (neutrino factories) has gained considerable interest among its possible future clients. The original interest started with the study of muon colliders [9],[10]. These colliders could open the way to lepton collisions at extremely high energies. Circular electron colliders are limited in energy due to the high synchrotron radiation emitted by the electrons. Although this radiation decreases with larger radius of the accelerator, it increases with the fourth power of the relativistic J factor. For this reason it seems unrealistic to build circular machines with higher energies than LEP. The only possibility for higher energies seemed to be linear colliders with all their technical challenges. Another, more straightforward solution is the use of heavier leptons, as the synchrotron radiation at the same energy is much reduced because of the smaller J which is inversely proportional to the rest mass. Muon beams seem to be possible candidates for this purpose. Muons can be readily produced by the decay of pions, which in turn can easily be produced by bombarding a target with high energy protons. The "only" remaining problem is the production of muon beams with the required density in phase space, necessary for collider operation. In spite of some impressive progress towards this goal, no technically feasible solution has yet been found. A substantial R&D effort will be required to make progress.

With the apparent discovery of neutrino oscillations and the increased interest in neutrino physics in general, the situation has changed drastically. What appeared to be almost science fiction in the context of muon colliders is now, due to the reduced requirements for a neutrino factory, much closer to reality. The R&D effort for the muon colliders turned out to be very useful for a neutrino factory, and the increased interest from the physics side has produced a high activity on the achieve an optimum intensity, the energy spread and the transverse emittance have to be reduced.

2.1 Purpose

Neutrino factories would provide [11],[12]:

(i) ν_e and $\overline{\nu_e}$ beams, as well as ν_μ and $\overline{\nu_\mu}$ beams !

(ii) High event rates. With $2 \cdot 10^{20}$ muon decays per year in the beam forming straight section of a 50 GeV neutrino factory the ν_μ event rates in a distant detector would be about a factor of 60 higher than the corresponding rates for the next generation of conventional beams (NUMI at FNAL for example). These neutrino factory rates would yield tens of thousands of ν_μ events per year within a reasonable sized detector on the other side of the Earth (L $\sim$ 10000 km). In addition, a near-detector a few hundred meters from the end of the beam-forming straight section of a 50 GeV neutrino factory would measure of the order of a million events per year per kg ! This fantastic rate would enable a revolution in non-oscillation neutrino experiments, which could be based on silicon pixel targets, polarized hydrogen targets, and detectors with fine segmentation and good particle identification.

(iii) Narrow ν and $\overline{\nu}$ energy spectra. Neutrinos from a neutrino factory have a much narrower energy spectrum than provided by a conventional "wide band" beam. Hence, a neutrino factory beam can be thought of as being "narrow band".

(iv) Low systematic uncertainties. Since the muon decay spectrum is very well known, the systematic uncertainties on the flux and spectrum of neutrinos at a distant experiment are expected to be significantly less than the corresponding uncertainties for a conventional beam. This would be expected to improve the ultimate precision of ν_μ disappearance measurements.

(v) Polarization. In the forward direction the ν_e flux at a neutrino factory is sensitive to the polarization of the muons in the storage ring. Hence, by controlling the polarization the ν_e component within the initial beam can be varied. In principle this could be very useful, although a compelling case for muon polarization has yet to be demonstrated in a detailed analysis.

Thus, compared with the next generation of conventional neutrino beams, neutrino factories offer the prospect of higher intensity neutrino and antineutrino beams containing ν_e as well as ν_μ, lower systematic uncertainties, a narrower beam energy distribution, and perhaps beam composition control via polarization. In addition the intensity increase would initiate a revolution in non-oscillation experiments. Its easy, therefore, to understand the current interest in neutrino factories.

2.2 Physics

Conventional neutrino beams are produced from a beam of charged pions decaying in a long (typically several hundred meters) decay channel. If positive (negative) pions are selected, the result is an almost pure $\nu_\mu(\overline{\nu_\mu})$ beam from $\pi^+ \rightarrow \mu^+\nu_\mu$ ($\pi^- \rightarrow \mu^-\overline{\nu_\mu}$) decays, with a small (1%) component of ν_e from three body kaon decays. The ν_e component is not large enough to be useful for $\nu_e \rightarrow \nu_x$ measurements. Hence, if one wants ν_e and $\overline{\nu_e}$ beams one will need a different sort of neutrino source.

An obvious way to try to get ν_e and $\overline{\nu_e}$ beams is to exploit the decays $\mu^+ \rightarrow e^+\nu_e\overline{\nu_\mu}$ and $\mu^- \rightarrow e^-\nu_\mu\overline{\nu_e}$. To create a neutrino beam with sufficient intensity for a new generation of oscillation experiments will require a very intense muon source. With a millimole of muons per year we can imagine producing high energy beams containing 10^{20} neutrinos and antineutrinos per year. However, to achieve this a large fraction f of the muons must decay in a channel that points in the desired direction. Muons live 100 times longer than charged pions. Since the decay fraction f must be large we cannot use a linear muon decay channel unless we are prepared to build one that is tens of kilometers long. A more practical solution is to inject the muons into a storage ring with long straight sections. The useful decay fraction f is just the length of the straight section divided by the circumference of the ring. It has been shown that $f \sim 0,3$ is achievable [13]. The resulting muon storage ring is sufficiently compact that it can be tilted downwards at a large angle so that the neutrino beam can pass through the Earth [11], and very long baseline experiments ($L \sim 10^4 km$) can be imagined.

Thus the "neutrino factory" concept [11] is to create a millimole/year muon source, rapidly accelerate the muons to the desired storage ring energy, and inject them into a storage ring with a long straight section that points in the desired direction. Typical parameters for a "reference scenario" would be a 50 GeV ring delivering 10^{20} muon decays per year in the beam forming straight-section, yielding data samples 10^{22} kt-decays after a few years of running.

2.3 Production of Neutrinos - Neutrino Factory

[14],[15]

2.3.1 Overview Neutrino Factory

The first part of a neutrino factory is a proton driver which delivers a high-power proton beam onto a target; a system for collection of the produced pions and their decay products, the muons. The resulting muon beam has to be accelerated and, to achieve an optimum intensity, the energy spread and the transverse emittance have to be reduced. This is done by phase rotation and ionisation cooling. After acceleration with a linac and RLAs (Recirculating Linear Accelerators) the muons are injected into a storage ring or rather decay ring, where they decay in long straight sections in order to deliver the desired neutrino beams.

The first part of a neutrino factory is the "proton driver" which, in order to provide an intensity of 10^{21} neutrinos/year, should deliver a beam power of the order of 4 MW. This linac accelerates H^- ions and operates at 75 Hz and a pulse duration of 2.2 ms with 11 mA. The beam is injected into an accumulator (charge exchange injection) and subsequently into a compressor ring to produce the necessary short bunch lengths of the order of nanoseconds. 140 bunches at a frequency of 40 MHz will be sent onto a target to produce short pion bunches decaying into muons which are captured, and reduced in energy spread and in transverse emittance. The muons are then accelerated to 50 GeV and injected into a storage ring (decay ring) where they are kept for the duration of their lifetime (1.2 ms at this energy). The muons decaying in the long straight sections of this ring produce the required neutrino beams.

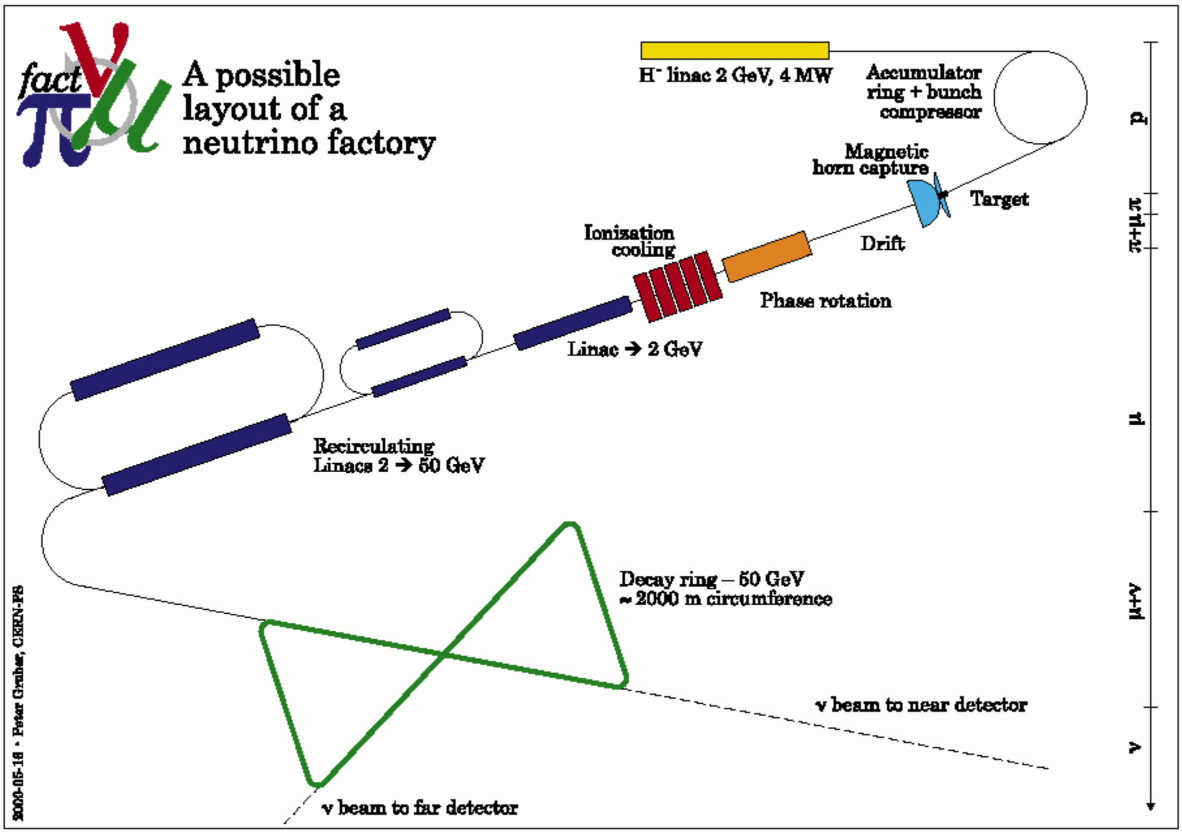

Figure 2.1: Possible Layout of a Neutrino Factory

2.3.2 Driver, Target and Capture

As mentioned above, the first element of a neutrino factory is the proton driver. That is, the protons produce pions which, subsequently, decay into muons. The driver must be intense, we talk of 1 to 4 MW of proton beam power, which is high, but in the same range as a spallation neutron source. The present AGS, at Brookhaven, produces 0.2 MW of proton beam power and improving the rep rate, alone, would bring it to 1.0 MW. At Fermilab there is talk of building a new booster, at 16 GeV, that satisfies the needs of a neutrino factory. Solid carbon targets may be used, although liquid mercury jets give an enhanced flux by about a factor of two and are therfore the prefered solution (but are harder to operate). The target should be placed at a small angle both with respect to the proton drive beam and the surrounding solenoid, so as to reduce pion re-absorption. The production is not only spread over energy but also over angles. To capture as large a number of pions as one is able, a very strong magnet is put over the target region. The considered provides 20 T, which is large, but far from the most powerful solenoid made. However, lifetime and operation in the intense radiation field are issues that result in employing smaller field strength. The captured muons are (about) 0.6 per proton.

2.3.3 Phase Rotation and Cooling

The muons, resulting from pion decay, are spread in energy as shown in Figure 2.2. If the bunch is now allowed to drift then the higher energy muons, being faster, will move to the front of the bunch and vice-versa. In short a correlation will be developed between energy and position.

At the same time, the energy spread, at any position, will be decreased. The length of the drift region is determined by making the energy spread sufficiently small that the beam can be accepted by down-stream components. (Of course, the longer the drift the more muons are lost for their mean survival length, at the low energies considered, is only 660 m.). The correlation between energy and position must now be removed and that can be done with an induction accelerator which, unlike rf, has a pulse length as long as the muon bunch. In combination with the drift, the muon beam can now be bunched and longitudinally accepted by the rest of the factory. However, the transverse size of the muon beam must still be reduced. To this end, ionization cooling is employed. The cooling effect results from absorption of the energy in tanks filled with H_2, so longitudinal and transverse momenta are both reduced. In each cooling unit, RF re-acceleration restores the longitudinal momentum, not the transverse one and the angle of the particle with the axis diminishes. The multiple Coulomb scattering counteracts the reduction of the angle. But within the present parameters, this effect is weak. The optics of the cooling line is setup to maintain a high divergence and thus make the cooling efficient.

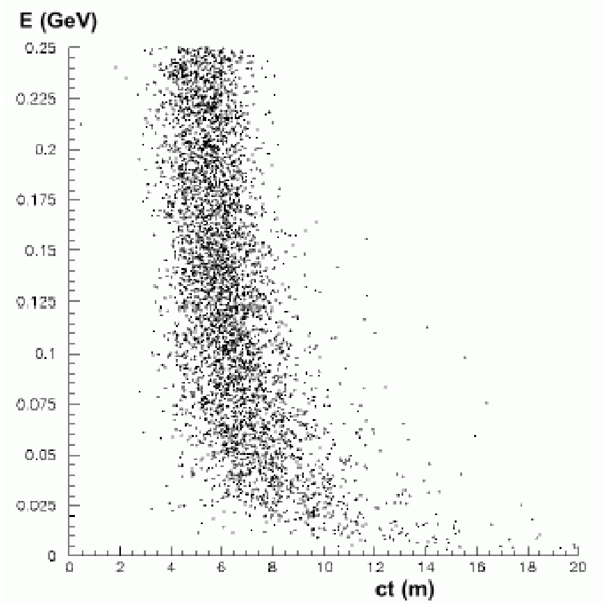

Figure 2.2: Distribution in Energy and Longitudinal Position of Muons just after Capture

An R&D program would consist of making an induction unit, developing high gradient rf cavities, engineering a cooling channel and actually demonstrating cooling. This R&D program is called MUCOOL and is described on their home page [16].

2.3.4 Acceleration and Storage

Once a muon beam has been developed, by the rather difficult procedures described in the previous sections, which takes about half a kilometer, rather than a few meters (as would be the case for another lepton; namely, an electron), acceleration and storage is much simpler than producing a beam of muons. Acceleration must be rapid, of course, and the method of choice is the use of recirculating linacs. (Other methods, such as FFAG, are being studied.) First, the beam must be accelerated in a linac so as to obtain some adiabatic damping in both transverse and longitudinal (energy- rf phase) phase space. Second, when the beam is adequately small, which occurs at about 1 GeV, it is injected into a superconducting re-circulator operating at a low frequency of 200 MHz. It appears that only four re-circulations are possible, because of the difficulty of separating large beams (despite the adiabatic damping, the beam is still large compared, say, to an electron beam). Third, the beam is extracted and then injected into a second superconducting re-circulator (operating at 400 MHz) where, perhaps, five re-circulations are now possible. Naturally, a good bit of simulation and design has been done and that can be found in Ref. [20]. An R& D program is needed on the rf superconducting cavities employed in the accelerating re-circulators. A number of types of storage rings have been considered; a triangle being particularly attractive. The rings must, of course, be properly oriented and, furthermore, slope down so that the neutrino beam will hit the detector. The simplest is a race track. A draw-back of his geometry is that only one of the neutrino beams is directed to a far detector (the other points up).

Chapter 3

Pion Production Target

[21]

3.1 Critical Issues

3.1.1 Target Material

Solid or Liquid Target

The muons of a muon collider will arise from the decay of pions produced in the interaction of some $11 \cdot 10^{15}$ protons/s on a primary target. If these protons have 2.2 GeV energy, the beam power is 4 MW. The target will be about 2 interaction lengths long and will absorb about 10% of the beam power, i.e., about 400 kW. So each beam pulse deposits about 30 kJ of energy in the target at 75 Hz.

Target Cooling The target is in the form of a cylinder, about 1 cm in radius, 30 cm in length, with a volume of about 100 cm^3. If the target material has a density of 10 g/cm^3, then the target mass is about 1 kg. Thus the beam-energy deposition in the target averages about 30 J/g. Taking the heat capacity of a typical metal as $0.2J/(g \cdot K)$, the temperature rise of a metallic target is about $150^{\circ}K$ per pulse. If the target were not cooled, it would melt (if solid) or boil (if liquid) after a few beam pulses. However, the goal of collecting the maximal number of muons per proton is not consistent with typical cooling schemes in which the target material is in immediate contact with a large thermal reservoir. Radiative cooling of the target appears to be unfeasible. At 2000 °K, the radiated power would be only 3.6 kW, well minor in comparison to the 400 kW beam load. Thus, scenarios are considered in which the target is in motion, with any subunit of the target exposed to only one or a few beam pulses before being transported away from the interaction region, to be cooled by a remote thermal reservoir. For similar reasons, targets at multimegawatt neutron spallation sources are expected to be based on owing liquid metal, usually mercury [22], [23],[24],[25],[26],[27],[28].

Thermal Shocks The simplest option would be use of a owing liquid metal contained within a (static) metal pipe [29],[30],[31]. However, when a large pulse of energy is deposited in a material in a time that is short compared to the transit time of a sound wave ($\approx 3\mu s/cm$), a pressure (stress) wave results [32],[33],[24],[35],[36],[37],[38]. Since the proton pulse for a muon collider is expected to be only about 2 ns long, stress waves will be excited in the target, and consequent damage to the target and adjacent material is a concern. This issue is often called "thermal shock". The pressure wave front propagates out- wards at roughly the speed of sound in the target material. However, thermal shock is not necessarily associated with bulk transport of matter at the speed of sound.

The Initial Pressure Wave If the beam-induced stress exceeded the tensile strength of the target material, it would fracture. Here a simpliffied model to estimate the regime in which a pressure wave will "tear" the target apart, whether solid or liquid is presented (see also refs. [32],[39]). When an energy density ΔU (per gram) is deposited quickly in the target, we first calculate the temperature change ΔT that would occur, assuming no thermal diffusion. Then, we calculate the strain, $\Delta l/l$ corresponding to that ΔT, and evaluate the stress P corresponding to that strain. Tearing is likely to occur if the stress exceeds the tensile strength. In this model, tearing occurs during the phase of the pressure wave when the material is under tension, i.e., for negative pressure. In liquids, this phenomenon is called cavitation [40][41],[42]. It is supposed that the effective tensile strength of a liquid metal is similar to that of the same metal in solid form. For example, the tensile strength of sea ice is reported as about 8 atm [43], while that of water can exceed 200 atm in a static measurement [44] but was measured as 8 atm by an explosive technique [34] that has much in common with the present concerns; see also [40], [41]]. For most metals, the tensile strength (pressure) P is about 0.002 of the modulus of elasticity E (Young's modulus). If the target tears, it is possible that the fragments do damage to the surrounding vessel. Thus, it is encouraging that if a liquid target were dispersed into droplets by the beam, the droplets would do little damage to the surrounding vessel. However, this should be confirmed by experiment.

The Reflected Pressure Wave Even if target parameters are chosen such that the initial pressure wave does not tear the material, there is another concern. When the pressure wave reaches the surface of the target, it will, in general, be reflected. In the case of a cylindrical target, the reflected wave converges on the axis of the target and will typically result in higher peak pressures than exist in the initial outgoing wave. Hence, there is a serious prospect for localized fracture or vaporization of the target material close to the target axis, whether the cylindrical target is solid or liquid. In the case of a liquid, this is likely to induce localized damage to the target pipe, particularly on the upstream wall.

The destructive effects of pressure waves and cavitation on liquid-metal targets in pipes have been demonstrated at the CERN ISOLDE facility [45], as shown in Figures 3.1-3.2 and also at the Budker Institute [46], as shown in Figure 3.3. Practical targets based on liquid metals in pipes require sufficiently long beam pulses and/or target geometries (e.g., planar) in which imploding pressure waves do not occur. Therefore, liquids in pipes are not considered further for a muon-collider target. Likewise, a moving solid cylindrical target is very problematic at a muon collider.

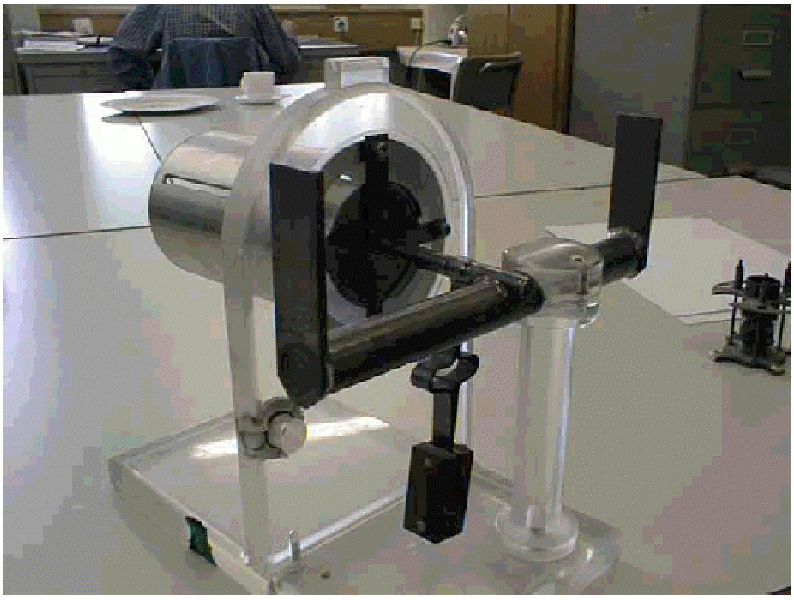

Figure 3.1: Full-scale model of an ISOLDE-target (2-cm-diameter, 20-cm-long tantalum cylinder containing molten lead)

Beam Induced Radioactivity The high flux of protons into the target will induce some radioactivity, no matter what the target consists of. A thorough study of this issue will be needed before a final decision as to the target material is taken. A first study will be made using a MARS simulation of the hadronic cascade in the target. For any target material with an atomic number greater than or equal to that of mercury, radioactive isotopes of mercury will emerge in the vapor phase. These are only the most prominent among other radioactive vapors that will be produced. Hence, a high-Z target must be enclosed in a gas-tight system that includes capture tanks for the vapors, including those exhausted from any pumps. This proposal does not cover R&D towards such a system, which would be modeled after the target-containment system at the ISOLDE facility at CERN.

Figure 3.2: ISOLDE liquid-lead target, ruptured around the upstream window after a few beam pulses

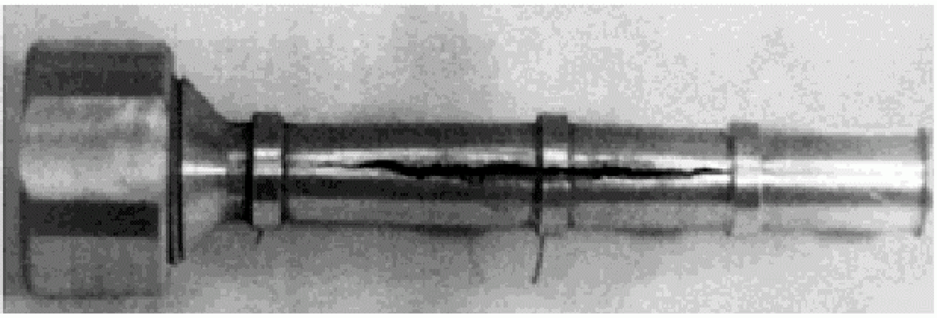

Figure 3.3: Mercury target contained in an aluminum cylinder, ruptured after exposure to a beam (deposition 1 kJ/g per pulse)

Candidate Liquid Metals

Liquid metals have long been used as coolants for nuclear reactors, and a useful summary of candidate materials has been given by Lyon [47]. The best target materials are high-Z, high-density materials for the most efficient pion production. High electrical resistivity is helpful in reducing the eddy-current problem of a jet entering a magnetic field. In many ways mercury is an excellent candidate, but its vapor is toxic.

Lead alloys (solder-like materials) are good candidates. Rather low melting temperatures are obtained by alloying with indium, which, however, wets most solid metals so much as to make it difficult to produce liquid jets. Lead-bismuth alloys have the drawback of relatively high production of polonium when activated by the proton beam. Gallium alloys are nontoxic and can be liquid at room temperature. The relatively low atomicnumber, low density and low resistivity of gallium is somewhat undesirable for use in the final target.

Overall seen, mercury seems to be the most advantageous target material. And as mercury most likely will be the prefered material for the final Neutrino Factory target, all further investigations and studies will be made referring to mercury.

3.1.2 Jet Velocity

To be useful as a target, a pulsed liquid jet must have a minimum velocity, so that each pulse is sufficiently distinct from the others, and so that the jet is reasonably straight.

Effect of 50 - 75Hz Repetition Rate

We consider the use of a pulsed jet, leading to a series of cylinders of liquid, each of length l and radius r, and moving with velocity v. The frequency f of the pulse is nominally 50 to 75Hz. If the material from one pulse is not to overlap that of the next, then the jet velocity must obey

$$v > fl \tag{3.1}$$

For example, if the length of each pulse is be about two nuclear interaction lengths (about 30 cm for a dense, high-Z material), then with $f = 50Hz$, one needs $v > 15m/s$ and with $f = 75Hz$, $v > 22,5m/s$ is neeed. The jet velocity will have to be several times this to create gaps between adjacent pulses, so that the proton beam interacts with only a single jet pulse.

Effect of Gravity

The trajectory of the jet will be a parabolic arc, due to the acceleration of gravity. If the jet velocity were too low, the curvature of the jet would be large, and the proton beam would not be able to intersect the jet pulse over its whole length. The ends of the jet are displaced downward from the ideal straight trajectory by amount

$$\Delta y = \frac{gt^2}{2} = \frac{gl^2}{8v^2} \tag{3.2}$$

noting that the time for the center of the jet to reach its end is $t = l/2v$. For example, with $\Delta y = 1/8cm$, as might be desired for a jet of radius 1cm, $l = 30cm$, then $v \approx 1000cm/s = 10m/s$ is needed. Thus, as the effects of pulse frequency requres the higher velocity, the jet velocity has to be at least about 20 m/s.

Jet Velocity vs. Pressure

Suppose the liquid metal is stored in a tank of area A perpendicular to the ow, and the pressure is P above ambient. A valve lets a jet of liquid escape through an aperture of area $a \ll A$. Then Bernoulli's equation tells us that the flow velocity v out the aperture obeys

$$\frac{1}{2}\rho v^2 = P + \frac{1}{2}\rho V^2 \tag{3.3}$$

where ρ is the density of the liquid and V is the velocity of the liquid surface of area A in the tank. The equation of continuity for an incompressible liquid tells us that $av = AV$, so that

$$v = \sqrt{\frac{2P}{\rho(1-(a/A)^2)}} \approx \sqrt{\frac{2P}{\rho}} \tag{3.4}$$

For example, with a Bi-Pb alloy of density $\rho \approx 10g/cm^3$

$$v[m/s] \approx \sqrt{20P[atm]} \tag{3.5}$$

Thus, to reach $v = 20m/s$ would require 20 atm overpressure in the storage tank.

The Interaction of a Liquid-Metal Jet with a Magnetic Field

As a jet of liquid metal enters the magnetic field that surrounds the beam interaction region, it will be repelled according to Lenz' law. The effect is due to the Lorentz force on the eddy currents induced in the moving metal. In an extreme case the jet would not reach the center of the interaction region.Analytic estimates of the effects of eddy currents reach the tentative conclusion that they would visibly alter the trajectory of the liquid-metal jet, but would not prevent the jet from functioning as a target. However, there appears to be little safety margin, suggesting the need for laboratory experiments to confirm that the proposed liquid-metal jet is viable. Additional details of the analytic arguments can be found in refs. [48],[49],[50].

Chapter 4

Design Details and Parameters

The Neutrino Factory target will be designed as a pulsed jet of mercury interacting in a strong magnetic field with a high energy proton beam. Some global numerical studies and analytical estimations of the behavior of the mercury jet under such energy deposition and in the magnetic field are presented in the next chapter.

In this chapter one can find a summary of given design parameters for the final target due to physical requirements.

4.1 Target

The target is shown schematically in Figure 4.1. It will contain a series of mercury jet pulses of about 1 cm in diameter and 30 cm in length. Each pulse will be shot at a velocity of about 20 m/s into a 20 Tesla magnetic field at a small angle to the axis of the magnetic field (∼6°). When the jet reaches the center of the magnet it is hit by a proton beam pulse with 140 5ns bunches. Each proton pulse will deposit about 30 J/g of energy in the mercury.

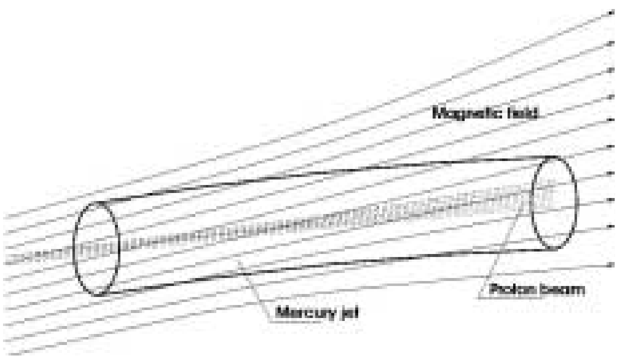

Figure 4.1: Schematic view Neutrino Factory target

4.1.1 Material

As already mentioned before, mercury is the target material of choice. For proton beam energies greater then 10GeV (as required for a Neutrino Factory), the pion/myon yield reaches a high peak at an atomic mass of 200 (see fig. 4.2). And mercury with the atomic mass of 200.6 seems to be perfect for a maximum number of myons produced.

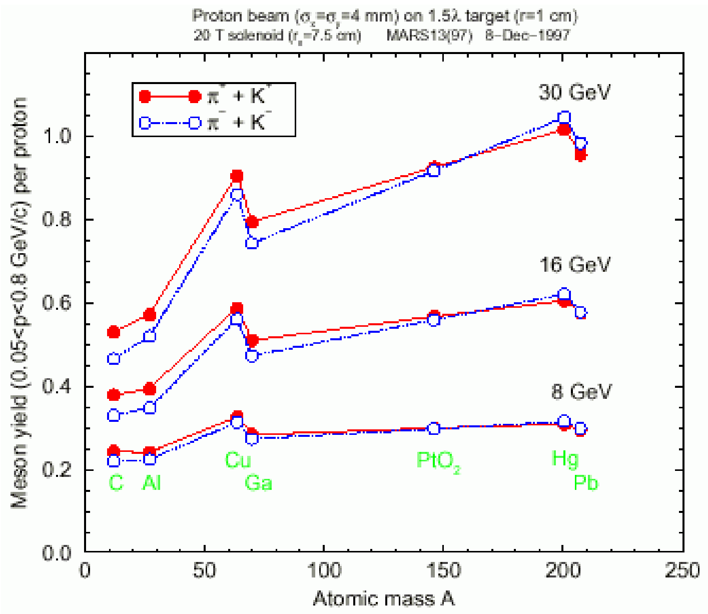

Figure 4.2: Atomic mass vs. meson yield

4.1.2 Geometry

The best target radius and tilting angle (between mercury jet and axis of the magnetic field) can be estimated in fig. 4.3 and 4.4.

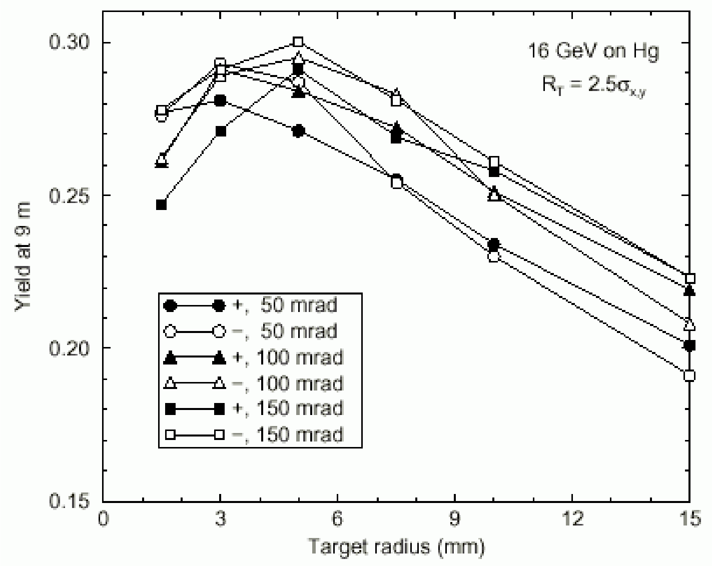

Figure 4.3: Target radius vs. meson yield

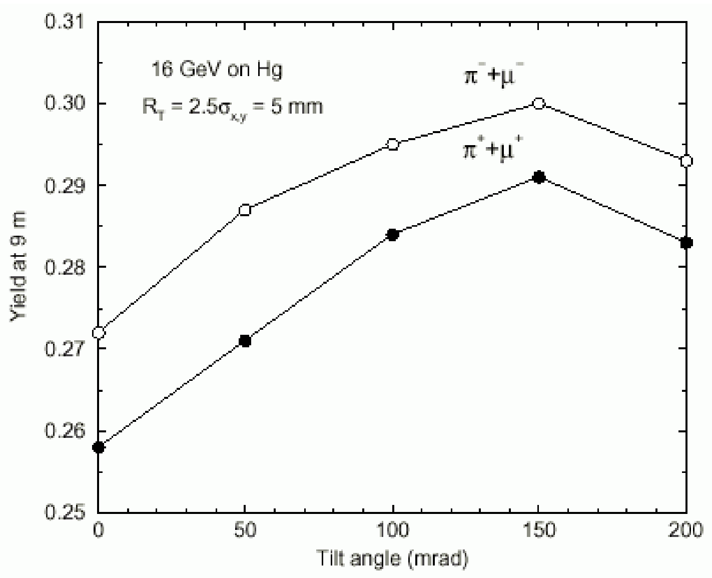

Figure 4.4: Tilting angle vs. meson yield

Target radius should be ∼5mm, and the angle should be ∼100-150mrad (∼6°).

4.2 Proton Beam

The Superconducting Proton Linac (SPL) accelerates protons up to 2.2 GeV kinetic energy in bursts of 2.2 ms duration, at a rate of 75 Hz. The mean current during the pulses is 11mA for an average beam power of 4 MW. For the neutrino factory the beam burst is accumulated over 660 revolutions of the accumulator ring that transforms it into a 3.3 μs train of 140 bunches (see fig. 4.5). These are then individually reduced in length in a compressor ring before being sent to the pion production target.

The linac cannot directly provide a suitable beam, hence it will inject the protons into an accumulator ring. Bunches will be formed in this ring with suitable rf cavities. They will be transferred into a compressor ring for further shortening of their length. The repetition rate is 75 Hz.

The main characteristics of the SPL-accumulator-compressor-beam are listed in the following table:

Parameter	**Unit**	**Value**
beam current	mA	11
averagce beam power	MW	4
kinetic energy	GeV	2.2
pulse frequency	Hz	75
pulse duration	μs	3.3
pulse intensity	p/pulse	$1.51{\cdot}10^{14}$
number of bunches		140
bunch length	ns	5
bunch spacing	ns	22.7
bunch intensity	p/bunch	$1.1{\cdot}10^{12}$

Table 4.1: Characteristics SPL-Accumulator-Compressor

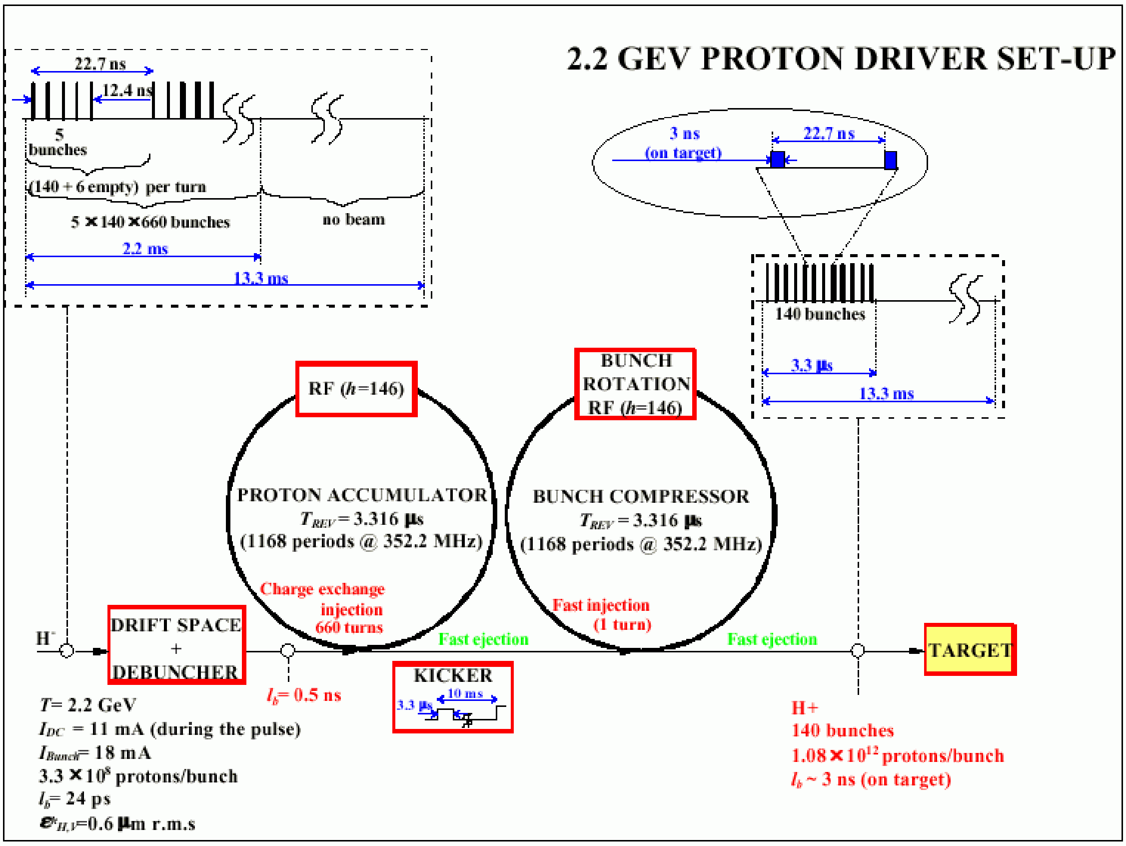

Figure 4.5: SPL-Accumulator-Compressor Layout

4.2.1 Energy Deposition

When a particle beam travels through matter, the particles lose energy (primarily by ionization). The mean rate of energy loss (or stopping power) is given by the Bethe-Bloch equation. The energy loss dE/dx is given in the unit [MeV cm^2/g].

$$-dE/dx = D\frac{Z}{A}\rho z^2\Phi(\beta)(1+v) \tag{4.1}$$

with

$$\Phi(\beta) = \frac{1}{\beta 2}(\log(\frac{2m_e c^2\gamma^2\beta^2}{I(1+\gamma m_e/M)}) - \beta^2 - \frac{\delta}{2} - \frac{C}{Z}) \tag{4.2}$$

where

E	=	projectile energy
M	=	projectile energy
β	=	projectile velocity (in units of c)
γ	=	$1/\sqrt{1-\beta^2}$
z	=	projectile charge (in units of elementary charge)
x	=	path length
D	=	$4\pi r_e^2 m_e c^2 N_A = 0.30707 MeV cm^2/mole$
re	=	$2.817938 \cdot 10^{-13} cm$=classical electron radius
me	=	$0.511003 MeV/c^2$=electron rest mass
N_A	=	$6.022 \cdot 10^{23}/mole$=Avogadro number
Z	=	atomic number of the medium
A	=	atomic weightnof the medium [g/mole]
ρ	=	mass density of the medium [g/cm^3]
I	=	average ionization potential
δ	=	density correction
C	=	shell correction
v	=	higher order correction

The ionization energy loss depends mainly on the projectile velocity. It decreases with $1/\beta^2$ for increasing velocity until reaching a minimum (minimum ionization), then starts to rise logarithmically (relativistic rise) and leveling off finally at a constant value (the Fermi plateau).

Taking the target to be a static cylinder of mercury, 20 cm long and 1 cm in diameter, irradiated by a 2.2 GeV proton beam of 1 mm diameter, calculations indicate that approximately 10% (or 0.4 MW for a 4 MW beam power) of the beam power is deposited in the target, with most of the power deposited in the first few centimetres of length. This is shown in Figure 4.6 as a function of radius. For the Gaussian beam distribution there is a strong dependence in the power density as a function of the radius. The consequence of this is that there will be strong temperature differences in the target, radially and longitudinally, and some internal parts of the target may reach the boiling point and thus limit the total power that can be absorbed in the target.

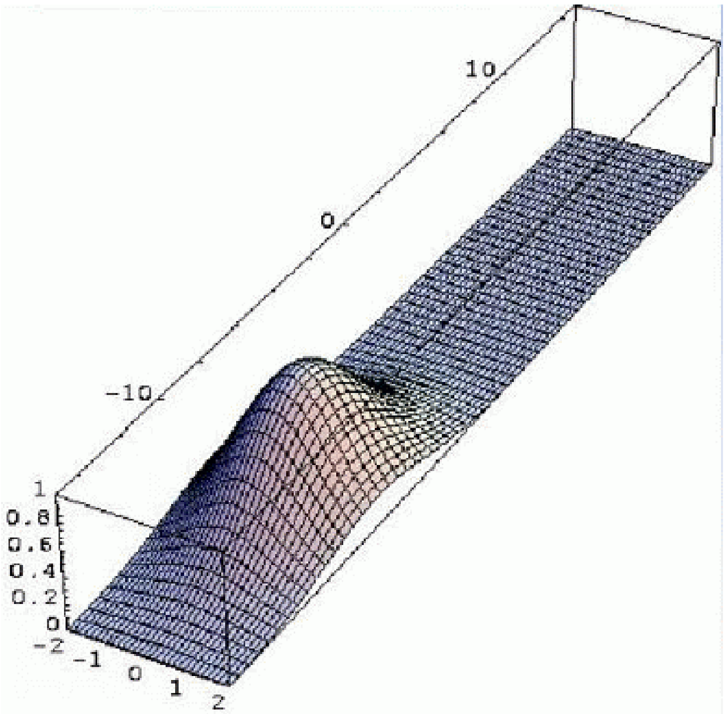

Figure 4.6: Energy deposition profile

4.2.2 Temperature Profile

The deposited energy is converted mainly into heat and causes a target temperature profile which follows in principle the ionization energy loss profile as in fig. 4.6.

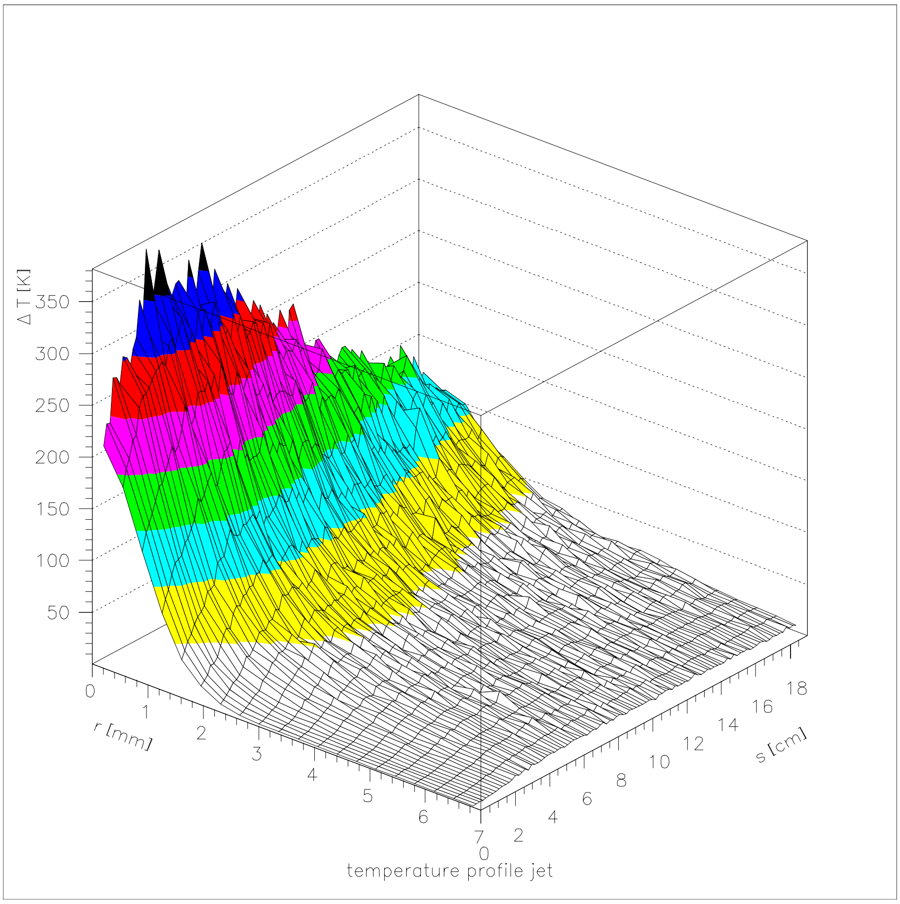

Figure 4.7: 3D target temperatur profile: ΔT vs. target lenght s and radius r

4.3 Magnetic Field

As mentioned in 2.3.2, a magnetic Field of 20T is needed for collecting the pions produced after proton beam impact and forcing them into one direction. There are three possibilities for applying this magnetic field:

(1) Using the magnetic field of a solenoid (4.3.1) or

(2) using a magnetic horn (4.3.2) or

(3) using the magnetic field produced by a high current sent through the target itself ("Pulsed Target") - (4.3.3).

4.3.1 Solenoid

A superconductive or a conventional conductive solenoid could be used for focusing the pions. Fig. 4.8 shows a principle sketch of the target station with a surrounding solenoid. There are indicated in blue the mercury jet, in red the proton beam and in light red the produced secondary particled (pions). The red dots symbolize the magnetic field lines.

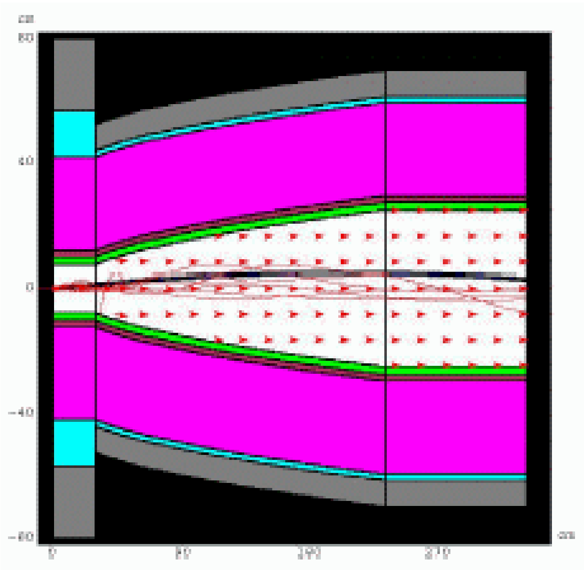

Figure 4.8: Sketch of Target Station with surrounding Solenoid

4.3.2 Magnetic Horn

An other method for producing a pulsed magnetic field is a so called magnetic horn. A magnetic horn is an electrical conductor with an surface formed like a horn. It consists of an inner and an outher conductor. When a high current is driven through the conductor by applying a voltage between the inner and the outher conductor, a magnetic field forms inside the horn.

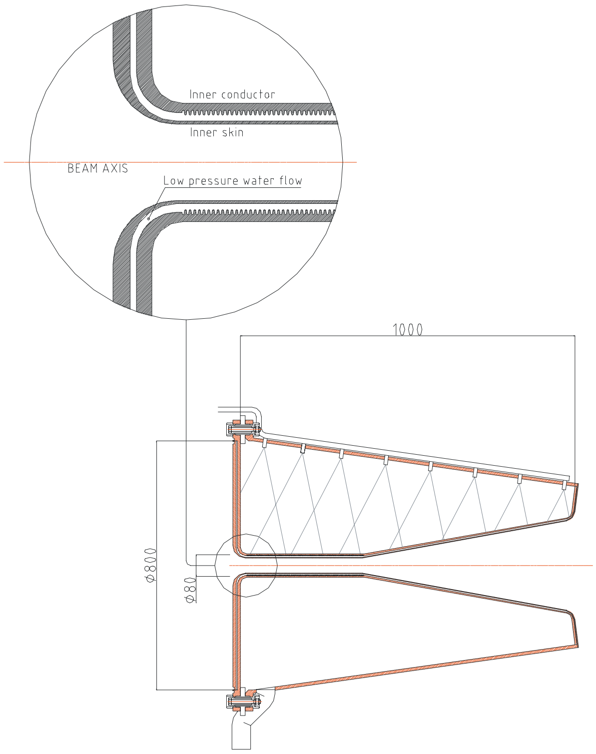

Figure 4.9: Preliminary design of a water cooled magnetic horn for a Neutrino Factory

4.3.3 Pulsed Target

It would also be possible to send a current directly through the target in order to produce a magnetic field around the target. To get a suitable magnetic field, a current of about 1MA would be necessary. The energy deposited in the target by the current would then be about 1MW, wich corresponds to two times the energy deposition by the proton beam.

The option "Pulsed Target" is mentioned here just for completeness, because the most plausible scenarios are the solenoid or the magnetic horn.

Chapter 5

Mercury

As mercury is one of the most promising material considered for the target for the neutrino factory, its properties and hazards have been studied.

5.1 Description

Mercury is the only common metal liquid at ordinary temperatures. It only rarely occurs free in nature. The chief ore is cinnabar (HgS). Spain and Italy produce about 50% of the world's supply of the metal. Worldwide production of mercury in the 1960s was estimated at 15 million pounds by the U.S. Geological Survey. Environmental concerns have slowed the growth of mercury as an industrial chemical. The metal is obtained by heating cinnabar in a current of air and by condensing the vapor[51]. It is a heavy, silvery-white metal; a rather poor conductor of heat, as compared with other metals, and a fair conductor of electricity. It easily forms alloys with many metals, such as gold, silver, and tin, which are called amalgams. The metal is widely used in laboratory work for making thermometers, barometers, diffusion pumps, and many other instruments. It is used in making mercury-vapor lamps and advertising signs, etc. and is used in mercury switches and other electrical apparatus. Other uses are in making pesticides, mercury cells for caustic soda and chlorine production, dental preparations, antifouling paint, batteries, and catalysts. Mercury is a virulent poison and is readily absorbed through the respiratory tract, the gastrointestinal tract, or through unbroken skin. It acts as a cumulative poison and dangerous levels are readily attained in air. It is estimated that 30,000 to 150,000 tons of mercury vapor is emitted annually into the earth's atmosphere through natural evaporation from the earth's crust[52]. Air saturated with mercury vapor at 20 deg C contains a concentration that exceeds the toxic limit many times. The danger increases at higher temperatures. It is therefore important that mercury be handled with care. Containers of mercury should be securely covered and spillage should be avoided.

5.2 Properties / Physical Data

Mercury is a naturally occurring metallic element;

Number 80 on the periodic chart;

Chemical symbol Hg for hydrargyrum;

Molecular weight 200.6 grams/mole;

Silvery, extremely heavy liquid at room temperature at 13.59 grams/cc (water 1 gm/cc);

Melting point -38.85 °C (-38 °F); boiling point 356.6 °C (699.48°F);

Soluble in nitric acid and lipids, insoluble in water, alcohol and ether;

Surface tension 480 dynes/cm at 20 °C (water 73 dynes/cc), the highest for any liquid;

Vapor pressure at room temperature 0.002 mmHg; at 50°C 0.013 mmHg. A standard atmosphere saturated with mercury will contain approximately 18 mg Hg/$m^3$of air;

Non-combustible;

Odorless

Chrystal structure: rhombohedral

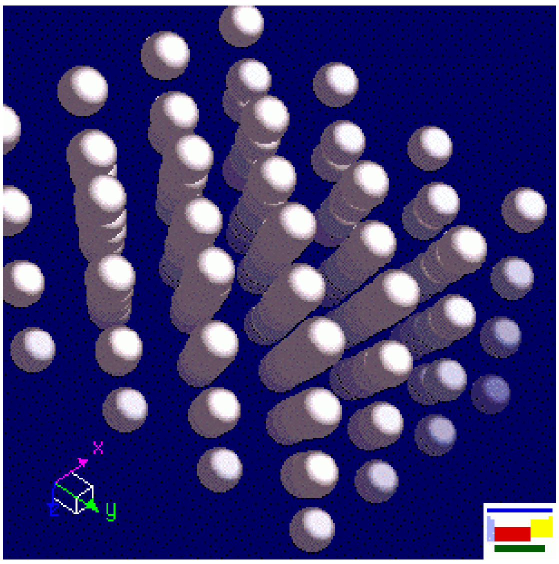

Figure 5.1: Rhomboheral chrystal structure of mercury

5.3 Phase Diagram

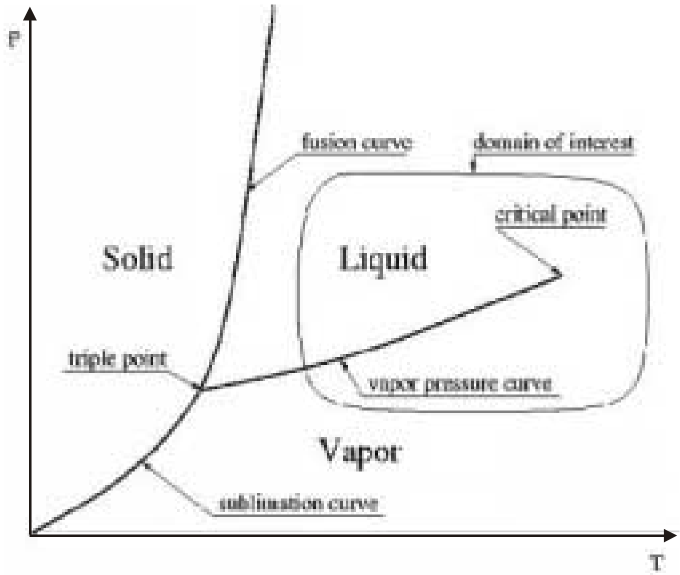

Figure 5.2: Mercury Phase Diagram

Critical point:

$T_C = 1750K$

$P_C = 172MPa$

$V_C = 43cm^3mol^{-1}$

Boiling point:

$T_b = 629.84K$

$P_b = 0.1MPa$

$\rho = 13.546g \cdot cm^{-3}$

Analytical expression for the vapor pressure curve:

$$P = 133.3exp(18.41 - 7318/T) \tag{5.1}$$

[P]=Pa, [T]=K

5.4 Safety Aspects

5.4.1 Potential Health Effects

Inhalation:

Mercury vapor is highly toxic via this route and causes severe respiratory tract damage. The symptoms include sore throat, coughing, pain, tightness in chest, breathing difficulties, shortness of breath, headache, muscle weakness, anorexia, gastrointestinal disturbance, ringing in the ear, liver changes, fever, bronchitis and pneumonitis. Mercury can also be absorbed through inhalation with symptoms similar to ingestion.

Ingestion:

May cause burning of the mouth and pharynx, abdominal pain, vomiting, corrosive ulceration, bloody diarrhea and may be followed by a rapid and weak pulse, shallow breathing, paleness, exhaustion, tremors and collapse. Delayed death may occur from renal failure. Gastrointenstinal (through the stomach) uptake of mercury is less than 5% but its ability to penetrate tissues presents some hazard. Initial symptoms may be thirst, possible abdominal discomfort.

Skin Contact:

Causes irritaton and burns to skin. The symptoms include redness and pain. Skin contact may cause skin allergy and sensitization. Mercury can also be absorbed through the skin with symptoms similar to ingestion.

Eye Contact:

Causes irritation and burns to eyes. The Symptoms include redness, pain, blurred vision and may cause serious and permanent eye damage.

Chronic Exposure:

through any route can produce central nervous system damage. It may cause muscle tremors, personality and behavior changes, memory loss, metallic taste, loosening of the teeth, digestive disorders, skin rashes, brain damage and kidney damage. Chronic exposure can also cause skin allergies and accumulate in the body. Repeated skin contact can cause the skin to turn gray in color. It is a suspected reproductive hazard and may damage the developing fetus and decrease fertility in males and females.

Aggravation of Pre-existing Conditions:

Persons with nervous disorders, or impaired kidney or respiratory function, or a history of allergies or a known sensitization to mercury may be more susceptible to the effects of the substance.

5.4.2 Safety Measures

Organisatorial Measures

- All persons who will work with mercury have to be instructed in emergency procedures and informed about the potential risks and hazards.

- All of the persons working with mercury are known by the TIS (Technical Inspection and Safety) department and the medical service.
- Before starting the work with mercury everyone has to undergo a medical examination.
- All mercury is stored in a locked cupboard in the mercury laboratory and each amount taken out or put back has to be recorded.

Mercury Laboratory

- There are warning signs at the entrance of the laboratory.
- There has been installed a sealed floor.
- The air is continously monitored by a mercury vapor detector (Mercury Instruments VM3000).
- Breathing masks and respirators are available everytime.
- A special mercury vacuum cleaner is available at the fire brigade.

Chapter 6

Simulations

In the following section a few examples of simulations done for mercury injected into a magnetic field and for the interaction of a proton beam with mercury will be presented. In fact there exist many more and there is still a lot of simulation work going on.

6.1 Mercury in Magnetic Field

6.1.1 Peter Thieberger: Approximate behaviour of a conductive cylindrical jet coaxial with a long solenoid.[17]

One of the important issues that needs to be addressed when considering the injection of a fast, liquid-metal jet target into a strong magnetic field are the perturbations of the jet motion and shape due to the presence of large field gradients at the entrance of the solenoid. Lebedev [18] developed simple arguments claiming that the magnetic pinch effect caused by $I \times B$ forces on the induced eddy-currents, when a mercury jet enters such a 20T solenoid, will tend to produce large incremental velocities. The approach followed here is similar, but the results and conclusions are much less pessimistic, and much more in line with the initial estimates [21].

P. Thieberger has used the so called ballistic or impulse approximation in which forces, accelerations and velocities are calculated while displacements are assumed to be negligible during the duration of the interaction. This is the same type of assumption made by others dealing with this problem when they postulate a constant radius for the jet. The interaction time is the length of the fringe field region, divided by the velocity of the jet. Thus, for displacements to be small, the velocities generated in the frame of reference of the incoming jet must be small compared to the jet velocity. If the velocities resulting from the calculation fulfill this condition, then one can rely quantitatively on the results.

Calculation parameters:
Field: $2 \cdot 10^5$Gauß
Solenoid radius: $10cm$
Jet radius: $0,5cm$
Jet velocity: $2000\frac{cm}{s}$
Material: Hg (Density: $13,6g/cm^3$)
Conductivity: $9.10 \cdot 10^{15}[\Omega m]^{-1}$

The result for the accelerations at the core and at the surface of the jet are shown in figure 6.1. The magnetic pinch effect, i.e. the interaction of the eddy currents with the z-component of the field is entirely responsible for the acceleration at the core and the interaction of the eddy currents with the r-component of the fringe field causes the acceleration at the surface. The surface is always decelerated, while the core is decelerated at first and then accelerated after entering the solenoid. This last effect is the result of the radial pressure tending to squeeze out material towards both the front and the back of the jet.

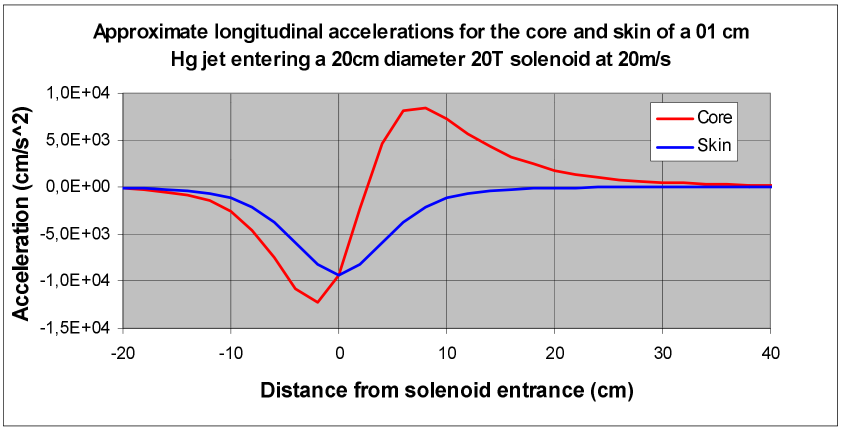

Figure 6.1: Longitudinal Acceleration for the Core and Skin of a Hg Jet Entering a Magnetic Field

Figure 6.2 shows the velocity increments at the core and five radii as functions of the distance from the entrance to the solenoid. The values shown in these curves are independent of the initial jet velocity. This must be so, because the forces are proportional to that velocity and the interaction time is inversely proportional to it. The impulse approximations, which is very good at 20 m/s will become less accurate for much smaller velocities.

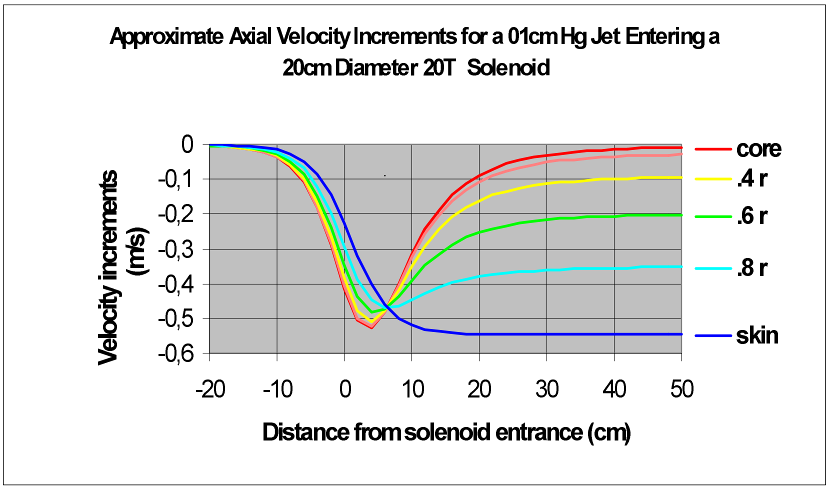

Figure 6.2: Axial Velocity Increment of a Hg Jet Entering a Magnetic Field

The radius of the jet can be evaluated, using average jet velocities computed at each point from the previous six values, properly weighted with their respective cross-sectional areas, and using the fact that the volume-per-second of liquid crossing a plane must be constant for steady-state flow. The result is shown in figure 6.3. We see that in this case there is only a 2.3% variation of the radius, further confirming the validity of the approximations.

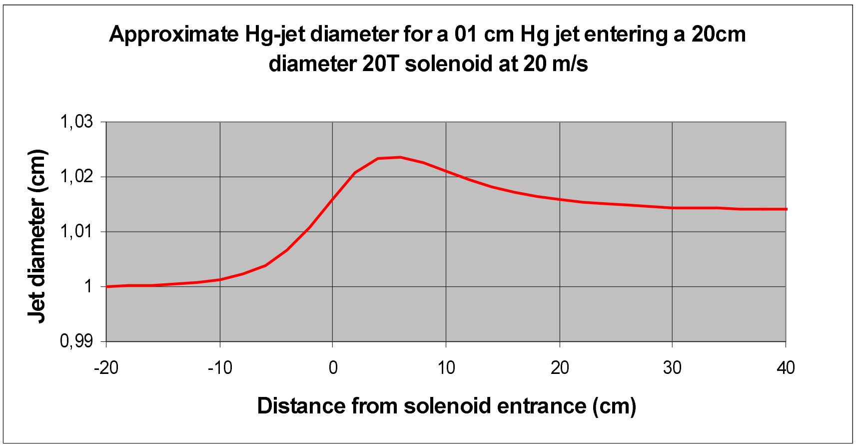

Figure 6.3: Hg Jet Diameter Propagation as a Function of the Position inside the Solenoid

The data of figure 6.2 were used to compute the deformation of an initially flat surface perpendicular to the jet, as the jet enters the solenoid. The result is shown in figure 6.4 where the retardation and deformations are exaggerated by a factor 10 to make them more visible. The grid lines to the right of each surface indicate the position were the surfaces would be in the absence of magnetic effects.

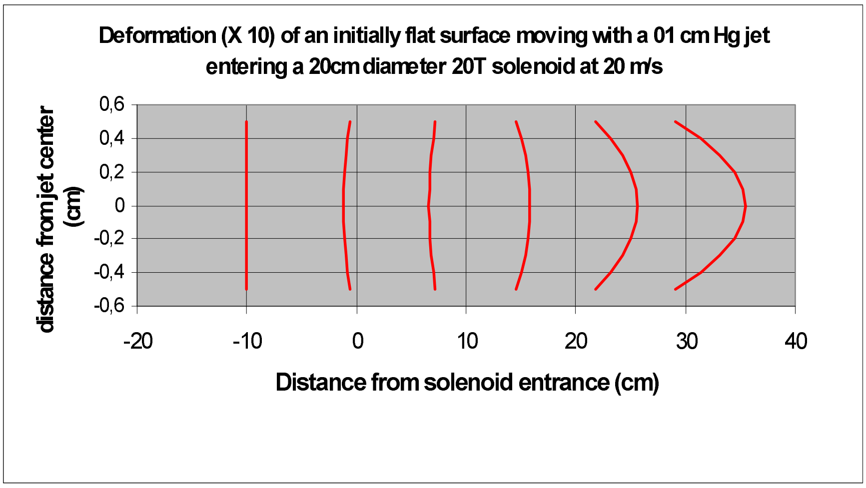

Figure 6.4: Deformation of the Hg Jet Surface when Entering a Magnetic Field

6.1.2 Roman Samulyak (Center for Data Intensive Computing BNL /U.S. Department of Energy): Effects of the Magnetic Field

This very imposing simulation should just give a quantitive impression of what could happen with a mercury jet when injected resp. leaving a 20T magnetic field.

A set of images describing evolution the state of the liquid jet as it enters and leaves the solenoid is depicted in Figure 6.5. The strong nonuniform magnetic field near the solenoid entrance squeezes and distorts the jet. The magnetic field outside the solenoid stretches the jet which results in the jet breakup.

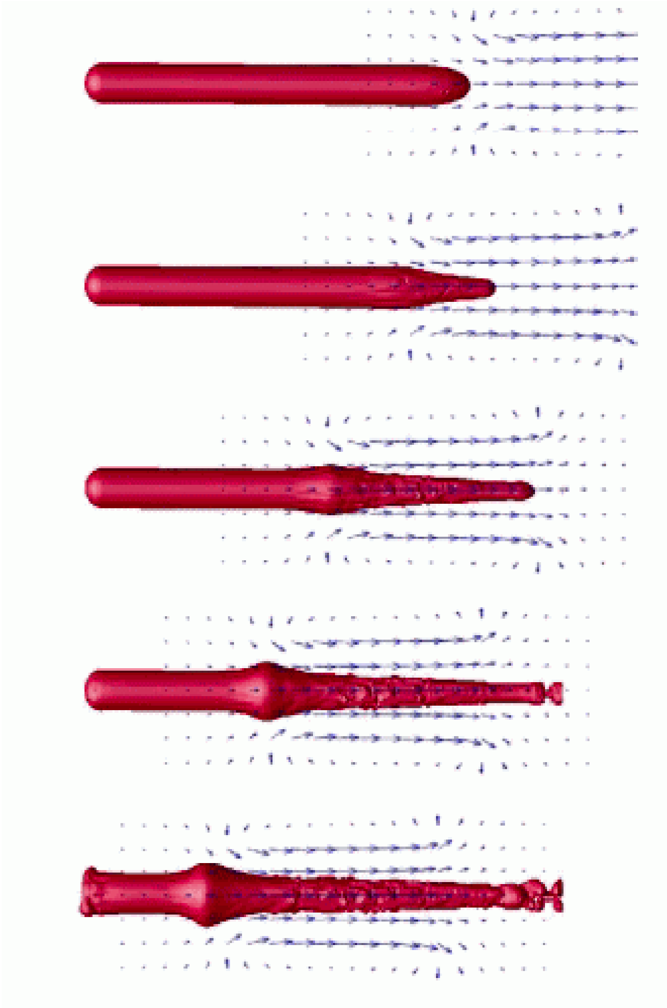

Figure 6.5: Simulation of a conducting fluid entering and leaving a 20T magnetic field

6.2 Interaction with Proton Beam

6.2.1 Roman Samulyak (Center for Data Intensive Computing BNL /U.S. Department of Energy): Effects of Proton Energy Deposition

This simulation has been done using the FronTier code and gives also a nice impression of the evolution of a mercury jet when hit by a proton beam.

The FronTier code was developed to model the propagation of three dimensional fluid jets and is based on front tracking, a numerical method which allows the computation of dynamically evolving interfaces. Surfaces are separating two phases of matter, each of which may be solid, liquid or gaseous. An interface is not a geometric surface but a thin layer that has properties differing from those of the bulk material on either side of the interface. In general, interfaces can model many types of discontinuities in a medium such as shock waves in gas dynamics, boundaries between fluid-gas states, different fluids or their different phases in fluid dynamics, component boundaries in solid dynamics etc. This method often doesn't require highly refined grids and it has no numerical diffusion.

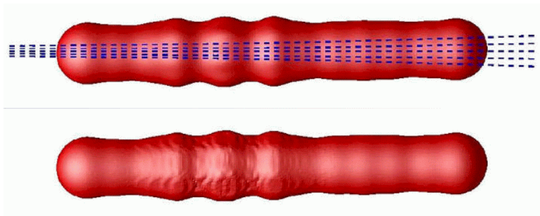

Figure 6.6: Mercury target: evolution after the first proton pulse ($0 - 10\mu s$)

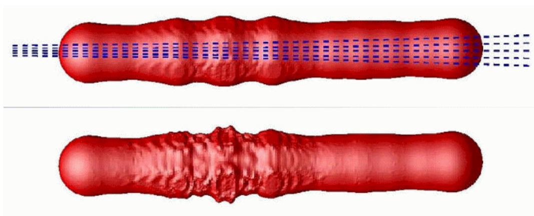

Figure 6.7: Mercury target: evolution after the first proton pulse ($10 - 20\mu s$)

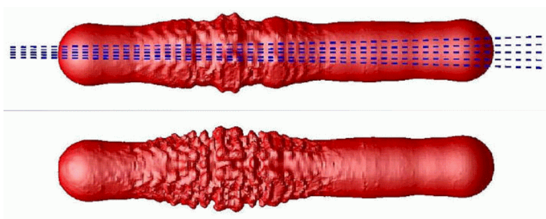

Figure 6.8: Mercury target: evolution after the first proton pulse ($20 - 35\mu s$)

6.2.2 Peter Sievers: Response of Solid and Liquid Targets to High Power Proton Beams for Neutrino Factories. [19]

Among the main issues for pion production in solid or liquid targets for neutrino factories are the evacuation of the average power deposited by the intense proton beam incident on the target and the instantaneously (within a few nano-seconds) deposited energy leading to rapid temperature rises and stresses in the material. In this basic assessment the response of the target material to the rapid heating will be evaluated, assuming material constants independent of temperature and pressure. This study serves to identify relevant parameters and critical areas where non-linear effects become important and where more sophisticated methods and tools have to be applied.

Input Parameters

The following calculations have all been made for mercury as target material.

For the proton beam an average power of 4 MW is considered, incident on the target in short energy pulses (bursts) of 80 kJ/burst each, at 50 Hz. A parabolic radial energy deposition density ρ is assumed, dropping to zero at the outer radius R = 1 cm and being uniform along the target:

$$\rho(r) = \rho_0 \left[1 - (r/R)^2\right] \tag{6.1}$$

$$\rho 0 = 40 J/gr.$$

With this assumption about 25% of the incident energy remains in the considered target of 2 cm diameter and 25 cm length.

First Order Approximations

Converting the peak energy density per burst into an instantaneous temperature rise along the center of the target, yields:

$$\Delta T = 286 K \tag{6.2}$$

Now, since the rise time of the temperature is of the same order of magnitude as the deposition of the beam energy, which is 10^{-9} s, thermal expansion is initially prevented by the mass inertia of the material. The resulting instantaneous pressure (P) rise at time t = 0 is given by:

$$\Delta P(r) = \frac{\alpha_V \Delta T(r)}{\kappa} \tag{6.3}$$

where α_V is the volume thermal expansion coefficient and κ is the compressibility.

For the above parameters this yields along the center:

$$\Delta P_0 = 1150MPa \tag{6.4}$$

Assuming now linear elastic behaviour of the target, the instantaneously pressurized material will start to oscillate since at time zero it is not in its equilibrium position. This can readily be compared to a pendulum for which the location of its "equilibrium" suspension is instantaneously be shifted. If this shift occurs slower and within times comparable to the pendulum frequency, its oscillation amplitude will be smaller, and if this shift occurs very slowly it will not oscillate at all. The latter case corresponds to a "slow" heating with "quasi-static" thermal expansion.

Note that the response of material to rapid heating is different from that induced by the impact of a supersonic bullet which actually displaces material radially with supersonic velocity along its path. This would be equivalent to displacing the mass of the pendulum with supersonic speed which is different from displacing rapidly its equilibrium suspension.

For liquid targets it is relevant to assess the energy E_c stored in the material due to the initially prevented thermal expansion of the target as this might be converted into kinetic energy ripping the liquid apart. The energy density dE_C/dV is given by:

$$dE_C/dV = \frac{(\alpha_V \Delta T(r))^2}{2\kappa} \tag{6.5}$$

By integration over the volume, the total energy E_C , convertible to velocity for the assumed Hg-target with a length of 25 cm is about

$$E_C = 780J/pulse \tag{6.6}$$

and the "average" kinetic power, W_c to be handled in the vicinity around this "exploding" liquid is

$$W_C = 39kW \tag{6.7}$$

This is with the assumed parameters about 4 % of the total deposited power.

The order of magnitude of the velocity with which the boundary of the liquid target material can explode in radial direction is simply given by the radial, thermal expansion at the boundary divided by the time over which the sound travels across the radius of the target:

$$\overline{v}/c \approx \alpha_V \Delta T_0/4 \tag{6.8}$$

$$c...velocity\ of\ sound$$

This estimate yields for the considered cases that the material velocities during oscillations or at explosion are only of the order of a percent of the sound velocity. As a consequence one may believe that supersonic shock phenomena are not yet relevant at the above-assumed parameters. Still, the problem is unsolved whether the liquid will explode once the pressure turns to negative during its oscillation, rather than sustaining negative pressures and continuing to oscillate, as one may expect for solids.

The involved frequencies of the radial oscillations are of the order of

$$f_R = c/4R \tag{6.9}$$

With the sound velocity of 1.3 km/s for Hg respectively this yields

$$fR \approx 32kHz \tag{6.10}$$

which is within the ultra-sound region.

Results

Fig. 6.9 and Fig. 6.10 show the pressure and the material velocity respectively vs. radius at different times. The pressure is given in units of $\alpha_V \Delta T_0/\kappa$, the velocity in units of $c\ \alpha_V \Delta T_0$, the radius in units of R and the time parameters in R/c. These plots are generally valid for any material constants with a parabolic energy deposition density. Fig. 6.11 and Fig. 6.12 show the pressure at r = 0 and the material velocity at r = R respectively vs. time. At times $\theta > 0.74$ (t > 5.7 μs for Hg) the pressure becomes negative, i.e. as of this instant cavitation (brake-up) of the liquid may occur and all subsequent pressure and velocity profiles are no longer valid. However, as can be seen in Fig. 6.12 the maximum velocity at the boundary is reached at the same time. Thus, in case of immediate cavitation for P<0 the material will fly off at the rim with a velocity of

$$\widehat{v}/c = 0.54\alpha_V \Delta T_0 \tag{6.11}$$

or

$$\widehat{v} = 36m/s \tag{6.12}$$

which is about double the value estimated in 6.8. This may be explained by the fact that there the average velocity is given while here the peak velocity is quoted. For illustration, a Hg-droplet flying off vertically with this velocity will ideally reach a maximum height of 65 m.

Again the central pressure and the velocity at the boundary are reduced by extending the time of heating as illustrated in Fig. 6.11 and Fig.6.12.

As can be seen from the above considerations the pressure and the material velocity both depend on the compressibility like

$$P \sim 1/\kappa \tag{6.13}$$

and

$$v \sim 1/\sqrt{\kappa} \tag{6.14}$$

Thus increasing the compressibility would have a beneficial effect. Indeed, liquid metals "loaded" with bubbles or liquid jets made of micro-droplets have been suggested which could substantially change the response of liquid targets modified in such a way.

As one can see from Fig. 6.12 the material at the boundary of the target moves radially similar to a harmonic oscillator. Since it is envisaged to place the Hg-target inside a solenoid with an axial magnetic field of 20 T one can estimate the change of the oscillation, associating it with an oscillator, magnetically damped by a term proportional to its velocity. The damping time δ is

$$\delta = 2\rho/\varepsilon B_Z^2 \tag{6.15}$$

$\varepsilon ...electrical\ conductivity\ of\ Hg$
$B_z ...magn.\ Field\ (20T)$
$\rho ...density\ of\ Hg$

Putting in the numbers, this yields:

$$\delta \approx 67\mu s \tag{6.16}$$

Since this is large compared to the time $t \approx 5.7\mu s$ to reach the first peak of velocity, damping can be neglected for the first oscillations, i.e. the velocities displayed in Fig. 6.12 over the first 20 μs will not be reduced significantly and, if the material brakes up at P<0 it will fly off at the velocity estimated above.

Still, these results must be considered as somewhat pessimistic, since nevertheless some internal friction and braking will occur due to surface tension and viscosity of the liquid. It may however be expected that these effects are even smaller than the magnetic friction.

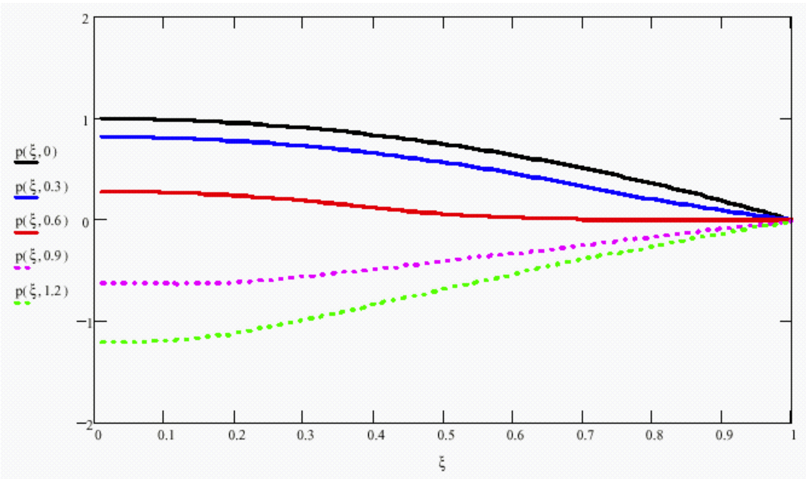

Figure 6.9: Pressure (in relative units) vs. radial position ξ (in units of R) in a liquid target at different times θ (in relative units of R/c) of 0, 0.3, 0.6, 0.9 and 1.2.

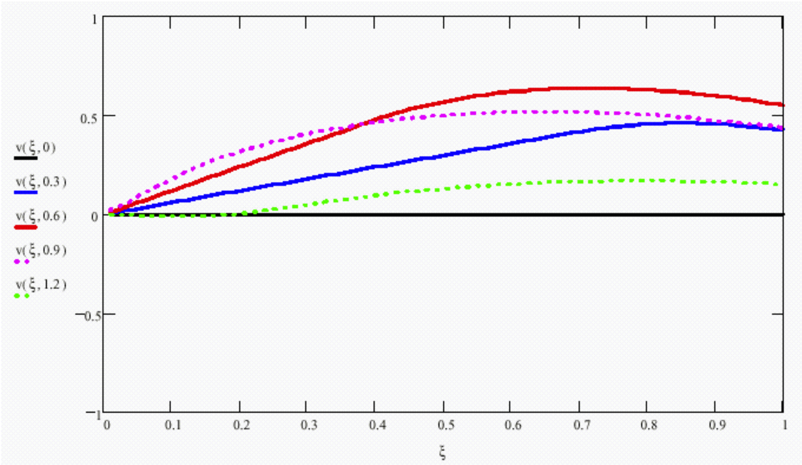

Figure 6.10: Material velocity (in relative units) vs. radial position ξ (in units of R) in a liquid target at different times θ of 0, 0.3, 0.6, 0.9 and 1.2 (è in units of R/c).

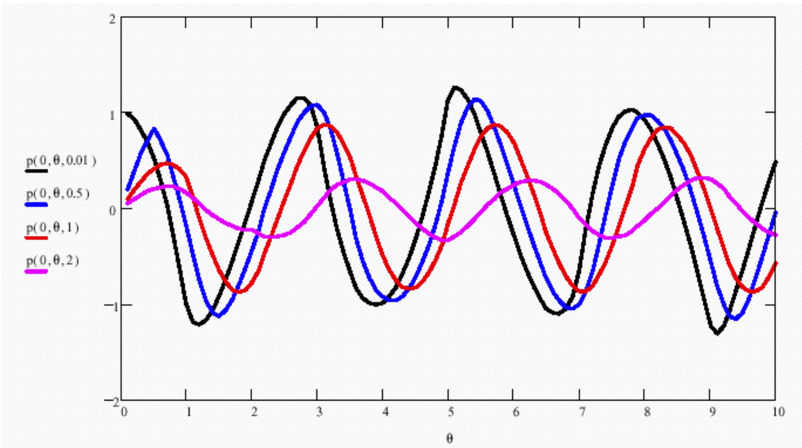

Figure 6.11: Pressure (in relative units) vs. time θ (in units of R/c) in the center of the liquid target. In addition to infinitely fast heating with , $\theta_0 = 0$ oscillations are shown for slower heating over the durations $\theta_0 = 0.5$,1 and 2

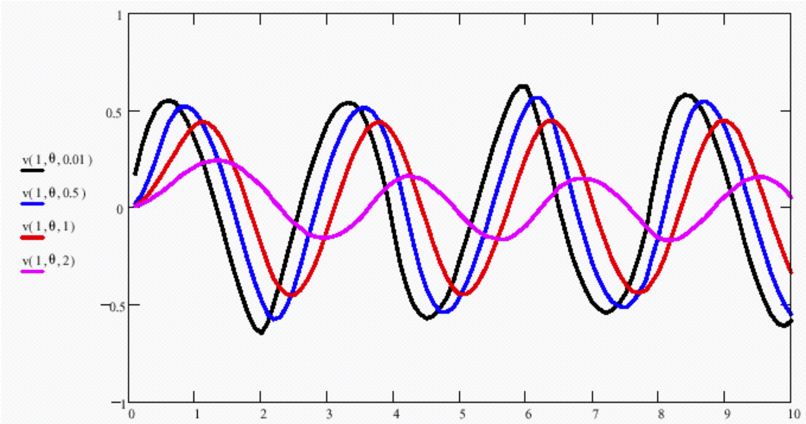

Figure 6.12: Material velocity (in relative units) vs. time θ (in units of R/c) at the outer radius of the liquid target. In addition to infinitely fast heating with , $\theta_0 = 0$, oscillations are shown for slower heating over the durations $\theta_0 = 0.5$,1 and 2

Conclusion

As a pessimistic assumption for liquid targets, cavitation may set in as soon as the pressure becomes negative in the target which is about 6 μs after the proton burst. Whether this starts in the center where the largest depression occurs first or close to the boundary where at moderate negative pressures the highest velocities arise, cannot be answered by this classical assessment. The strong magnetic field of 20 T of the solenoid around the target will not damp significantly the initial velocity of the target material vibrating or, in the case of cavitation (see 6.2.4), exploding in radial direction.

Material Constants

Material constants for mercury used for the calculations:

Density:	$\rho = 13.5 \cdot 10^3 kg/m^3$
Compressibility:	$\kappa = 0.45 \cdot 10^{-10} m^2/N$
Volume Thermal Expansion Coefficient:	$\alpha V = 18.1 \cdot 10^{-5} K^{-1}$
Specific Heat:	$c_V = 140 J/kgK$
Velocity of Sound:	$c = 1/\sqrt{\kappa\rho} = 1.3 km/s$
Electrical Conductivity:	$\varepsilon = 10^6 \, [\Omega m]^{-1}$

6.2.3 Stresses on the ESS target enclousure by thermal shock waves

At the research center in Jülich there exists a ESS (European Spallation Source) target mock up, which also contains mercury. This target consists of a stainless steel vessel containing the mercury.

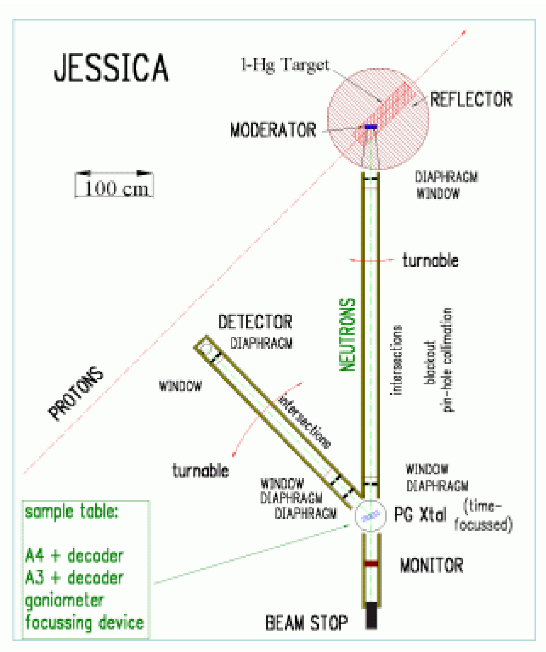

Figure 6.13: Sketch of JESSICA (Forschungszentrum Jülich)

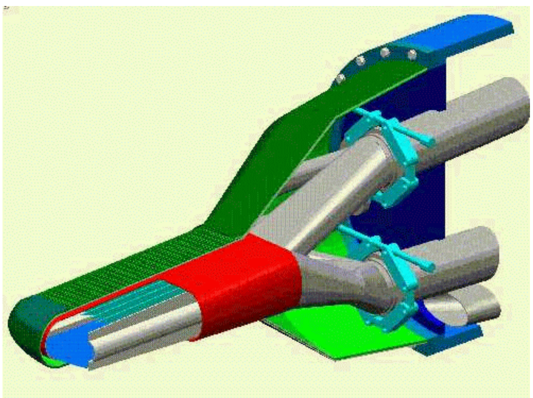

Figure 6.14: ESS Mercury Target Unit (overall length: 1300 mm)

The main diference between the ESS- and the Neutrino Factory-target is that the mercury in the ESS-target is enclosed inside a stainless steel housing (Fig. 6.14), while the Neutrino Factory-target most likely will be a free mercury jet.

Nevertheless the knowledge gained there about the rsponse of mercury to the interaction with a proton beam can be very usefull for the Neutrino Factory target development.

Figure 6.15: The JESSICA facility: proton beam line (from top centre), reflector vessel with target and moderator and primary neutron flight path (between reflector vessel and black detector box) (Forschungszentrum Jülich)

Figure 6.16: JESSICA target housing containing the mercury (Forschungszentrum Jülich)

The scientists and engineers at the research center in Jülich have made some calculations of the stresses by the thermal shock waves.

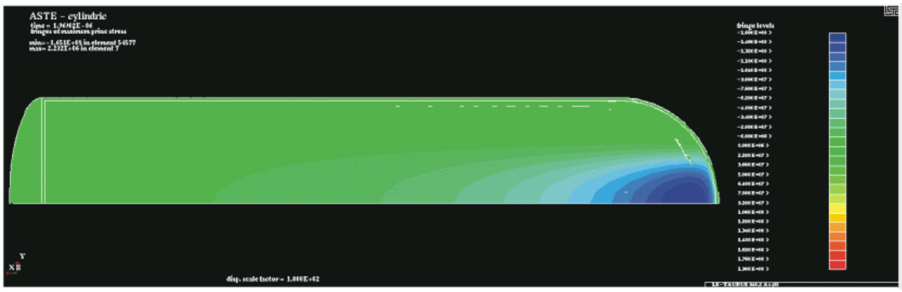

Figure 6.17: Target enclosure stress 2 μs after p-beam impact

As one can see in Fig. 6.17 (the figure symbolizes a cut-view and the upper half-part of the mercury enclosure; beam window on the right side), immediately after the proton beam impact a point of negative pressure arises. A few microseconds later, this negative pressure region builds most likely cavitation (see 6.2.4) and the result is a point of very high pressure. A shock wave travels through the mercury and displaces (bends) the wall of the target enclosure.

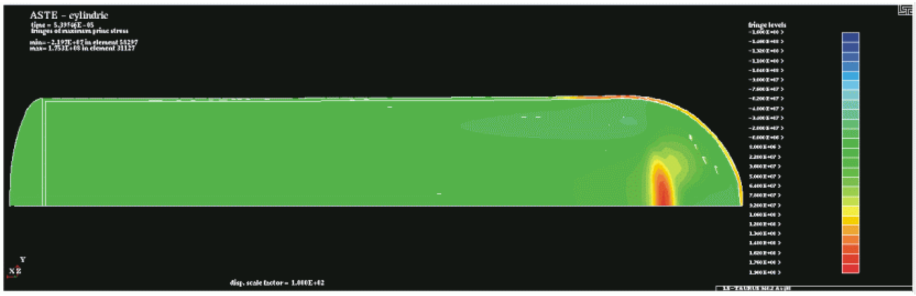

Figure 6.18: Target enclosure stress 54 μs after p-beam impact

This simulation shows also (see 6.2.2), that a negative pressure due to the proton beam impact is possible, and as a consequence cavitation occurs.

6.2.4 Negative Pressure - Cavitation

Cavitation, the formation of bubbles, is a familiar phenomenon. Whenever a liquid is agitated violently, there is a possibility that cavitation will occur (see, for example, figure 6.19). In the case of boat propellers or hydraulic machines, cavitation is a problem that engineers try to avoid. In other contexts, however, cavitation can be useful as, for example, in ultrasonic cleaning devices. Desirable or not, cavitation is a complex phenomenon because inhomogeneities in the liquidsuch as walls, dissolved gases, vortices, and impurities usually play a major role in the nucleation of bubbles. As a consequence, our understanding of cavitation is incomplete. To make some progress, research groups at Brown University in Providence (Rhode Island), at the National center for Scientific research and at the Ecole Normale Superieure in Paris, have examined cavitation in superfluid helium, a simple and pure liquid. It is the coldest liquid in nature and exists only at temperatures near absolute zero, where every other liquid is frozen. It can therefore be filtered very efficiently and prepared without impurities.

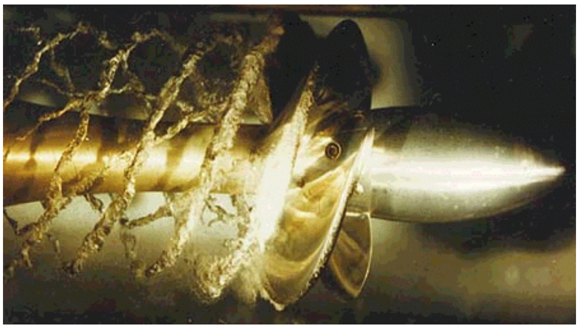

Figure 6.19: Vortex lines are generated at the edge of boat propellers in motion. (DGADCE, Bassin des Carenes, Paris)

Toward the core of the vortices, the liquid velocity increases and the pressure decreases. The lower pressure triggers cavitation, and the resulting bubbles produce noise, vibrations, and erosion of the propellers.

How a liquid "breaks"

Measuring the tensile strength of a solid involves applying an increasing stress until the solid breaks. The study of cavitation in liquids follows a similar path. Suppose that some water is put into a cylinder that is sealed with a piston. If the piston is above the water and has a weight placed on top of it, the water will be under a positive pressure. The pressure will be equal to the weight divided by the cross-sectional area of the cylinder. But if the apparatus is turned upside down and a weight hung from the piston, what happens? The correct answer depends critically on some details of the situation that we have not yet specified. If there is an air bubble in the water above the piston, then when the weight pulls on the piston, the bubble will grow and the piston will fall. If there is no air bubble and the weight is small, the piston will move down a short distance but soon come to rest. In that equilibrium position, the force exerted by the weight is balanced by a force that the water exerts. The water is thus under negative pressure that is, under positive stress. If there is no air bubble and the weight is heavy enough, then the piston will move down, the water will be stretched, and eventually a bubble will spontaneously appear within the liquid or possibly on the wall of the container.

At low pressure P, the equation of state for air (or any other gas) is the well-known ideal-gas law. As P decreases toward zero, the volume V varies as the inverse of the pressure. Consequently, when an air bubble is present in the water, the size of the bubble grows without limit as soon as the weight pulls on the piston. But what happens when there is no bubble and the water is able to stay in a state of tension? This state is only metastable: If a bubble forms, the piston will be able to move, and that movement will clearly lower the potential energy of the system. Before a large bubble can be formed, however, the system has to overcome an energy barrier.

The existence of an energy barrier against nucleation is very general. The barrier arises because the liquid-gas transition is discontinuous, or first order. Such a barrier exists for any first order transition because the interface between the two phases has a finite energy per unit area. In our example, this energy is nothing but the surface tension α of water. Since α is nonzero, the formation of a bubble with radius R has an energy cost of $4\pi R^2\alpha$. When such a bubble forms, the energy of the whole system also contains the work of the negative pressure over the bubble volume, so that the total energy cost of forming the bubble is

$$\Delta E = 4\pi R^2\alpha + \frac{4\pi}{3}R^3 P \tag{6.17}$$

At negative pressures, this energy has a maximum for a critical radius $R_C = 2\alpha/|P|$. The energy at this radius establishes the energy barrier (see figure 6.20) at

$$\Delta E = \frac{16\pi\alpha^3}{3P^2} \tag{6.18}$$

A thermal fluctuation may enable the system to pass over the energy barrier. The probability of such an occurrence is proportional to the factor

$$\exp(-\Delta E/kT), \tag{6.19}$$

where T is the absolute temperature and k is Boltzmanns constant. In this simplified model, it is clear that cavitation should be a random process that depends on temperature. This discussion of the energy required to form a bubble is inadequate in one very important respect. Equation 6.19 says that to maintain a given probability that nucleation will take place, the ratio of the energy barrier ΔE to kT must have a particular value; this requirement would lead to the conclusion that as the temperature decreases, the pressure at which nucleation occurs should diverge as $T^{-1/2}$. But such reasoning ignores the obvious fact that there is an upper limit to the force one molecule in a liquid can exert on another, so that for some negative pressure of finite magnitude, the liquid will stretch without limit (that is, the compressibility will become infinite). The pressure at which that happens is called the spinodal limit. When it is reached, the sound velocity becomes zero and the barrier to nucleation vanishes.

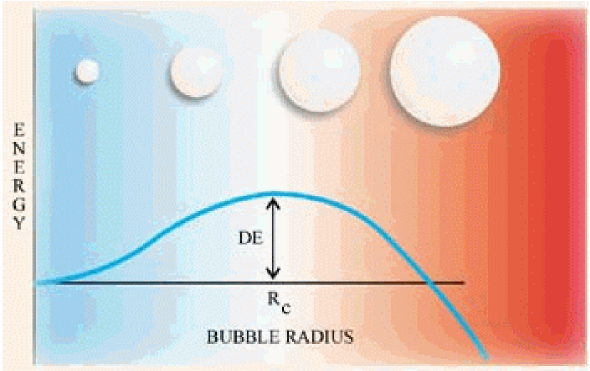

Figure 6.20: Energy of a small bubble in a liquid under negative pressure, as a function of bubble radius

For small bubbles, the energy increases with radius because the surface energy makes the largest contribution to the energy. Above a critical radius R_C, the energy begins to decrease because of the negative energy associated with the work done by the applied negative pressure. When its radius reaches R_C, a bubble can grow without limit. Thus, the liquid "breaks".

Given these considerations, one can see that if the applied pressure is only slightly negative, the energy barrier is very large and the chance that a bubble will form is very small. Then the liquid can exist in a state of negative pressure for a long time - but only if the liquid is very clean. If the liquid contains dirt or dissolved gas, the formation of bubbles is usually much likelier. Bubbles also tend to form preferentially on the walls of a container. Bubble production associated with walls or impurities is called heterogeneous nucleation - as distinguished from homogeneous nucleation, which takes place within the volume of an ideal bulk liquid and is an intrinsic property of the liquid.

Chapter 7

Experiments and Results

7.1 Overview

Two main types of experiments were proposed to be done. One experiment is the investigation of the behavior of a liquid metal (mercury) injected into a magnetic field, while the second experiment is to shot a proton beam onto mercury to observe the effects of the thermal shock induced by the energy deposition in the material.

Before any experiment with a mercury jet can be performed, an apparatus to establish a jet has to be developed, built and tested. And as there exists no similar apparatus and also no basic knowledge about establishing a stable mercury jet, to build such an apparatus can be seen as a own experiment, which, by the way, was one of the most challenging tasks.

The following tabe represents and overview of all scheduled experiments.

Exp. No	Experiment Type	Individual Experiment	Remarks
1.0	*Establishing a mercury jet*	study jet at different velocities, testing camera and illumination	
1.1		calibration, measurements without magnetic field	horizontal and tilted jet
2.0	*Mercury jet in magnetic field*	injection into 1.3T solenoid / CERN	horizontal jet
2.1		injection into 13T solenoid / GHMFL	vertical jet
2.2		injection into 20T solenoid / GHMFL	Postponed
3.0	*Mercury in proton beam*	mercury at rest / BNL	
3.1		mercury jet / BNL	
3.2		mercury at rest / CERN (ISOLDE)	Postponed

Table 7.1: List of single experiments

7.1.1 Experiment Series 1

The first task -or experiment- in the pool of all experiments was to produce a pulsed mercury jet. The following sketch (figure 7.1) shows how this problem was solved. To produce a pulsed mercury jet, the mercury is put under pressure via a pressure increasing device. This device (piston pump) converts an air pressure into a pressure on the mercury, which is 16 times higher. The high pressure mercury is lead through a valve into the nozzle and from the nozzle escapes a pulsed mercury jet. A detailed description of the setup can be found in chapter 7.4.

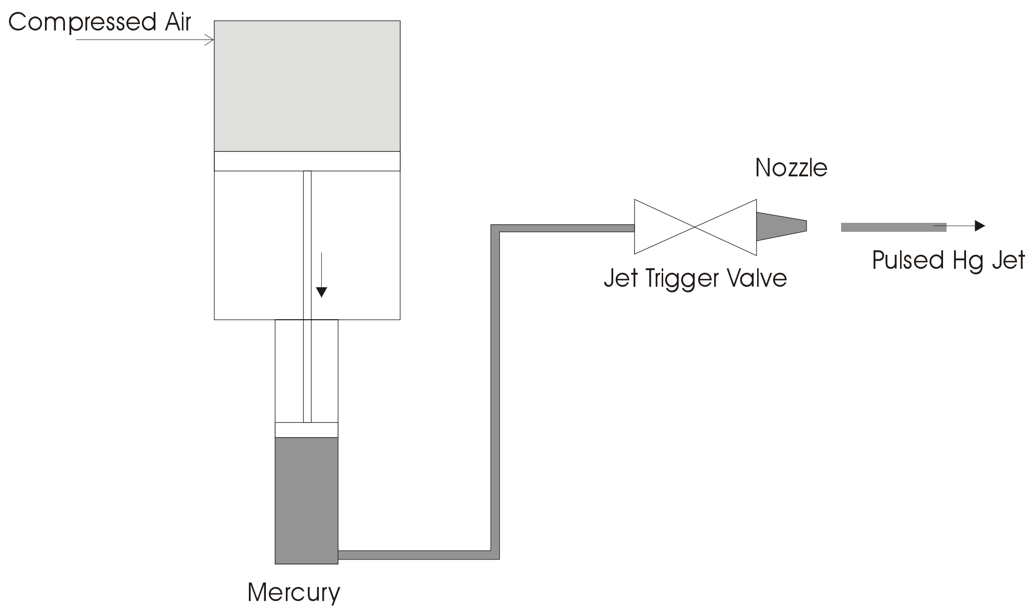

Figure 7.1: Principal Sketch - Mercury Jet Production

7.1.2 Experiment Series 2

The next experiment series deales with the injection of a mercury jet into a magnetic field. The function overview of the experiment 2.0 (injection into a horizontal magnet) can be seen in figure 7.2.

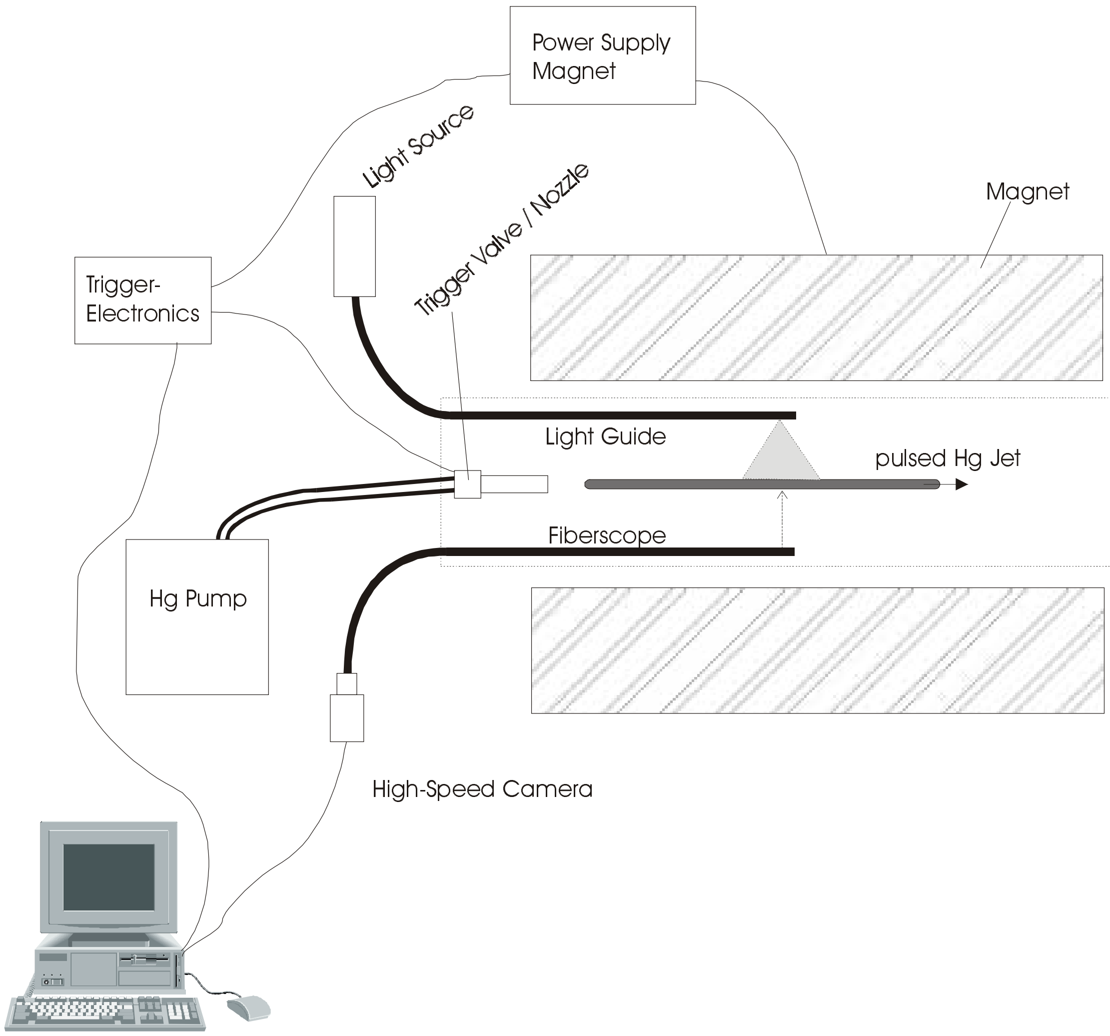

Figure 7.2: Pricipal Sketch - Hg Jet Injected into Horizontal Magnet

Figure 7.3 shows the principle of experiments 2.1 and 2.2 (injection into a vertical magnet). Detailed descriptions of these experiments are in chapter 7.7 and 7.8.

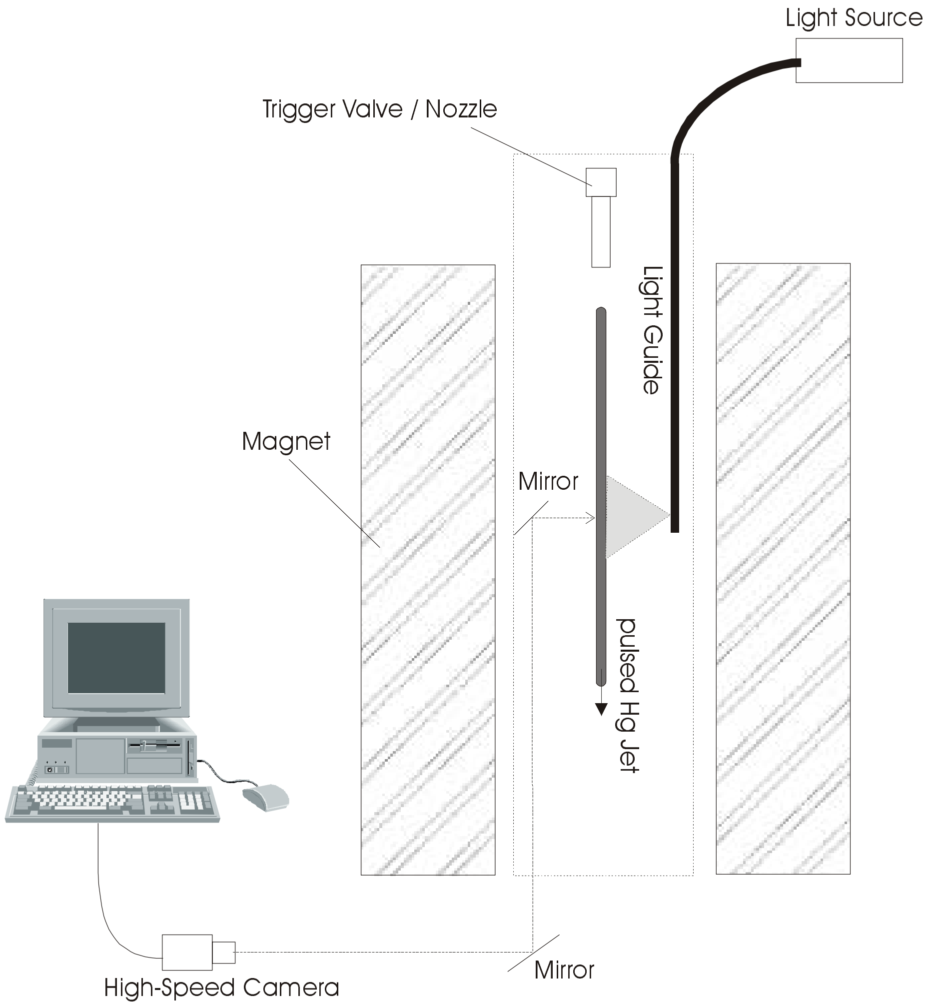

Figure 7.3: Principal Sketch - Hg Jet Injected into Vetical Magnet

7.1.3 Experiment Series 3

Experiment 3.1 comprises the collision of a proton beam with a small amount of mercury. The mercury is held in a "thimble" or through drilled into a stainless steel plate. Figure 7.4 shows a sketch of the experiment setup.

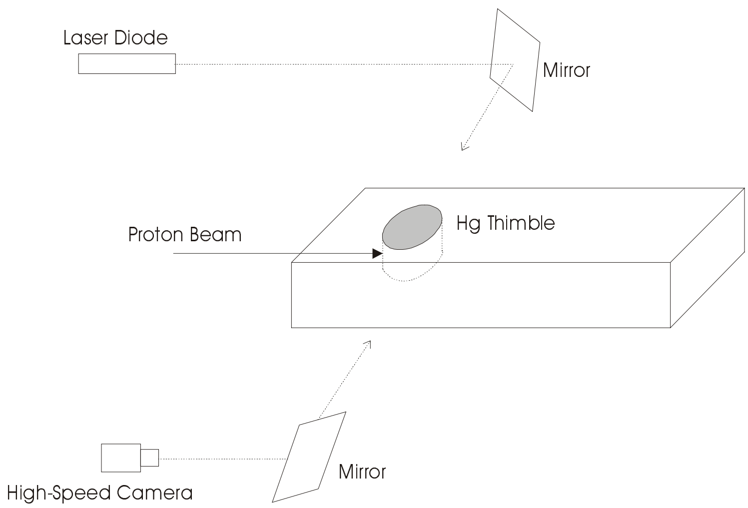

Figure 7.4: Principal Sketch - Mercury at Rest in Proton Beam

The Collision of a proton beam with a mercury jet is the experiment 3.2. The pricipal sketch is the Figure 7.1. For detailed descriptions see chapter 7.9 and 7.10.

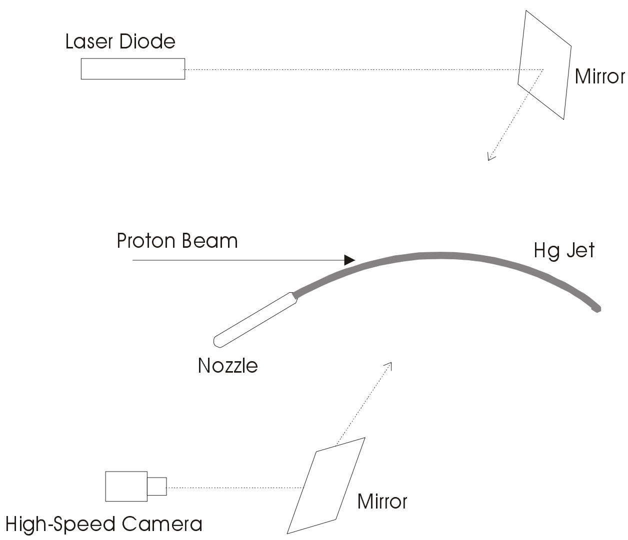

Figure 7.5: Principal Sketch - Hg Jet in Proton Beam

7.2 Purpose

Many calculations and simulations of the reaction of a liquid metal to a proton beam pulse or a magnetic field have already been made. Some of these simulations showing very different results and one can not guarantee that they corespond to the reality because there exists no knowledge obtained by any experiments. Therefore the results of the experimental investigations should be used as a benchmark for the simulations. Also some of the parameters are very difficult or even impossible to calculate.

7.3 Observation Equipment

7.3.1 High Speed Camera System

In order to observe the response of the mercury to magnetic field, a high-speed camera system will be used to record the mercury when injected into the magnetic field. The resulting slow-motion videos can then be used to calculate parameters like the acceleration (or decceleration) of the mercury jet or deformation of the jet shape. But they are also useful to "see" what happens, to get a qualitative picture of the process. The same system will be used for the In-Beam experiment.

For some of the experiments the high-speed camera system Olympus Encore Mac PCI, which is able to record at up to 8.000 fps, has been used. This system consists of the camera head with the CCD-sensor (low-light version) connected to a PCI-card, which is installed in an industrial PC. The system software allows besides setting up the recording speed and shutter time also to make measurements like acceleration and velocity.

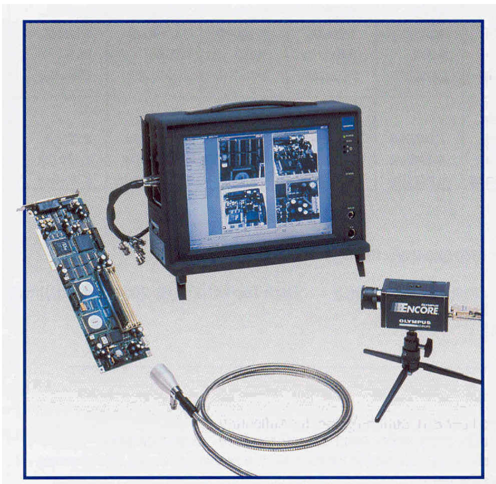

Figure 7.6: Olympus Encore High-Speed Camera System (Olympus Europe)

Measuring Capabilities

The fastest movements will be in the proton beam experiments. As the estimated perpendicular velocity of the droplets when the mercury jet is hit by the proton beam is in the order of up to 50 m/s, it is possible to measure the speed of the escaping drops at 4.000 frames/s with a field of view of minimum 12,5 mm (ref. 7.1).

$$\frac{50m/s}{4000fps} \Rightarrow 12,5mm/frame \tag{7.1}$$

Respective twice this area if the first picture is taken when the droplet is already somewhere in the field of view.

The resolution of the optical sensor at 4000 fps is 100 x 98 pixel. If the field of view is 50 mm x 50 mm, the accuracy of the measurements is 0,5 mm in horizontal and in vertical direction. What means, the resolution of the measurement of the velocity is 0.125 m/s (ref. 7.2).

$$\frac{0,5mm}{4ms} = 0,125\frac{m}{s} \tag{7.2}$$

4.000 fps was chosen for this example calculation because previous tests have shown that recording at this speed is possible with a reasonable expenditure of illumination.

General Specifications

Sensor Array	658x496 pixels, each pixel 7.4 microns square
Image Resolution	up to 480x420 pixels
Recording Rates	60, 125, 250, 500, 1000, 2000, 4000, 8000 fps
Shutter Speed	1/60th sec. to 10 µs
Frame Storage	16.384 frames
Playback Rates	1, 2, 3, 4, 5, 10, 15, 25, 30, 50, 60, 125, 500, 1000, 2000, 4000, 8000 fps, forward and reverse
External Connections	Trigger, Strobe, Data Record, Video Out and Phase Lock In-Out
Trigger Input	Standard TTL signal, up tp 30 Volts DC. BNC connector
Video Output	RS-170 NTSC and PAL. BNC connector
Data Recording	2 TTL inputs. 2 BNC connectors
Strobe Output	TTL impulse normally low, goes high during exposure. BNC connector
Lens	Standard C-mount
Camera Size	6.2cm H x 6.2 cm W x 10cm L
Camera Weight	0.7kg
Operating Environment	-18°C to 40°C

Table 7.2: Specifications Olympus Encore High-Speed Camera

Camera Head

The camera head is a 6.2cm x 6.2 cm x 10cm enclosure that contains a CCD sensor and imaging circuits. The camera head accepts any c-mount lens. The enclosure has a 1/4-20 and a 3/8-16 threaded hole in the top and bottom of the enclosure to mount the camera head onto a tripod or other fixed mount. There are no controls or indicators on the camera head. A coarse adjustment ring in the lens mount allows to adjust the back focus of the lens.

Shutter Speed / Exposure Time

The Table 7.3 gives exposure times for the shutter speeds at different record frame rates.

Frames/Sec.	60	125	250	500	1,000	2,000	4000	8000
Shutter Speed	1X							
Exposure (sec)	1/60th	1/125th	1/250th	1/500th	1/1,000th	1/2,000th	1/4,000th	1/8,000th
Shutter Speed	2X							
Exposure (sec)	1/120th	1/250th	1/500th	1/1,000th	1/2,000th	1/4,000th	1/8,000th	1/16,000th
Shutter Speed	3X							
Exposure (sec)	1/180th	1/375th	1/750th	1/1,500th	1/3,000th	1/6,000th	1/12,000th	1/24,000th
Shutter Speed	4X							
Exposure (sec)	1/240th	1/500th	1/1,000th	1/2,000th	1/4,000th	1/8,000th	1/16,000th	1/32,000th
Shutter Speed	5X							
Exposure (sec)	1/300th	1/625th	1/1,250th	1/2,500th	1/5,000th	1/10,000th	1/20,000th	1/40,000th
Shutter Speed	10X							
Exposure (sec)	1/600th	1/1,250th	1/2,500th	1/5,000th	1/10,000th	1/20,000th	1/40,000th	1/80,000th
Shutter Speed	20X							
Exposure (sec)	1/1,200th	1/2,500th	1/5,000th	1/10,000	1/20,000th	1/40,000th	1/80,000th	N/A

Table 7.3: Exposure Times for Shutter Speeds and Frame Rates

Light Value Requirements

The exposure of each frame is reduced at the higher frame rates. So more illumination is required as the frame rate increases. The camera head imager must receive enough light to see details of the image, and recorde the subject at the optimum size so that the significant parts of the motion can be seen clearly. The standard camera has an infrared filter to give subjects the correct gray scale appearance. The low-light camera option does not have the IR filter, which increases the sensitivity of the system at low light levels. Table 7.4 gives minimum incadescent (tungsten) light requirements for the standard and low-light camera at a 1x shutter setting.

	Standard Camera	**Low-Light Camera Option**
Frame Rate [fps]	**LUX Value**	**LUX Value**
60	1.03	0.10
250	4.3	0.43
500	8.6	0.86
1000	17.2	1.72
2000	34.4	3.44
4000	68.8	6.88
8000	137.6	13.76

Table 7.4: Light Value Requirements for the High-Speed Camera

Imager Responsivity

The camera has a TC237 (monochrome) CCD imager installed. The imaging sensor has an imaging area of 658x496 pixels, each pixel being 7.4 microns square. The imager has an integration time of 16.67 ms.

Imager Base Characteristics Figure 7.7 gives the responsivity and sensitivity of the TC237 CCD imager across the range of visible light without a filter.

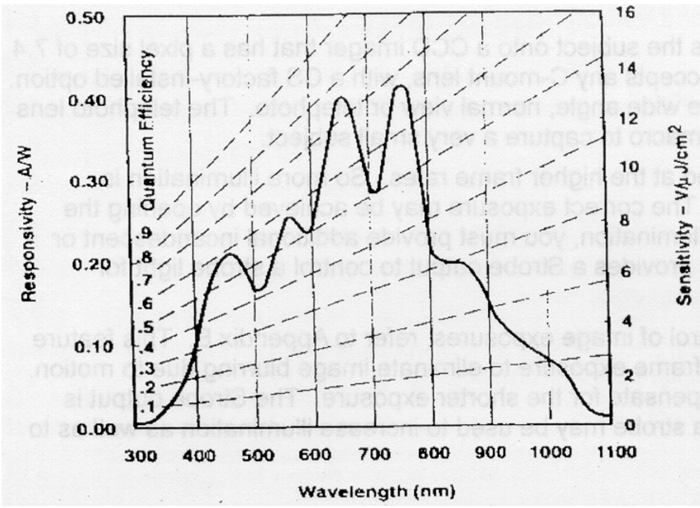

Figure 7.7: Spectral Characteristics of the TC237 Sensor

Data Record Inputs

The PCI card shipped with the camera is equiped with two data recording inputs. Each provides a square marker at the top left corner of the monitor to identify a specific frame. Normally each input is held to a high TTL level, and the marker appears as a white square. A contact closure to ground pulls the input to 0 volts and turns the marker black. With this feature it is possible to determine when a specific event occurs. In that way one can determine at what time an event occured when the marker turns black in the recorded video.

Trigger Input

The trigger circuit on the controller board supplies a +5 volt level to the trigger connector by a 6.8K pull-up resistor, see fig. **??**. The microprocessor monitors the trig-in lead and detects when a trigger signal is transmitted from an external source to the trigger input. A signal from an external source when the system is recording stops the record sequence at a point determined by the trigger point setting.

7.3.2 Illumination

As described in the previous section, a huge amount of light is necessary for high-speed imaging. But it is not possible to place big lights at the experimental setup. So liquid light-guides were used to direct the light to the place were needed. To produce the light two Olympus industrial light sources ILK-6 were available. This unit is fitted with a 150W quartz halogen lamp. Light output is controlled by opening or closing a shutter within the light source. In addition a halogen lamp with either a 650W or a 1250W light bulb was used.

Quantity	**Equipment**	**Description**
2	ILK-6 light source	150W halogen light source for light-guides
2	liquid light-guide 3m	
2	liquid light-guide 2.5m	
2	light-guide connector	to connect two lightguides
2	light-guide lens	with adjustable focus
1	halogen lamp	with 650W and 1250W light bulb

Table 7.5: Illumination Equipment

7.3.3 Fiberscope

To be able to take pictures inside a solenoid or in high radiation areas, a fiberscope as well as a mirror system was used. To find a suitable fiberscope was one of the most time consuming work. A fiberscope is used in medicinal and engineering applications to get images of objects for example inside the human body or machines and other constructions like aviation engines. It guides the light reflected from the object through an objective located at the tip of the fiberscope and glas fibers to the eye piece where an image of the object can be observed.

External light is guided through a different pair of fibers to the so called distal end of the fiberscope to illuminate the object to be observed (for illustration see figure 7.8).

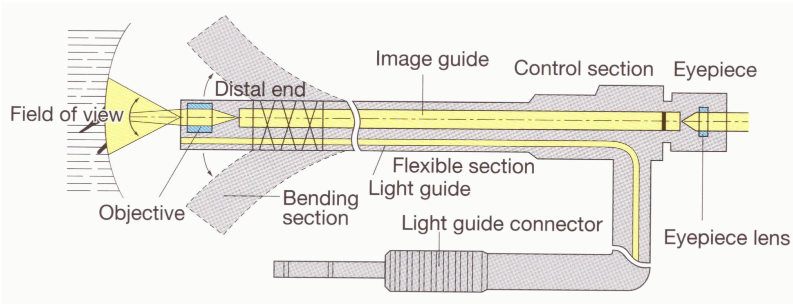

Figure 7.8: Structural drawing Olympus fiberscope (Olympus Europe)

The distal end can be moved (bended) via a remote control at the eye piece end (see figure 7.9).

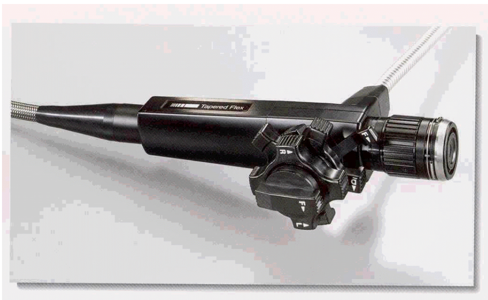

Figure 7.9: Olympus fiberscope remote control and eyepiece (Olympus Europe)

The specification of the needed fiberscope are very specific and there is no standard equipment which meets the requirements. The most important property is that the fiberscope has to be absolute anti-magnetic, due to the observation inside a very high magnetic field up to 20 T. Further requirements are a lenght of 6m, a side-view objective, the possibility to connect to the camera and a focus in a wide range. The only supplier which could offer a fiberscope with the required optical properties is Olympus. Table 7.6 summarizes the main features of the Olympus fiberscope. The mechanism for the remote control of the movement of the distal end is realised with steel wires which go through the whole system. This wires unfortunately are not anti magnetic. It was possible to take out this mechanism, because there is no need to move the distal end in our case.

Olympus Fiberscope	
Type	IF13D3-60
Diameter	13mm
Length	6000mm
tip articulation hor.	240°
tip articulation vert.	240°
Sideview	90° (with Adaptor)

Table 7.6: Specifications Olympus Fiberscope IF13D3-60

7.4 Mercury Jet Setup

7.4.1 Concept of Experimental Setup

The basic concept of the experiment is to put mercury under pressure by an air driven pump (air pressure to mercury pressure converter) and to trigger the jet which is produced by a nozzle and injected into an experiment chamber. This experiment chamber can be put in the bore of a magnet (solenoid). The mercury is lead back out of the chamber into a reservoir to be compressed again.

The main parts, the setup consists of are: the NORDSON 25B piston-pump, the NORDSON A7A ball tip valve, an injection nozzle, an experiment chamber and a Hg reservoir. The air driven pump sucks the mercury out of the Hg reservoir and pressurizes it. The to the high-pressure output of the pump connected ball tip valve triggers the jet through the nozzle into the experiment chamber. From there the mercury flows back into the reservoir driven by gravity.

The experiment chamber is designed to provide highest security against mercury escaping from the system. It is an airtight rectangular Plexiglas chamber surrounded by a Plexiglas tube that fits into the bore of the magnet. This tube is an additional protection if the inner chamber leaks. The back side of the inner chamber, where the mercury jet hits the wall is shaped in that way, that the jet will be deflected and flows back into the reservoir as fast as possible. There is a secondary housing containing the complete plumbing. Also the flexible high-pressure hoses, the hose for the back flowing mercury from the experiment chamber and the trigger valve are contained inside a safety housing.

The experiment chamber will be flooded with a noble gas (Argon) to prevent oxidizing of the mercury. For this there is a connector mounted to the experiment chamber. After this connector follows a needle valve and a flow control unit. Before doing an experiment with mercury, an Argon bottle will be connected and the experiment chamber will be flooded over the flow control and the open needle valve. The gas flows via the hose for the backflowing mercury to the Hg reservoir.

There is an additional pipe connected to the reservoir, which leads out of the safety housing. This pipe can be used for evacuating the reservoir if the experiment chamber is located lower than the Hg reservoir to pump the mercury back into the reservoir. Through this pipe the air exits, when the experiment chamber and the Hg reservoir are flooded with a noble gas.

7.4.2 Flow Chart

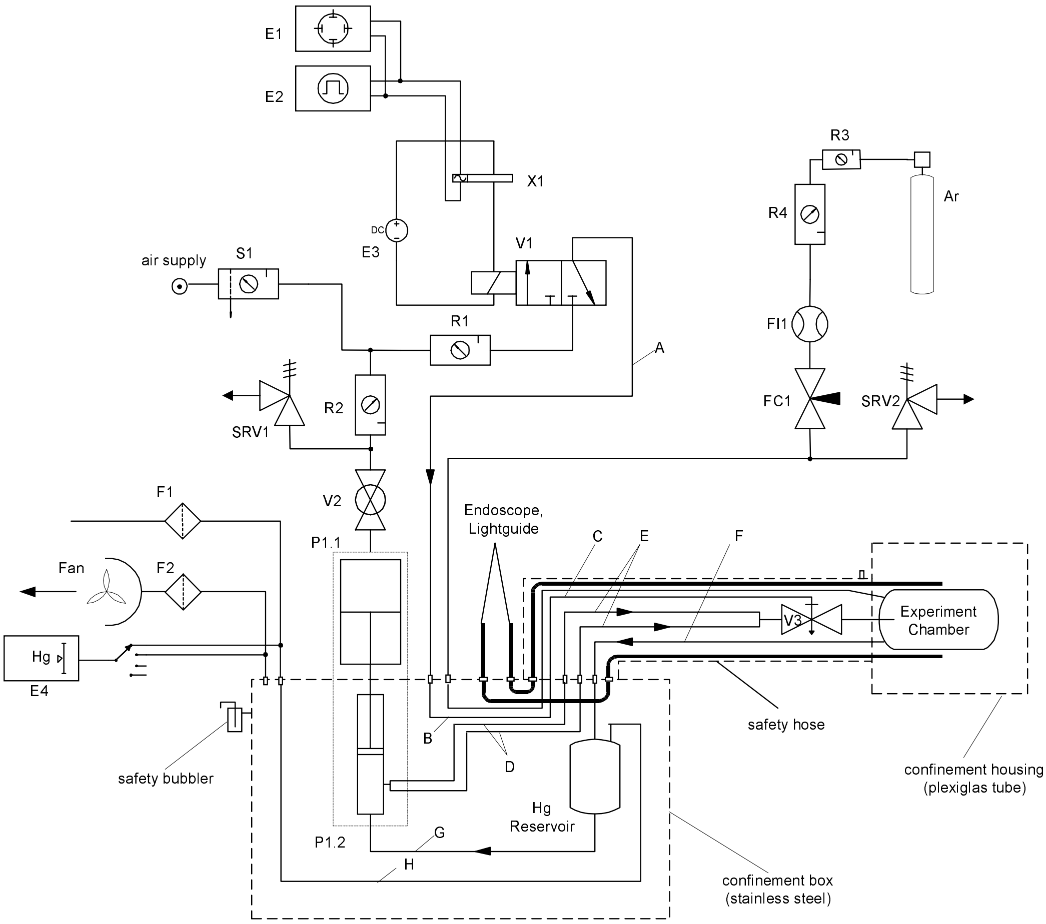

Figure 7.10: Flow Chart - Mercury Jet Setup

Description of the parts in figure 7.10:

E1....Oscilloscope Tektronix TDS3032 300Mhz, 2.5Gs/s
E2....Pulse Generator Philips/Fluke PM5786B 1Hz-125MHz
E3....Power Supply 24V DC
E4....Mercury Vapor Detector Mercury Instruments VM-3000
F1, F2....Charcoal Filter
FC1....Flow Control for Noble Gas
FI1....Flow Indicator (Flowmeter) 0-10l/min

P1.1....NORDSON 25B Piston Pump, Air Motor
P1.2....NORDSON 25B Piston Pump, Hydraulic Section
R1....Air Pressure Regulator
R2....Air Pressure Regulator
R3....Pressure Regulator for Argon LHC15 200bar à 15bar
R4....Pressure Regulator for Argon BS300/01 15bar à 10-100 mbar
S1....Air Service Station (Filter, Pressure Regulator)
V1....3/2 Pneumatic Valve
V2....Shut Off Valve for Air Motor of Piston Pump
V3....NORDSON A7A Ball Tip Valve (air actuated)
SRV1....Safety Relief Valve 4.1 bar
SRV2....Safety Relief Valve "Nupro" 0,2-3bar (calibrated to 0,2bar)
X1....Reed Relais 5V

Tube and hose types / Medium

A....4x6mm Rilsan (Polyamide) flexible hose; medium: compressed air
B....5x6mm stainless steel tube; medium: compressed air
C....4x6mm Rilsan (Polyamide) flexible hose; medium: compressed air
D....6x8mm stainless steel tube; medium: mercury (high pressure)
E....2x NORDSON high-pressure hoses, Teflon $\frac{1}{4}$", stainless steel nipples and swivel nuts; medium: mercury (high pressure)
F....6x8mm Rilsan (Polyamide) flexible hose; medium: mercury
G....$\frac{1}{2}$" plumbing (316 stainless steel); medium: mercury
H....6x8mm stainless steel tube; medium: Argon / (air)
I.....6x8mm stainless steel tube; medium: air

Feedthrough fittings: Gyrolok, stainless steel

7.4.3 Components

Pump

The pump which is used for the experiment setup is a NORDSON 25B double stroke piston pump. This pump is designed for heated or unheated high-pressure, airless paint spray applications. The present pump in stainless-steel construction is especially suited for corrosive and waterborne applications, as well as several non-paint applications including cold glue and adhesives, and food and drug applications. It is driven by compressed air and operates at 20-80 PSIG (1.4-5.5 bar), the maximum recommended air pressure is 100 PSIG (7 bar). The 16:1 fluid-to-air pressure ratio pump has a capacity of 0.05 l per cycle (one cycle = 2 strokes) and delivers 3.03 l at 60 cycles per minute. The maximum working pressure is 1500 PSIG (103.4 bar).

Figure 7.11: Nordson 25B Piston Pump (Nordson USA)

Function

Suction Stroke

Supply air enters the pump through the air valve. The air valve directs air through the connecting tube to the underside of the air motor piston, causing the piston to rise. Air above the piston is exhausted through the air valve and muffler. The piston pulls the hydraulic plunger up with it. The pressure ball check closes and the siphon ball check opens, allowing material to flow into the hydraulic section. The material above the pressure ball check is forced out of the pump. As the piston reaches the top of its stroke, the shifting mechanism is activated, shifting the spool inside the air valve, so that supply air is directed to the top of the piston and air below the piston is exhausted.

Pressure Stroke

Air above the air motor piston pushes the piston and hydraulic plunger down. The siphon ball check closes and the pressure ball check opens. Material below the pressure ball check is forced up through the plunger and out the pressure housing outlet fitting.

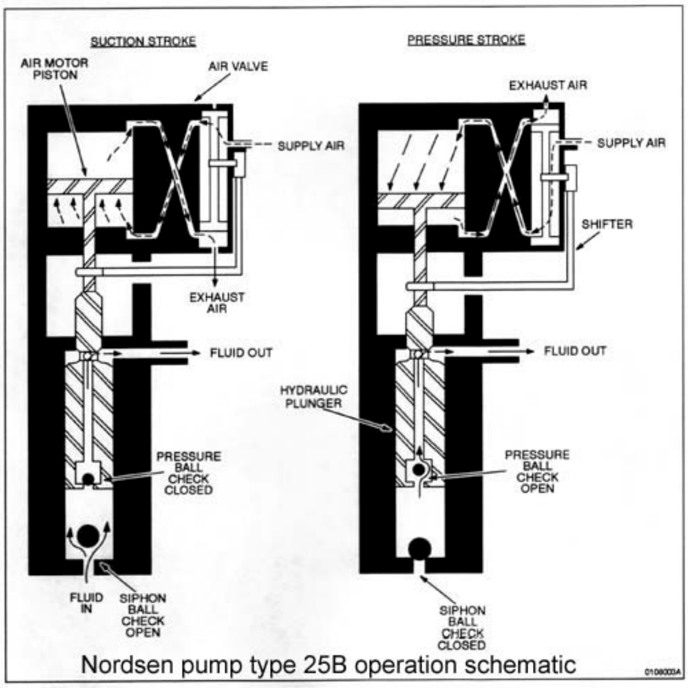

Figure 7.12: Nordson 25B - Operation Schematic (Nordson USA)

Trigger Valve

The valve used for triggering the jet is a Nordson A7A ball tip valve. Nordson A7A are used for automatic airless spray guns and are designed to deliver maximum reliability in high-production airless painting, sealant and adhesive applications.

It is an air-actuated valve and provides a response time of under 10 ms and a high-speed cycling capability of up to 2500 cycles per minute. The compressed air pressure range is 40-120 PSI (2.75-8.27 bar) and the maximum fluid pressure is 1700 PSI (117 bar) for the standard model.

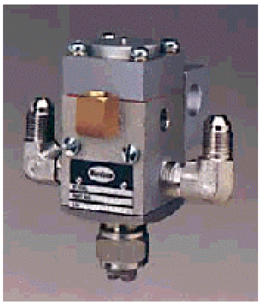

Figure 7.13: Nordson A7A Ball Tip Valve (Nordson USA)

Nozzle

The nozzle consists of an universal piece for connection to the valve with 8 mm inner diameter and interchangeable nozzle tips with different inner diameters (3, 4, 5 mm), which are inserted into the experiment chamber.

The shape of the nozzle is a very important parameter for producing a stable non-turbulent jet.

Plumbing

The high pressure mercury lines are 6 mm inner diameter stainless steel pipes, connected with "Gyrolok" connectors. The flexible connection between the pumping unit and the experimental chamber are two teflon hoses with stainless steel braid (Nordson), rated up to 107 bar. All other connections (for back flowing mercury, Argon, compressed air for trigger valve and connection between mercury reservoir and pump) are Rilsan (Polyamid) hoses.

Mercury Compatibility

The whole "mercury pump", including the Nordson pump, the trigger valve, the nozzle and the plumbing have been checked to be absolutely compatible to mercury. In addition the pump and the valve have been dismantled inside the vent hood in order to be prepared when the system has to be cleaned after operation or in the case of leaks.

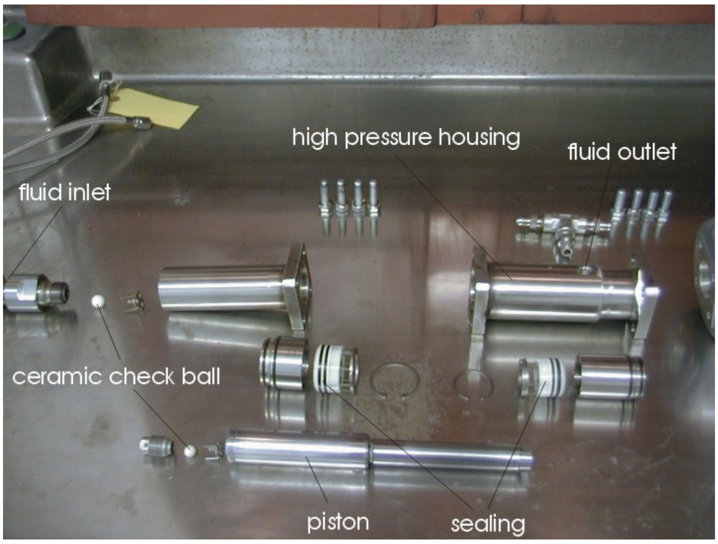

Figure 7.14: Dismantled Hydraulic Section of the Pump

Compatibility of Mercury with different materials

	Plastics																					Elastomers									Metals										Non-Metal		
	ABS	Acetal (Delrin)	CPVC	Epoxy	Hytrel	LDPE	HDPE	PP	PPCO	PMP	Nylon (Polyamid)	Teflon	ECTFE (Halar)	ETFE (Tefzel)	PC	PVC	PSF	PS	PVDF (Kynar)	Noryl	PPS (Ryton)	Nitrile (Buna N)	EPDM	Hypalon	Kel-F	nat. Rubber	Neoprene	Silicone	Tygon	Viton	304 stainless steel	316 stainless steel	Aluminium	Brass	Bronce	Carpenter 20	Cast iron	Copper	Hastelloy-C	Titanium	Carbon graphite	Ceramic Al203	Ceramic magnet
Mercury	B	A	A	A	B	A	A	A1	A1	A	A	A	A2	A2	D	A	A	D	A	A3	-	A	A	A	A	A	A	-	D	A	A	A	D	D	A	D	A	D	A2	A	C	A	A

- A Generally considered best choice, no effect after 30 days
- A1 compatibility above 50 degrees C not available
- A2 up to 50 degree C
- A3 at Room temperature
- B good resistance, minimal effect after 30 days
- C only usable under control
- D not compatible

LDPE	Polyethen Low Density
HDPE	Polyethen High Density
PP	Polypropylen
PPCO	Polypropylen Copolymer
PMP	Polymethylpenten
Teflon	FEP Fluroethylen propylen
Teflon	TFE Tetrafluorethen
Teflon	PFA Perfluoroalkoxy
PC	Polycarbonat
PVC	Polyvinylchlorid
PSF	Polysulfon
PSF	Polystyrol

Sources: Cole-Parmer
Foxboro
Bioblock Scientific

Figure 7.15: Mercury Compatibility Chart

Part	**Material**	**Compatibility**
25B Pump		
Housing	Stainless Steel	A, excellent
Plunger	Stainless Steel	A, excellent
O-Rings	Viton	A, excellent
Pressure Balls	Ceramic	A, excellent
Cage, Seat	Stainless Steel	A, excellent
Siphon	Stainless Steel	A, excellent
High-Pressure Fluid Hoses	Teflon, Stainless Steel	A, excellent
A7A Ball Tip Valve		
Housing	Stainless Steel	A, excellent
O-Rings	Viton	A, excellent
Ball Tip and Seat	Stainless Steel	A, excellent
Cartridge	Viton, Stainless Steel	A, excellent
Plumbing		
Tubes	Stainless Steel	A, excellent
Gyrolok Fittings	Stainless Steel	A, excellent
Nozzle		
Sealings	Neoprene, Teflon	A, excellent
Nozzle Body	Stainless Steel	A, excellent

Table 7.7: Hg Compatibility - Jet Setup

Max. Pressure Considerations

Pressure Ratios *NORDSON 25B pump*
Nominal operating fluid pressure range: 320-1280 PSIG / 22-90 bar
Maximum working pressure: 1500 PSIG / *103.4 bar*
Nominal operating pressure air motor of piston pump: 20-80 PSIG / 1.4-5.5 bar
Max. working pressure air motor of piston pump: 100 PSIG / *7 bar*
NORDSON A7A valve
Working pressure: 40-120 psi / 2.75-8.27 bar
Max. fluid pressure: 1700 psi / *117 bar*
Plumbing
Max. pressure (weakest part: flexible hoses): 1500 PSI = *103.4 bar*

Water Hammer A waterhammer is created by stopping and/or starting a liquid flow suddenly. Sudden closure of a control valve or stopping of a pump produces excess pressure in a pipeline. A common example of a waterhammer occurs in most homes everyday. Simply turning off a shower quickly sends a loud thud through the house; this is a perfect example of a waterhammer. Dishwashers and washing machines make these same sounds, because inside them small solenoid valves are being opened and closed quickly, producing this pulse noise. The hammer occurs because an entire train of water is being stopped so fast that the end of the train hits up against the front end and sends shock waves through the pipe.

The liquid metal on its way to the ejection might be interrupted by valves or by a reduction of the pipe cross section. An impact load causes pressure waves, which can easily exceed the working pressure at steady flow. At instantaneous, complete interruption of the flow a maximum pressure can be assumed by Joukowskis law: water hammer head H at instantaneous valve closure in a rigid pipe:

$$\Delta H_{max} = \frac{c}{g} v, \tag{7.3}$$

where c is the velocity of sound, g the gravitational constant and v the speed of the fluid through the open valve. The velocity of sound in a medium can be calculated as $c = \sqrt{\frac{K}{\rho}}$, where K is the bulk modulus (25GPa) and ρ is the density of the medium (13.6g/cm^3). With equation 7.3 the pressure is given by

$$P = \rho \Delta H. \tag{7.4}$$

Joukowskis law assumes an instantaneous stop of the liquid. But the valve closes in a finite time. For acceleration and deceleration of an incompressible liquid in a pipe, due to unsteady motion of changing velocity "dv" in time "dt" following term results:

$$\Delta H = \frac{L}{g} \frac{\Delta v}{\Delta t}, \tag{7.5}$$

where L is the length of the pipe. With L=0.4m and a (measured) closure time of the valve of 3ms, the induced pressure due to the water hammer results in (with equation 7.4 and 7.5):

$$P = \rho \Delta H = 13.6 \cdot 10^3 \frac{0.4}{9.81} \frac{20}{3 \cdot 10^{-3}} \approx 37 bar \tag{7.6}$$

The pressure caused by the hammer head is additionally to the working pressure generated by the pump. So the working pressure of the pump has to be limited by the water hammer in order to be sure not to exceed the pressure limitation of the pipes or other parts.

The "weakest" part are the flexible hoses connecting the pumping system to the trigger valve with a maximum pressure of 103.4 bar. Substracted the water hammer, thus the maximum pressure, the pump has to be limited yields:

$$103.4 - 37 = 66,4bar \approx 66bar \tag{7.7}$$

To limit the (secondary) pressure on the liquid, the (primary) compressed air pressure has to be limited by a safety relief valve. As the pump converts the air pressure into the 16 times higher pressure on the mercury, the maximum air pressure must be

$$\frac{66}{16} = 4,125bar \tag{7.8}$$

In agreement with TIS department (Technical Inspection and Safety), it was decided to limit the air pressure to 4,5bar, what equals 72bar on the mercury, because the assumptions made concerning the water hammer are the pessimistic side of life. And seen from the experimentalists side, the higher the pressure the better, in order to reach maximum mercury jet velocity.

Pressure Test After completing the setup, the high-pressure part of the experimental setup has been tested with the presence of a TIS member. For the pressure test the air pressure was increased to 5.5 bar (88 bar mercury pressure) and held for about 1 Minute. After that a safety relief valve set to 4.5 bar by TIS (SRV1 - ref. fig.7.10) was mounted in the compressed air supply piping.

7.4.4 Experiment Chamber

The whole chamber set up is made of plexiglas (PMMA - Polymethylmethacrylate) and the single parts are glued together with Cyanocrylate. The main experiment chamber, containing the mercury jet has a rectangular cross section of 100x40 mm (fig. 7.16 parts 2, 3, 4, 7). On the front of this chamber is mounted a holding plate (part 5) with a feedthrough for the nozzle (part 13) and a connection each for the backflowing mercury (part 14) on the bottom and for the Argon (part 12) at the top. This plate also holds the plexiglas tube (part 1) which builds the second confinement and fixes the chamber inside the bore of the solenoid. The backwall of the chamber is shaped to deflect the mercury jet and guide the mercury to the outlet of the chamber (ref. fig. 7.17). There is a plate above the bottom (part 6) to provide a protection against droplets hiting the main jet. At the inlet for the Argon (which could also be used for evacuating the chamber in future experiments) there is a bariere to prevent mercury going out through this connection (parts 9, 10, 11).

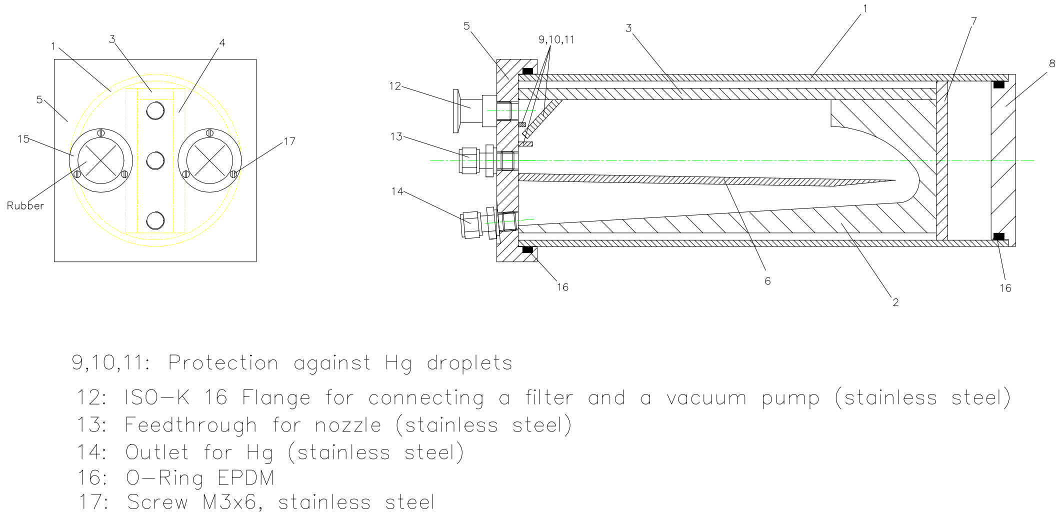

Figure 7.16: Experiment Chamber - Assembly Drawing

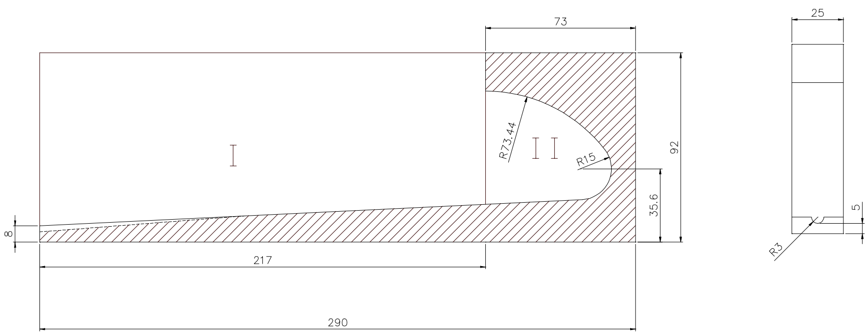

Figure 7.17: Experiment Chamber - Part 2

Figure 7.18 shows the experiment chamber immediately after shooting a mercury jet (there are still some mercury droplets). In the front one can see the fiberscope with the side view adaptor and in the back the light guide.

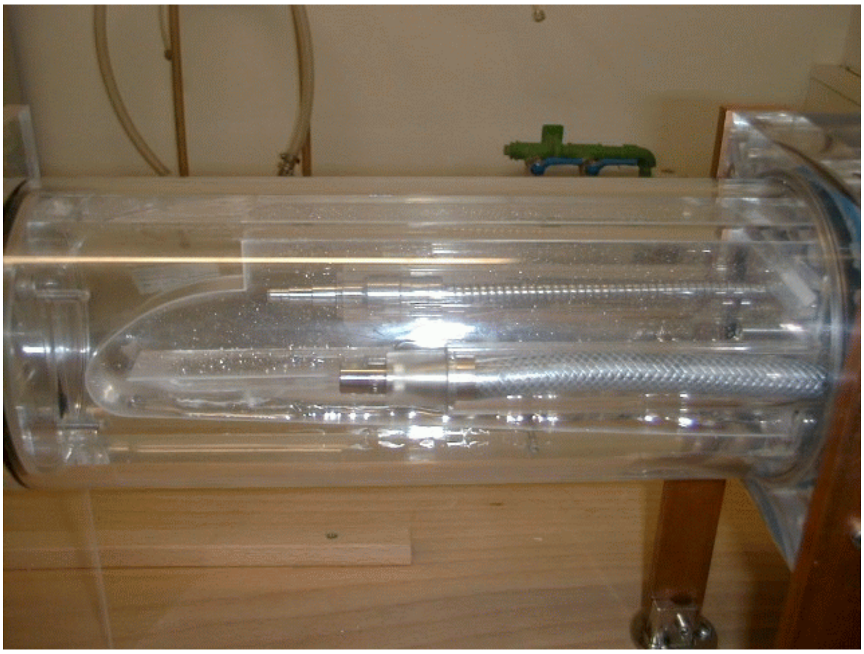

Figure 7.18: Experiment Chamber with Fiberscope and Light Guide

Stability

The glueing area at the side plates is:
(see fig. 7.17: 290·100-(I+II)):

$$290 \cdot 100 - (73,6 \cdot 217 + \frac{56^2\pi}{4}) = 10.565,8mm^2 \tag{7.9}$$

and the glueing area at the front is:

$$2 \cdot 100 \cdot 8 + 2 \cdot 25 \cdot 8 = 2.000mm^2. \tag{7.10}$$

The specification for the used cyanoacrylate glue (ThreeBond 1747) is a strength of 17N/mm^2.

The resulting force which can put on the side plates is then:

$$10.565,8 \cdot 17 = 179.618N \tag{7.11}$$

and the maximum force on the front results:

$$2.000 \cdot 17 = 34.000N. \tag{7.12}$$

As the inside area of the sides is (fig. 7.17 I+II):

$$\approx 73,6 \cdot 217 + \frac{56^2\pi}{4} \approx 18.434mm^2, \tag{7.13}$$

the maximum pressure results

$$\frac{179.618}{18.434} = 9,74\frac{N}{mm^2} = 97,4bar. \tag{7.14}$$

The inside area of the front is

$$84 \cdot 25 = 2.100mm^2, \tag{7.15}$$

so the maximum pressure on the front plate is

$$\frac{34.000}{2.100} = 16,19\frac{N}{mm^2} = 161,9bar. \tag{7.16}$$

7.4.5 Safety Measures

The complete set up for the magnetic field experiment has a consistent safety concept. All parts containing mercury are inside a second confinement. The hydraulic part of the pump and the mercury reservoir are inside a stainless steel box. The experimental chamber is souronded by a plexiglas tube and all connection hoses between the pump assembly and the experiment chamber are inside a big plastic safety hose. If there is a leak at any point of the mercury system, no mercury can escape.

HAZOP

To provide highest safety and operability, a HAZOP study has been done in cooperation with the TIS department. HAZOP stands for HAZard and OPerability Study. This is generally a qualitative study to identify the potential hazards and operating problems of a process. The technique was developed by ICI in the 1970's and is now used worldwide in the chemical industry to examine proposed designs and also to improve the safety and operating standards on existing systems.

HAZOP makes the assumption that a hazard or operating problem can only occur when there is a deviation from the design or operating intention (e.g. no flow when there should be forward flow). The process is examined line by line, vessel by vessel and section by section. It applies a combination of guide words and parameters to identify deviations from normal conditions in the process system. Where a cause of deviation is found, the consequences of the deviation require examination so that any necessary remedial actions can be taken.

Before the start of the study, the process is divided up into suitable sections (called nodes). Before each section is examined, its function and normal operating conditions are summarised.

For the HAZOP study see appendix.

For a safe operation of the set up also an operating instruction has been established (see appendix).

7.5 Experiment 1.0 Establishing a Mercury Jet

7.5.1 Experiment Setup with Experiment Chamber

Figure 7.19 shows the complete setup for producing pulsed mercury jets. On the right there is the mercury pump with the hydraulic section inside the steel box and the air motor with the air pressure reducer and the solenoid valve sitting on the top of the box. On the left side one can see the mercury jet chamber and in between are the connections inside the blue confinement hose.

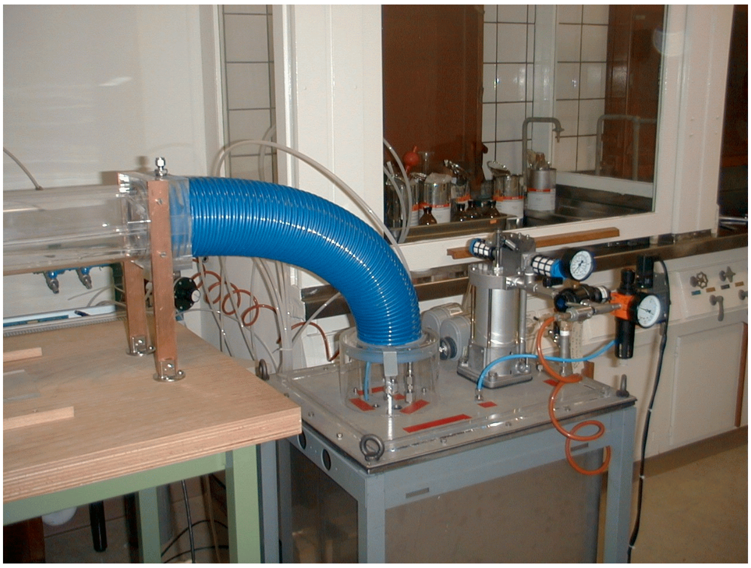

Figure 7.19: Complete Experiment Setup (Pumping System, Experiment Chamber)

The very first step in performing all the experiments was to test the setup and determine the optimal illumination and camera/fiberscope position. The very first mercury jet was captured in a picture (figure 7.20).

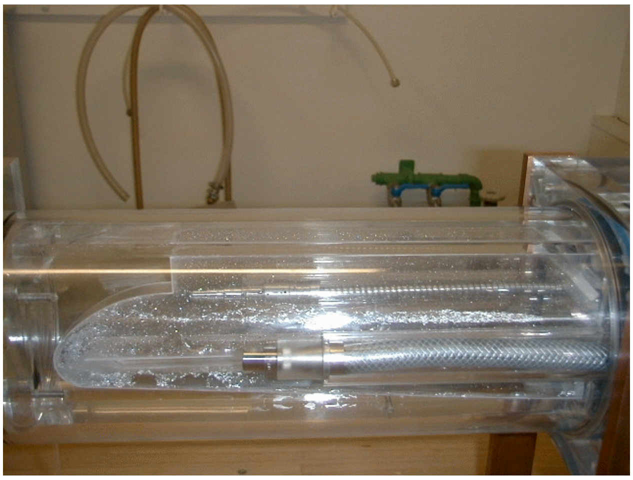

Figure 7.20: First Hg Jet

7.6 Experiment 1.1 - Calibration Measurements

In order to determine the jet velocity in dependence of the pressure, calibration measurements have been performed. To verify the plausibility of the measurements first the speed of the jet escaping from the nozzle has been calculated.

For this measurements the camera was directed directly to the experimental chamber without fiberscope (figure 7.21).

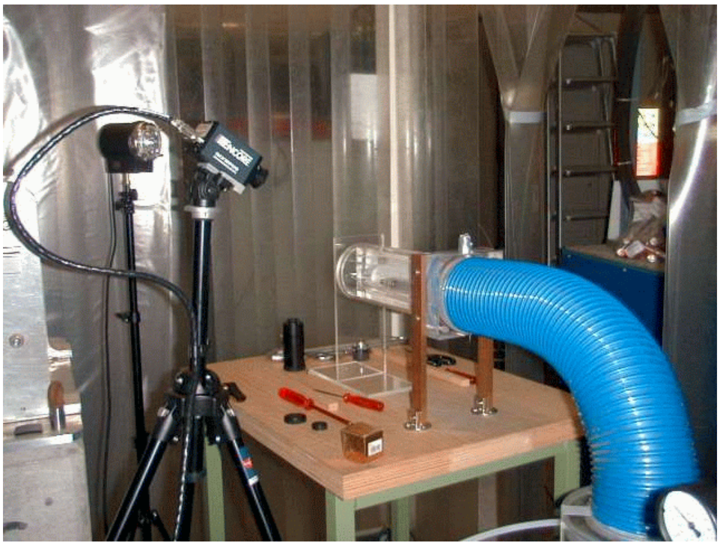

Figure 7.21: Experiment 1.1 - Positioning of the Camera

The measurement of the velocity has been made using the measuring feature inplemented in the Olympus Encore software (figure 7.22). This is a semi automatic modus for measuring positions, distances and velocities. First a defined distance with known length in the picture has to be marked to calibrate the software with the correct dimension. The video is played in single frame steps and in every frame the same point (which travels over the picture with increasing frame number) is marked. Then the software calculates the position of each point, the distance to each time the previous point and the velocity. This table can be exported in csv format to e.g. MS Excel for further analysis.

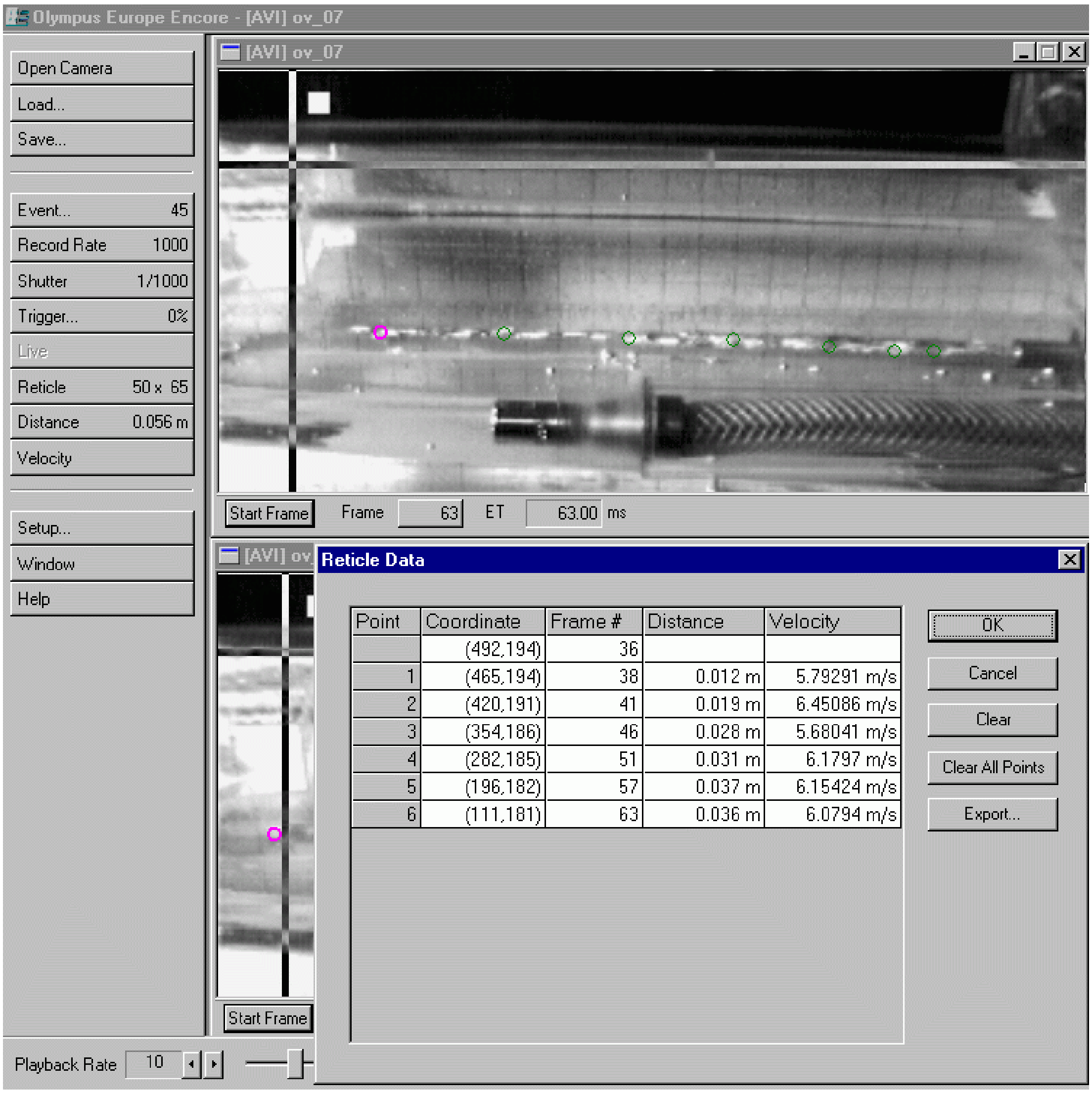

Figure 7.22: Velocity Measurements using the Olympus Encore Software

7.6.1 Compensation of Parallax Aberration

Due to different depths of the scale for calibrating the measuring feature of the Olympus software and the center of the experiment chamber (mercury jet) a parallax aberration would occur (see fig. 7.23). So if the software is calibrated using the scale in the background and then the mercury jet is measured, the results would be distorted. The measured values would always be larger than in reality.

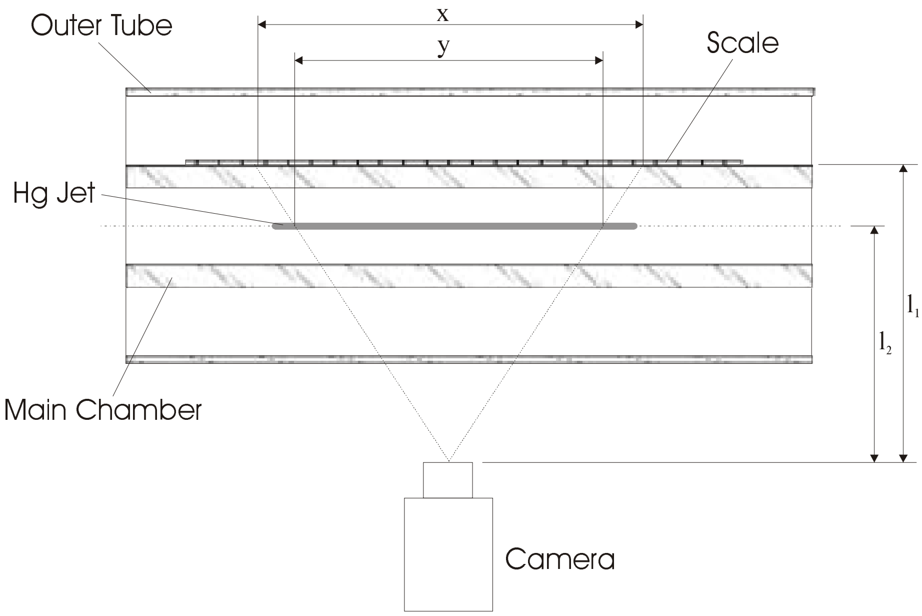

Figure 7.23: Compensation of Parallax Aberration

In order to compensate this aberration, an adaption calculation must be applied according to the following principle:

$$\frac{l_1}{x} = \frac{l_2}{y} \tag{7.17}$$

derives

$$y = \frac{l_2 \cdot x}{l1} \tag{7.18}$$

7.6.2 Result

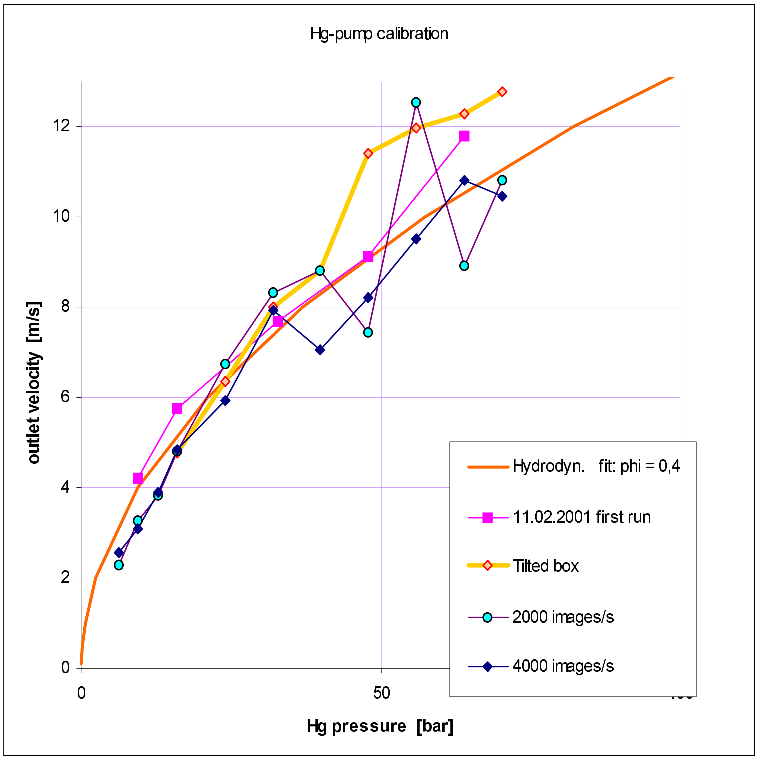

Figure 7.24: Hg-Pump Calibration - Hg Jet Velocity vs. Hg Pressure

The diagram 7.24 summarizes the results of four different measurment series and shows a fit of the calculation of the outlet velocity. The graph "Hydrodyn. fit" is based on the formula below (free flow due to a pressure). As the speed coefficient φ for mercury is not known, a fit was calculated with φ=0,4 (φ_{H2O}=0,97).

Formula for calculation:

$$v = \varphi \cdot \sqrt{2 \cdot \frac{p}{\rho}} \tag{7.19}$$

v...outlet velocity
φ...speed coefficient (fit: $\varphi = 0.4$)
p...pressure
ρ...density (13600 $\frac{kg}{m^3}$)

Until 40 bar / 8 $\frac{m}{s}$ the measured velocities agree very well with the calculation. The fluctuations of the measurements above about 40 bar arise because of jet instabilities and turbulances due to friction with the Argon with atmospheric pressure inside the experimental chamber. A further explanation of the fluctuations is that mercury droplets are remaining in the nozzle. When the valve opens and mercury streams into the nozzle, the gas layers between the droplets is compressed and when the mercury is ejected the gas expands again and causes a disruption of the tip of the jet. To show this effect also a series of measurements with a tilted box (nozzle showing upwards) has been made. With the tilted nozzle the fluctuation is damped but there is a leap in the velocity at the same point where the fluctuation start with the horizontal nozzle. This leap was not further investigated due to minor relevance.

7.6.3 Error Calculation

The velocities calculated by the software are given by

$$v = \frac{x_2 - x_1}{t_2 - t_1} \tag{7.20}$$

where x_i are the positions of the mercury tip at the times t_i. The error propagation of the error Δf is defined by

$$\Delta f(x_1, ..., x_n) = \sum \left| \frac{df}{dx_i} \right| \Delta x_i \tag{7.21}$$

what yields in

$$\Delta f(x_1, ..., x_n) = \frac{1}{t_2 - t_1}(\Delta x_1 + \Delta x_2) + \frac{x_2 - x_1}{(t_2 - t_1)^2}(\Delta t_1 + \Delta t_2) \tag{7.22}$$

The errors of the measurement are assumed to be $\Delta x_1 = \Delta x_2 = 2mm$ (mean error of placing the measuring point) for the postion and $\Delta t_1 = \Delta t_2 = t_{shutter} = \frac{1}{20.000}s$. The time between two points $t_2 - t_1$ is 10ms and the distance between two points $x_2 - x_1$ is 30mm. Put in the numbers in 7.22, the total error yields $\Delta f = \Delta v = 0,4\frac{m}{s}$.

7.7 Experiment 2.0 - Mercury in Magnetic Field (1,3T / CERN)

This initial experiment should produce first impressions about how mercury behaves in a magnetic field. It should also be a test of the setup and the observation equipment and demonstrate the feasibility of such a project before doing a experiment at the Grenoble High Magnetic Field Lab.

7.7.1 Parameters to be observed

Timing of the jet: is the jet accelerated or deccelerated by the field?

Deformation of the jet: increasing or decreasing of the jet diameter.

Jet instabilities: dumping of surface oscillations or increasing of instabilities?

7.7.2 Production of the Magnetic Field

The magnet available at CERN was a conductive solenoid whose parameters are summarized in table 7.8.

Bore Diameter	120mm
Magn. Field	1,3T (on axis)
Current	2000A
Pulse Duration	15ms
Frequency - cooled	<0,5Hz
Frequency - not cooled	<10Hz

Table 7.8: Parameters CERN 1,3T Solenoid

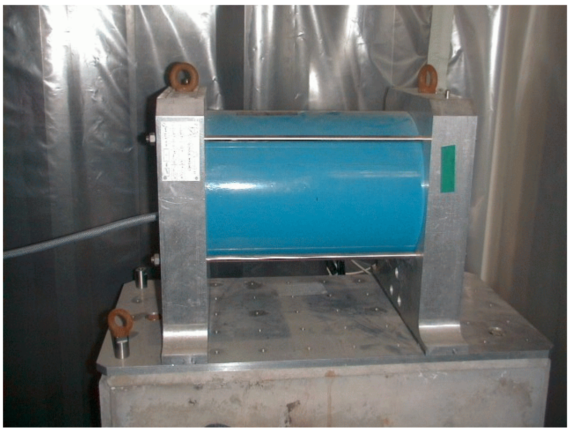

Figure 7.25: 1,3T Conductive Solenoid

7.7.3 Triggering Concept

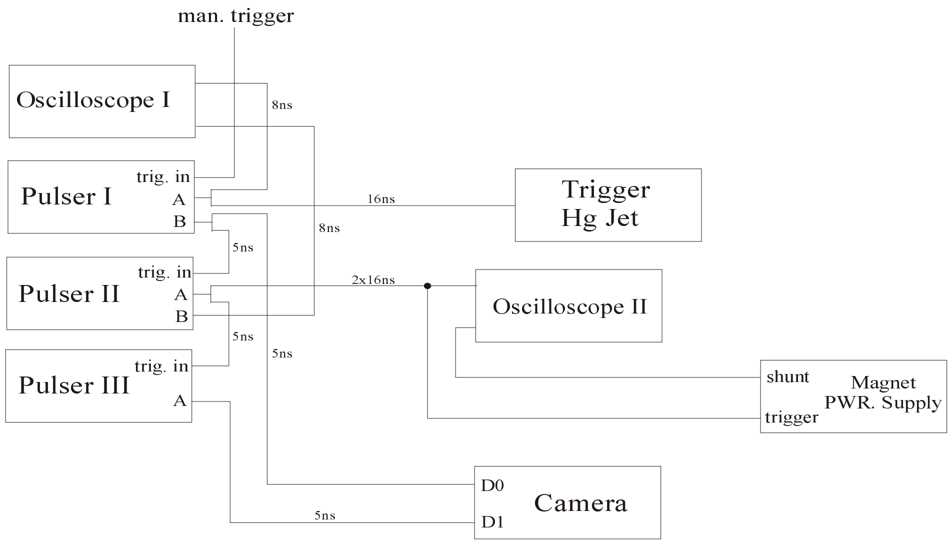

Figure 7.26: Triggering Concept Hg Jet - Magnet

Explanation Figure 7.26:

A manual trigger starts the pulser I which generates a single 5V pulse signal with a variable pulse duration. This signal triggers directly the solenoid valve (t1) which operates the pneumatic mercury jet valve. At the same time a second pulse generator (pulser II) is started and a signal is sent to the camera (Data Input 0) to indicate the trigger point of the mercury jet. The pulser II generates the trigger signal (t2) for the power supply of the magnet. The pulser III which is started by the output signal of pulser II generates a delayed signal to indicate the trigger point of the magnet (time of maximum magnetic field - t4) at the Camera (Data Input 1) - ref. figure 7.27. Oscilloscope I displays the trigger of the Hg jet and the magnet, and the delay between them and oscilloscope II displays the trigger of the magnet and the current output (via a shunt).

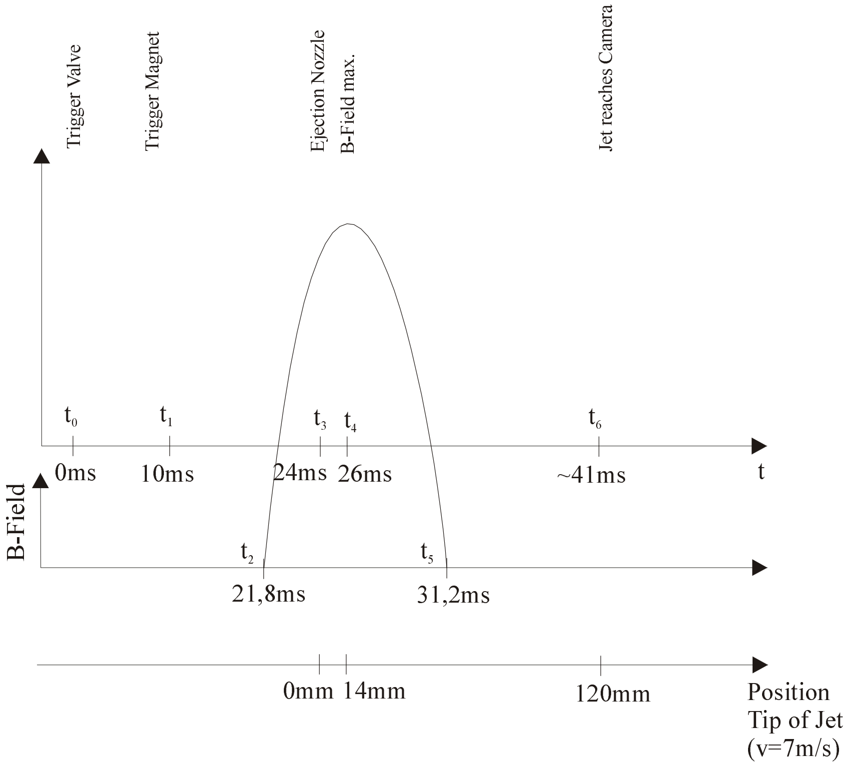

Figure 7.27: Timing Experiment 2.0

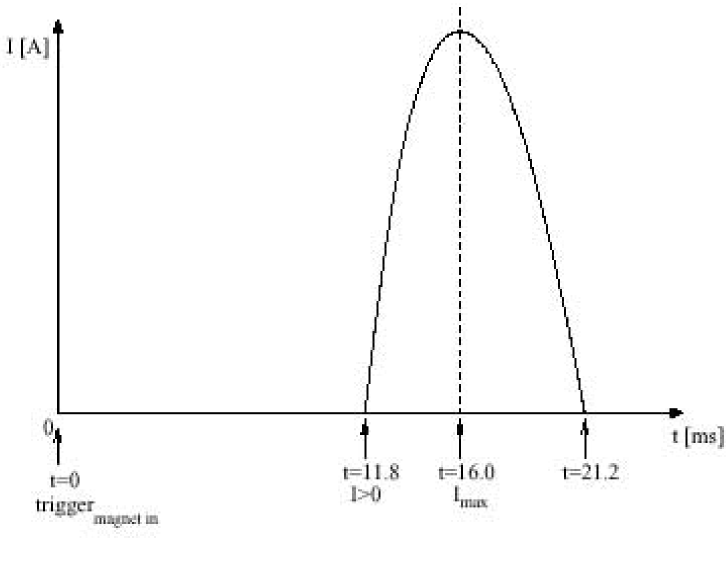

Figure 7.28: Timing 1,3T Solenoid

Figure 7.28 shows the timing of the Magnet. 11,8ms after the trigger point the condensers of the power supply start to discharge and 16ms after the trigger point the maximum current of about 2.070A and the maximum magnetic field of 1,3T is reached. Then the current falls again.

Figure 7.29: Hg Jet Setup with 1,3T Solenoid

7.7.4 Results

Timing of the Jet

In figure 7.30 are six frames of the tip of six different mercury jets of 4mm diamter taken with the fiberscope inside the solenoid. The three pictures at the bottom are taken without magnetic field and the three above with magnetic field (1.3 T). The single pictures are always taken at the same time after triggering the valve and the magnetic field. The boundaries of the jet are highlighted.

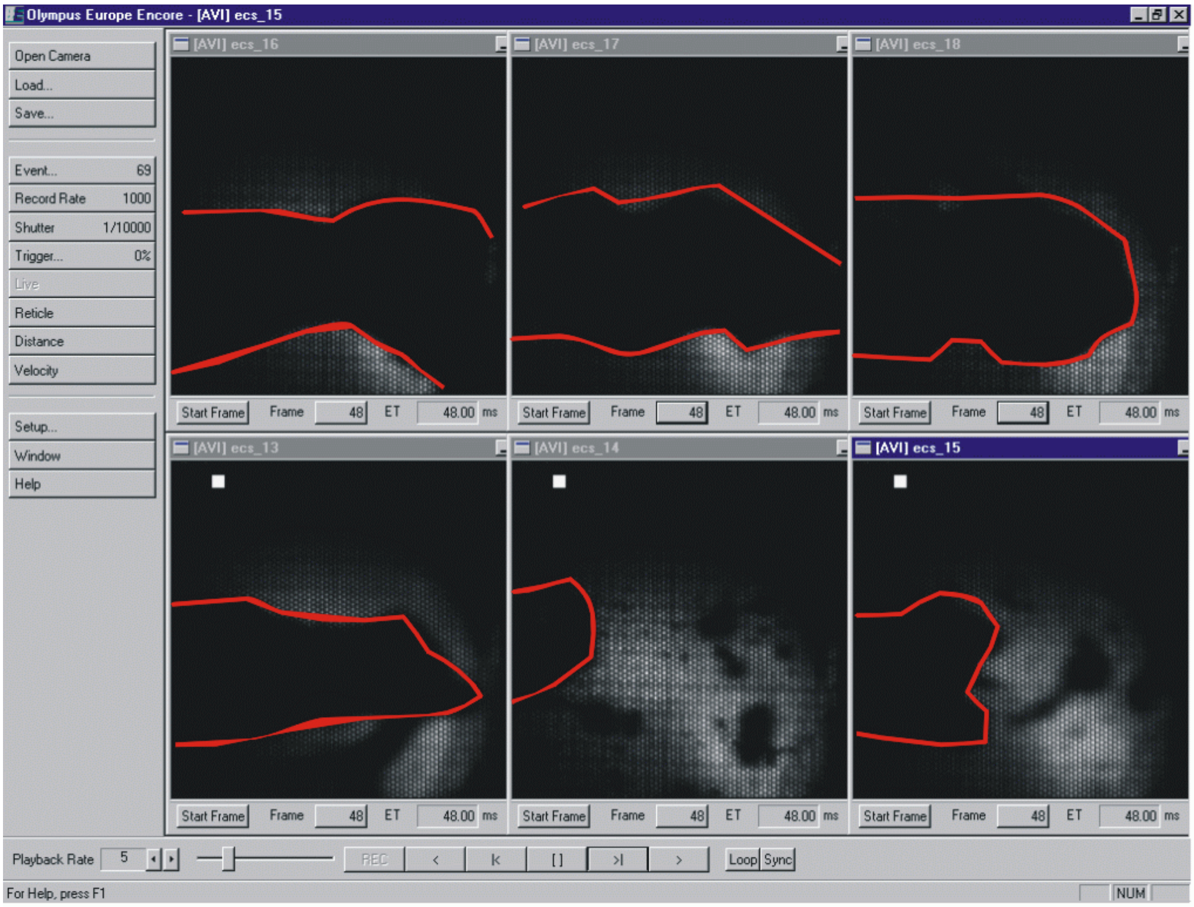

Figure 7.30: Timing of the Hg Jet with/without Magn. Field

One can see, that with magnetic field the tip of the jet arrives about 1ms earlier. When the tip reaches the field of view, it was travelling over 106mm after the magnetic field reached the maximum value. (At a record rate of 1.000fps, the time between two single frames is 1ms and the tip of the jet travells in one frame the half way from the left to the right border of the frame). See also fig. 7.31. This time shift corresponds to a difference in velocity of 0,57$\frac{m}{s}$.

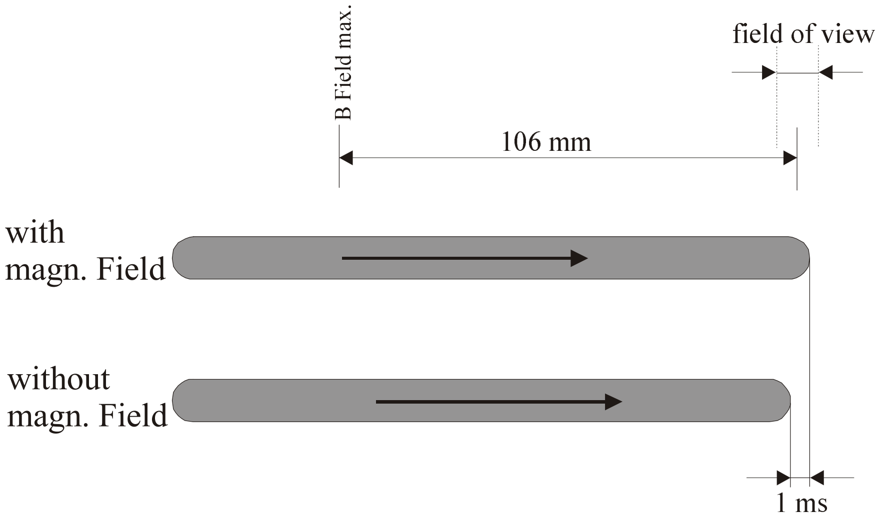

Figure 7.31: Acceleration of the Hg Jet in the Magnetic Field

This acceleration of the jet confirms the assumptions of the simulation in 7.1.1 and 7.1.2.

Jet Dimensions and Instabilities

Figure 7.32 shows the same jets as in 7.30 2ms later. Again the jets with the magnetic field are on the top. The jets without magnetic field are much more unstable. The magnetic field seems to have a damping effect on the surface instabilities. The overall diameter of the jets with magnetic field is slightly greater. This increased diameter appears due to a accumulation of material which is spread around the jets without magnetic field.

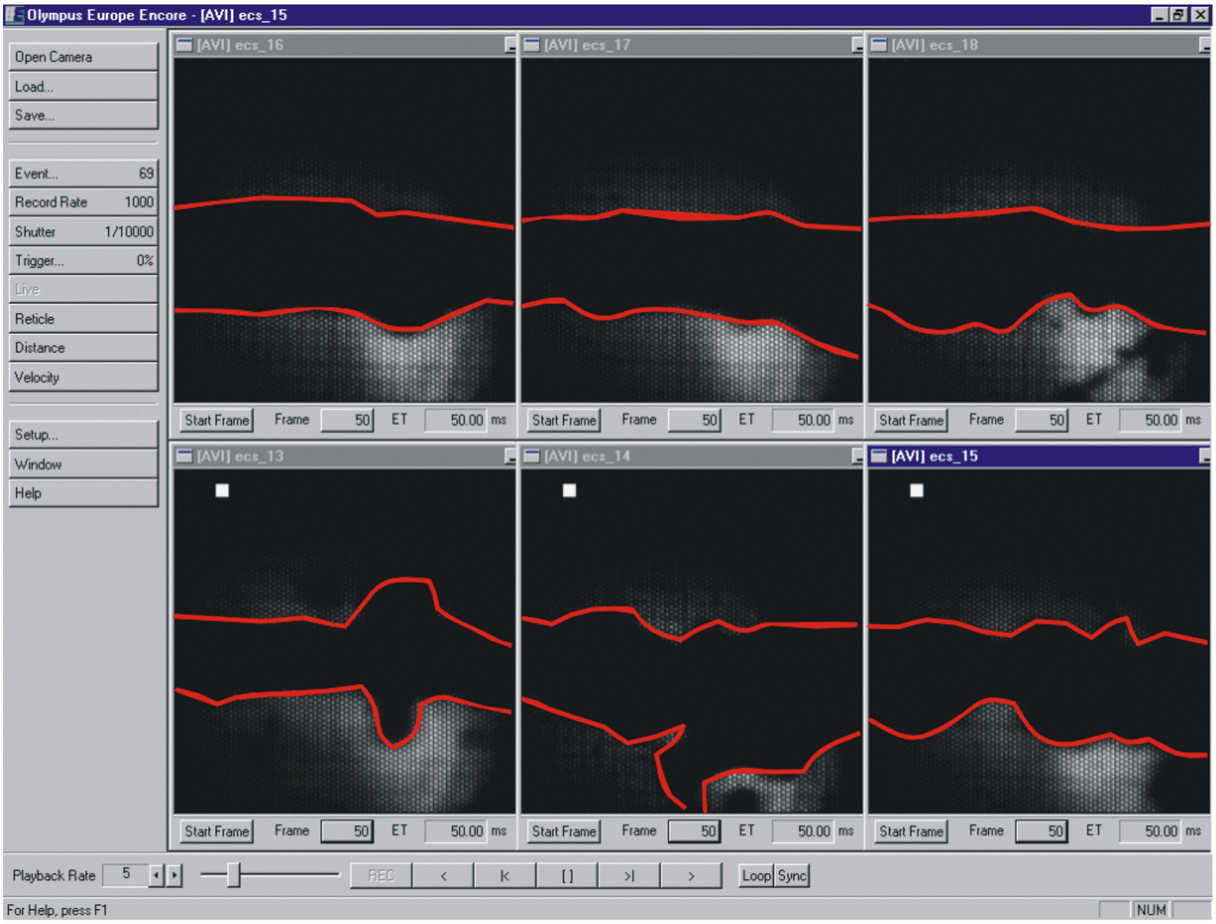

Figure 7.32: Jet Dimension and Instabilities

With these images it is not possible to estimate whether the bigger diameter is due to the increased volume flow per second as in 7.1.1 or only because of the concentration of material around the center of the jet. Also the effects as shown in 7.1.2 (squeezing of the tip of the jet, bulk at the fringe field entrance) can not be represented due to the too small field of view and the fact that the field of view is outside of the maximum field line gradients.

This experiment was done while Argon with atmospheric pressure was inside the experiment chamber. So many of the effects which occured were due to friction of the mercury and the gas. Especially the instabilities at the tip of the jet seem to be a result of this gas friction. The jet would most likely develop differently in vacuum. But this would bring along other difficulties like vaporisation of the mercury due to its low vapor pressure.

7.8 Experiment 2.1 - Mercury in Magnetic Field (13T / GHMFL)

7.8.1 Grenoble High Magnetic Field Laboratory

The Grenoble High Magnetic Field Laboratory - GHMFL (Laboratoire des Champs Magnetiques Intenses - LCMI), located inside the CNRS campus at the Polygone Scientifique Louis Neel, is a French-German laboratory (funded by the Centre National de la Recherche Scientifique and the Max-Planck Institute) and runs as a user facility which provides scientists access to its high field installation. The laboratory is equipped with six conductive magnets which can produce steady (DC) fields up to 30 Tesla. Due to the fact, that there is a much higher number of experiments at the stronger magnets ($>$ 20 T), it may be possible to use the magnet M5 (10 MW, 6T / 13T) without going through the whole process of application resp. it would be easier to get time on this magnet.

7.8.2 Experiment Setup

All magnets there have a vertical axis, so an experimental chamber for a vertical mercury jet has been developed. Also the optical concept of observation has been changed. Due to easier handling and higher resolution, here the camera "looks" via a zoom-objective and two mirrors through the downward bore of the magnet and the glas bottom of the stainless steel protection housing directly onto the Hg jet.

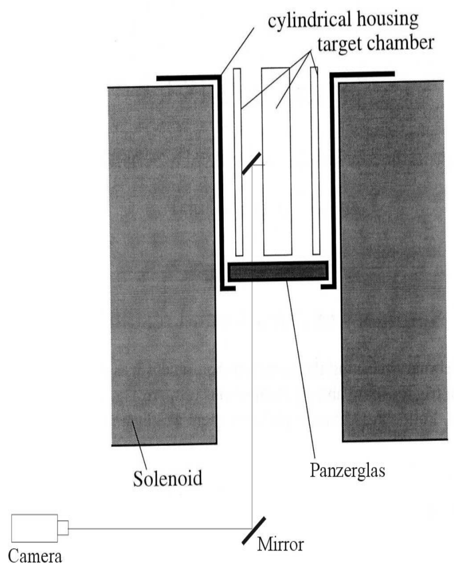

Figure 7.33: Experiment 2.1 - Setup

And as the mercury will not flow back just by gravity, also a system for the mercury recovery out of the vertical experiment chamber was supplemented (see fig. 7.34).

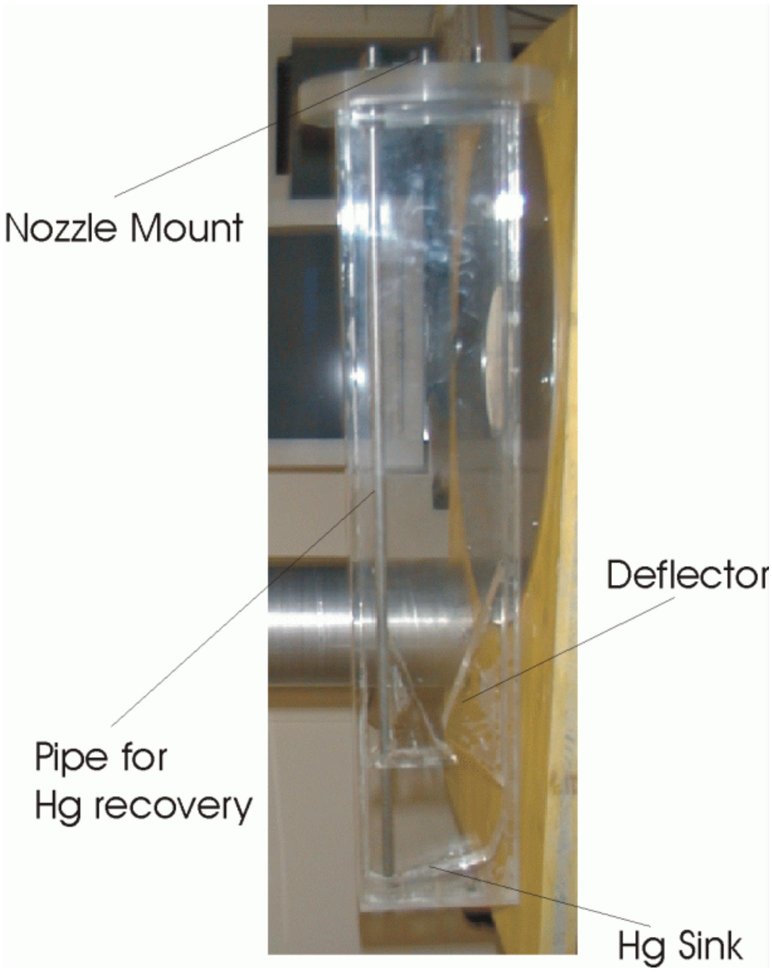

Figure 7.34: Inner Chamber of Vertical Hg Jet Experimantal Setup

The inner Hg jet chamber is installed in a stainless steel protection tube whose bottom is closed with a glas plate. In fig. 7.35, one can see the inner chamber with installed illumination, the mirror for the observation and the protection housing, which will be slided over the whole inner chamber.

Figure 7.35: Vertical Hg Jet Experiment Chamber

7.8.3 Magnetic Field

Table 7.9 summarizes the parameters of the M5 Magnet at the GHMFL.

Bore Diameter	130mm
Magn. Field	13T
Field Direction	vertical
Magnet Type	Bitter coil
Power	10MW
Voltage	400V
max. Current	25.000A

Table 7.9: Parameters GHNFL M5 Magnet

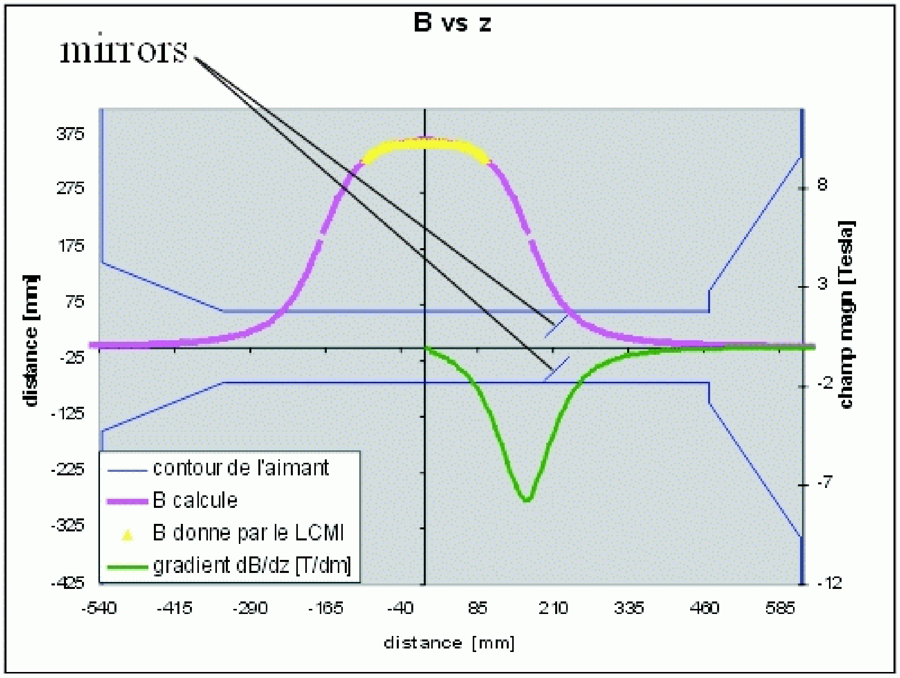

Figure 7.36: GHMFL Magnet M5 - B vs. z

Figure **??** indicates the magnetic field progression of the M5 magnet at the GHMFL. The line "contour de l'aimant symbolizes the bore of the magnet. The graph "B calcule" is the calculated B-field versus the z-axis and "B donne par le LCMI" is the B-field as given from the GHMFL (LCMI). As shown in the figure, are the mirrors for the observation of the mercury jet situated at the place of the maximum gradient dB/dz of 49 T/m.

7.8.4 Results

Figures 7.37 and 7.38 are a comparison between a 4mm mercury jet without and with a magnetic field of 13T.

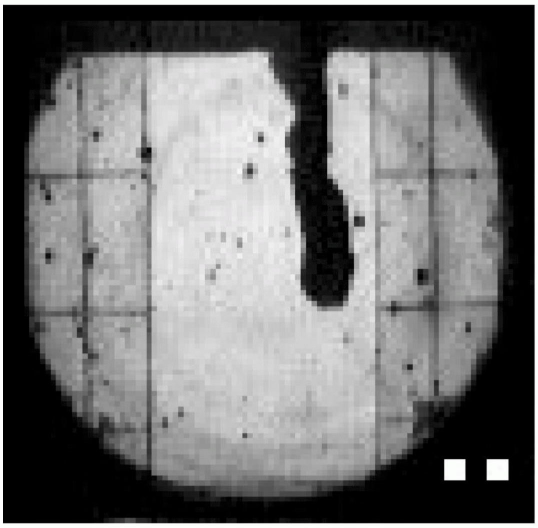

Figure 7.37: Vertical Hg Jet without Magn. Field

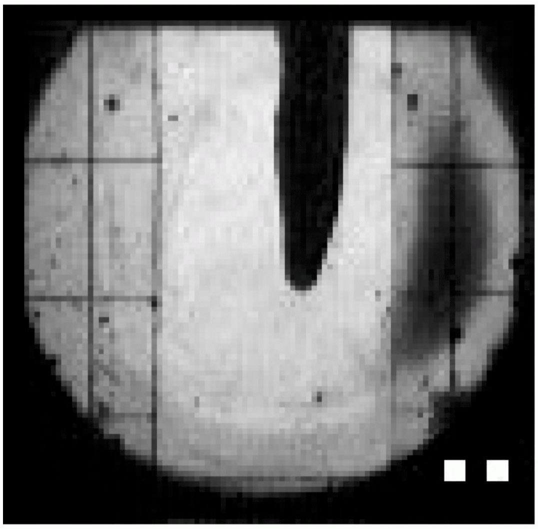

Figure 7.38: Vertical Hg Jet in 13T Magn. Field

The picture 7.38 represents the jet entering the magnetic field at the maximum dB/dz gradient. One can see that the tip is squeezed and formed like in 7.1.2. The instabilities are damped very intensely. Also the diameter of the jet is greater than without magnetic field.

7.9 Experiment 3.0 - Mercury in Proton Beam (Hg trough/BNL)

This experiment as well as experiment 3.1 (Mercury Jet) was performed at the Brookhaven National Laboratory (USA).

For this test it was foreseen, to shot a proton beam pulse onto a small amount of mercury.

7.9.1 Proton Beam Parameters

For these proton beam experiments the BNL AGS facility was used in the framework of the E951 collaboration between CERN and BNL.

The AGS receives protons from Brookhaven's 200 MeV linear accelerator (LINAC) and the AGS Booster.

The main parameters of the AGS beam line at the BNL are summarized in table 7.10.

E_p	26GeV
rep. rate	0.33Hz
ppp_{max}	$24{\cdot}10^{12}$
spot size	r=1.6x0.8mm

Table 7.10: AGS Parameters

7.9.2 Experiment Setup

The experiment setup used consists of a chamber in which a little trough was filled with mercury. The basic mercury volume consists of the half sphere at the bottom of the trough (=0.45 cm^3), the cylinder (=1.36 cm^3) and the meniskus (=0.067 cm^3). This is in total a volume of V=1.877 cm^3 (see principal sketch in fig. 7.40). At the front and the back there the chamber is closed with an observation window, mounted via a flange. The front view of the chamber, the side view and a cut of the chamber can be seen in fig. 7.39.

Before the experiment was performed, the chamber was evacuated and the valve at the small flange was closed. There was no permanent vacuum pump. The underpressure was very slight (in the range of a few 100 mbar).

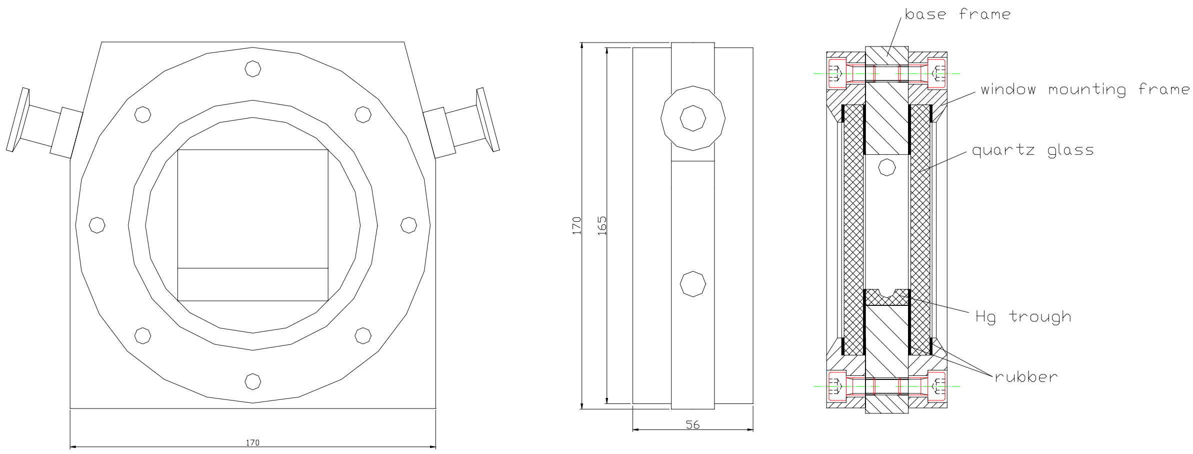

Figure 7.39: Drawing Experiment Chamber "Hg Trough"

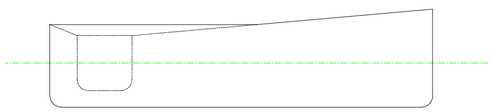

Figure 7.40: Principal Sketch Hg Trough

Fig. 7.41 shows the complete setup of the "Hg trough" chamber. The two big flanges are the beam entrance window on the left and the beam exit window on the right. The small flange on the left and the valve with the flange on the right are for evacuating the chamber and possibly distill the irradiated mercury after the experiment. In the front there is a charcoal filter which will be mounted after the valve to avoid Hg contamination of the vacuum pump.

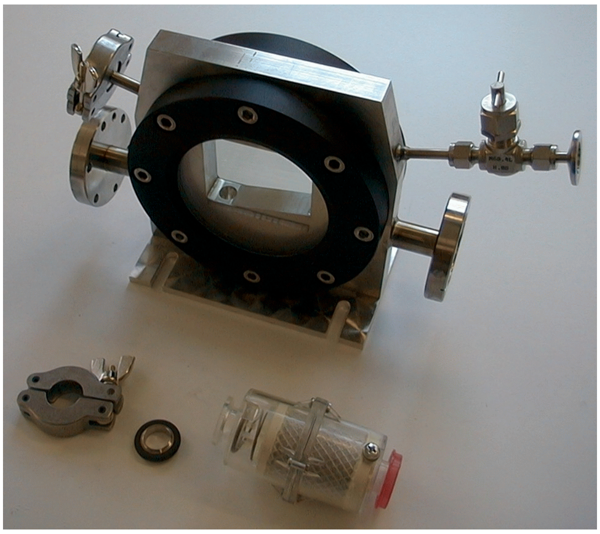

Figure 7.41: "Hg Trough" Experiment Chamber

At the beam entrance and exit windows a vacuum beam channel was installed to put the setup in the AGS beam line (fig. 7.42).

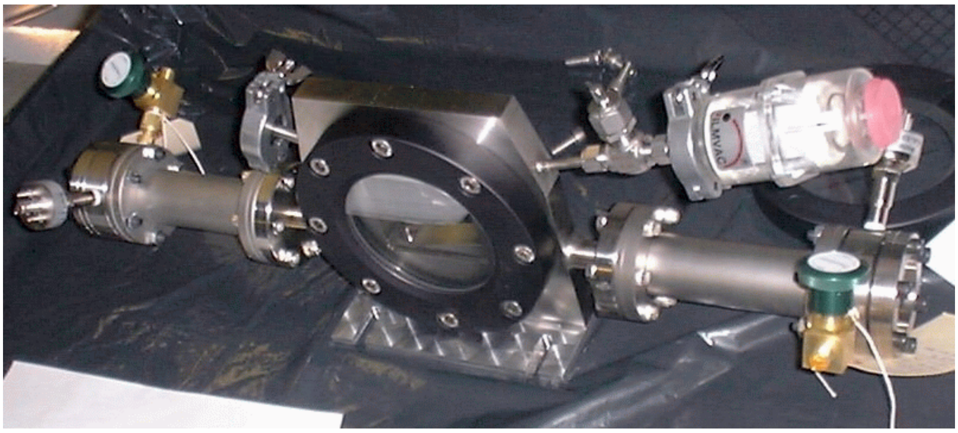

Figure 7.42: "Hg Trough" Experiment Chamber with Beam Channels

7.9.3 Results

Overview of Events

In table 7.11 the single experiment runs (events) are summarized. N_p gives the proton beam intensity (number of protons) in TP (Tera Protons = 10^{12} Protons).

A few single frames of the events are shown in figure 7.43. Each event represents the reaction of the mercury in the trough when hit by a single proton

Event #	1	2	3	4
N_p [TP]	0,6	1,75	3,3	3,7

Table 7.11: Experiment 3.0 - Events

pulse.

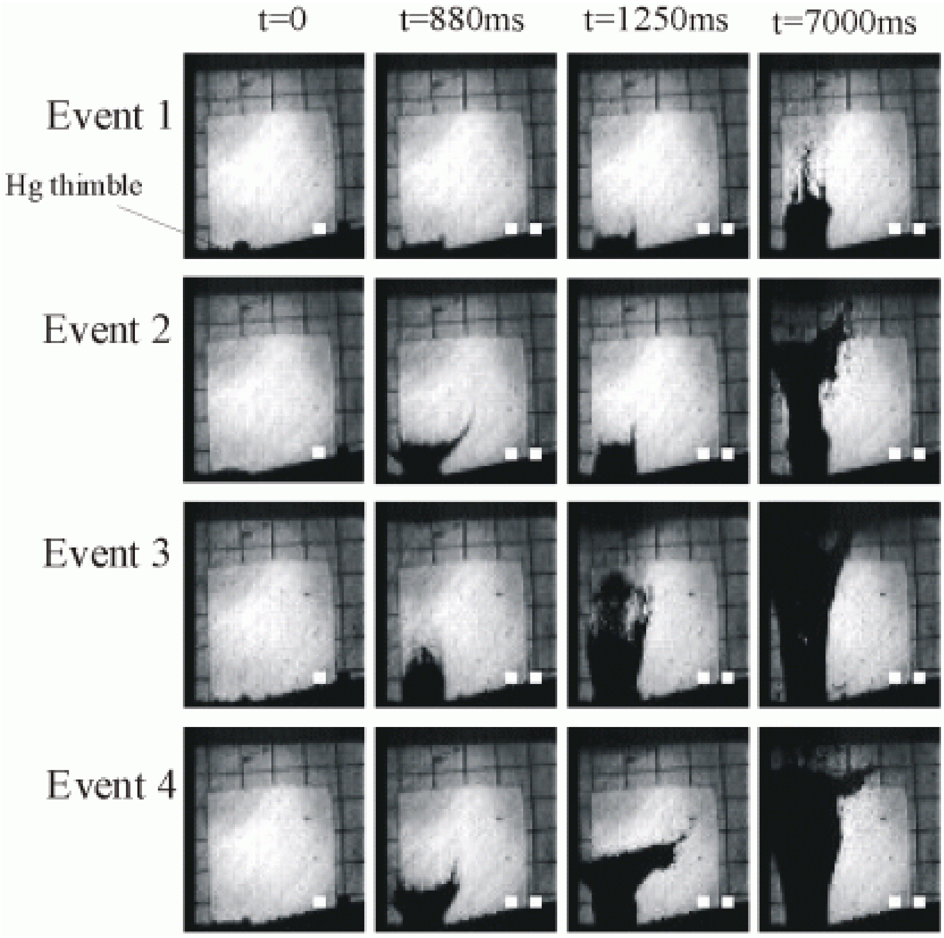

Figure 7.43: Experiment 3.0 - Example Pictures

As one can see, the deposited energy in the mercury deploys an imense force and the mercury is flinged out of the trough.

Event 1

meniscus-arms: overall 24,0$\frac{m}{s}$; start 32,0$\frac{m}{s}$

meniskus: 18,0; 12,9; 11,3; 5,2; 4,3$\frac{m}{s}$

start velocity: 18,8$\frac{m}{s}$

There is a cloud of mercury travelling much faster (at least 100$\frac{m}{s}$), but with the given spatial resolution it is only possible to guess it. The blocked area of the camera by the mercury is a section of 1cm x 7,2cm. Equally distributing the amount of mercury over this area gives an average thickness of 0,15mm. Or if distributed over a cylindrical shape, the column has a radius of 0,28cm. There is no explanation for these surprising numbers. From this measured areas it might be possible to estimate the remaining mercury in case of the events 2 and 3.

Event 2

start velocity: 7,8$\frac{m}{s}$

start meniskus: 5,8; 5,0; 4,2$\frac{m}{s}$

Event 3

meniskus-arms: 29,4; 18,1; 23,0; 16,4; 20,6; 12,5; 23,8; 22,0; 12,5; 18,3$\frac{m}{s}$

meniskus: 23,6; 24,2; 25,5; 6,7; 7,2; 7,7; 3,2$\frac{m}{s}$

Again, there could be observed a cloud of mercury travelling much faster (at least 100$\frac{m}{s}$).

start velocity: 27,3$\frac{m}{s}$

Event 4

meniskus: 22,0; 15,4; 16,8; 21,0; 23,1; 18,9; 25,9; 15,4; 24,4; 25,9; 19,6; 15,5; 19,6; 22,5$\frac{m}{s}$

meniskus 2: 12,6; 14,0; 6,0, 8,5; 10,6$\frac{m}{s}$

body: 6,3; 6,8; 7,0; 7,5$\frac{m}{s}$

start: 15 and 41$\frac{m}{s}$; because the thimble was not full, so less mass has been to accelerate.

In figure 7.44 are summarized the measured velocities. The four graphs show the relation of the beam energy and the perpendicular velocity of the "exploding" mercury. The graphs "full/not full thimble, start" represent the expanding velocity at the beginning of the expansion right after the proton beam impact. The main graphs represent the main value of the measured velocities over the whole expansion process.

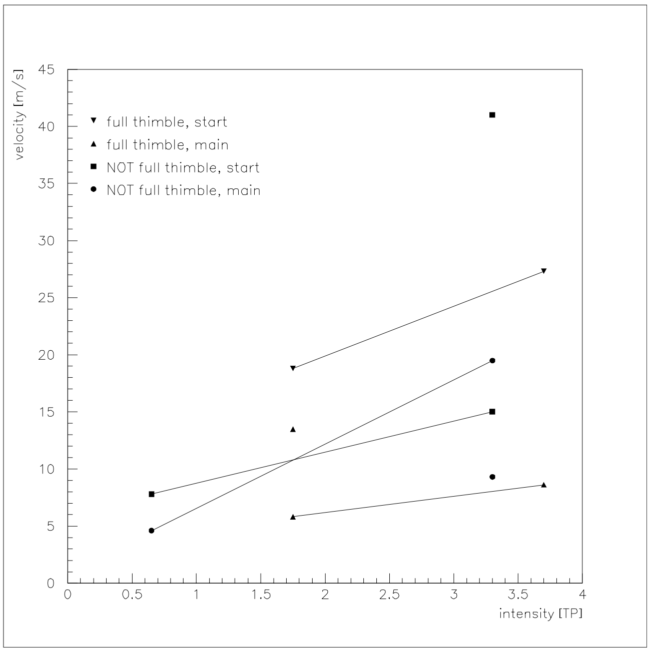

Figure 7.44: Experiment 3.0 - Measured Velocities vs. Proton Beam Energy

7.10 Experiment 3.1 - Mercury Jet in Proton Beam (BNL)

7.10.1 Experiment Setup

The continuos jet was ejected from a cylindrical nozzle (diameter 1 cm). The angle between horizontal plain and nozzle is 14,5°. The jet was observed with the above mentioned CCD camera.

The experiment setup exists as shown in figure 7.45 of a chamber or the ”mercury confinement”, which encloses the mercury jet, a mercury delivery tank of 2 liters capacity and some valves and tubes. To produce a jet, driving pressure (4,2bar) is applied to the delivery tank and the jet valve is opened. The mercury is driven through the nozzle and the jet establishes inside the mercury confinement, where it is collected in a sink. After shooting a jet, the jet valve is closed, the driving pressure is reliefed from the delivery tank and the mercury is recovered out of the confinement by applying a pressure to the confinement and opening the valve to the delivery tank. Then the mercury flows back into the tank.

The jet velocity was measured from three initial runs without proton impact and is stated as $2{,}51 \pm 0,13\frac{m}{s}$.

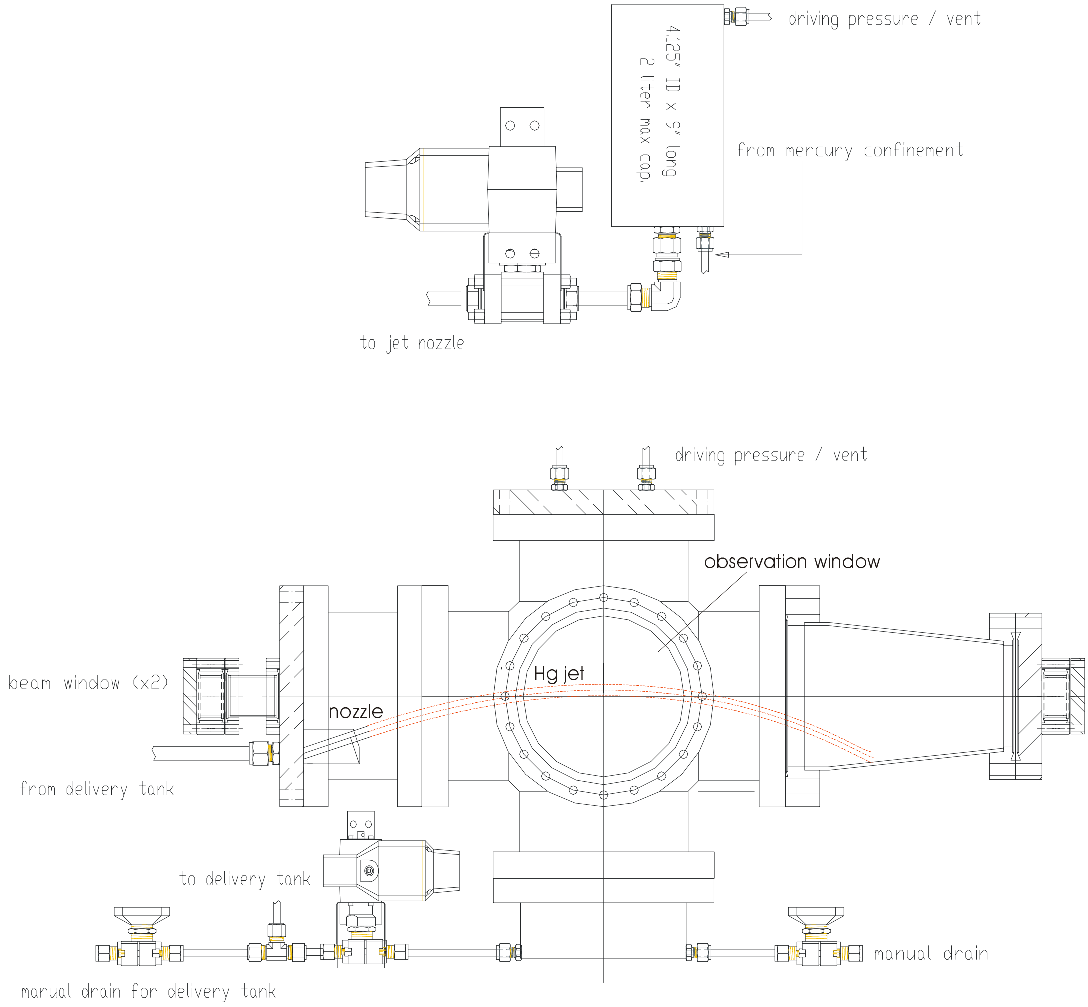

Figure 7.45: Experiment 3.1 - Setup

Figure 7.46 is a photograph of the setup as descriped above. On the left hand side one can see the beam entrance window, on the front there is the observation window, on the bottom the mercury sink and on the right hand side there is the mercury delivery tank.

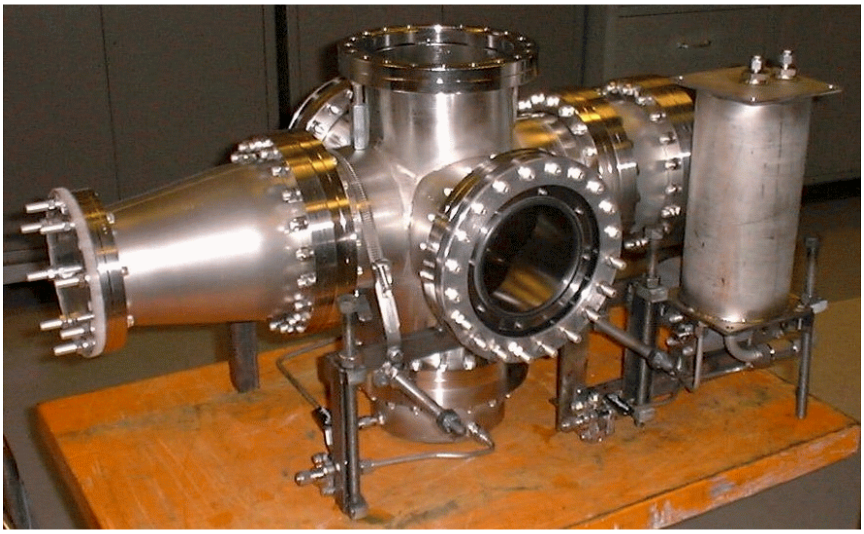

Figure 7.46: Photograph of Experiment 3.1 Setup

7.10.2 Observation Concept

Figure 7.47 shoes the principle of the observation setup. The illumination was setup with a 2mW laser, which was ran at 51,2mA, which corresponds to approx. 75% of the maximum ouput. The laser beam is fiber-coupled into the radiological controlled area where it is diverged at a full opening angle of 23° at the fiber output end. A lens then collimates the diverged light to an area of 150mm in diameter and illuminates the experiment setup. From the other side the camera is directed towards the experiment setup. A zoom lens was used. The distance between camera-target-illumination was 9 and 3m. The record rate was 4000 frames/s and the shutter was set to 1/40000 s. The lens aperture was set to maximum open. The errors resulting from the shutter time (~0,25 mm) is by far smaller than the spatial resolution (0,89 mm/pixel).

A trigger signal (tuned with the proton pulse) is delivered to the camera and a gage board installed in a PC located near the setup. The gage board generates a 16-pulse train per proton bunch. Each pulse has 0.5 microsecond duration in one microsecond period. The electrical pulse train is then used to trigger the Avtech current pulser. The laser diode is driven by an Avtech current pulser. This pulser is controlled by a LabView interface via an IEEE bus and is triggered by the gage board. The local PC is remote controlled by a second PC outside the beam-line area.

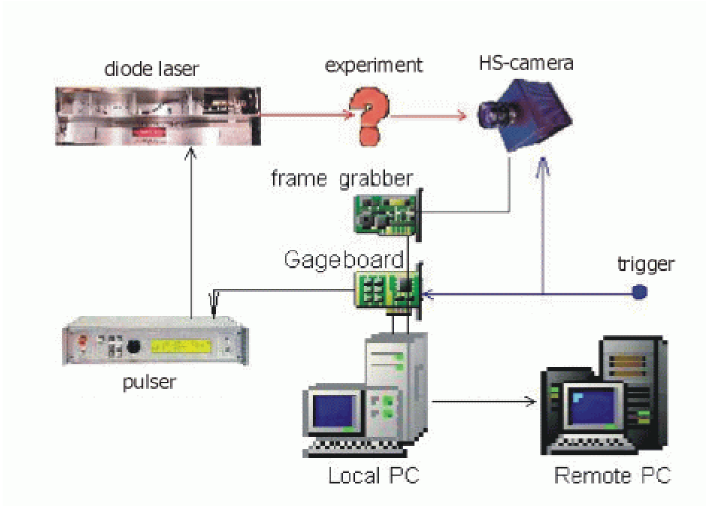

Figure 7.47: Experiment 3.1 Observation Setup

A typical basic view of the camera can be seen in Figure 7.48. The outer circle which limits the view area is caused by the camera and the illuminated cross section. The shadow ring at the outer line of the view area shows the grid which is printed on a transparency and placed on the viweing windows of the jet chamber. It indicates a 1cm grid. The lightest inner part has a diameter of approx. 7cm.

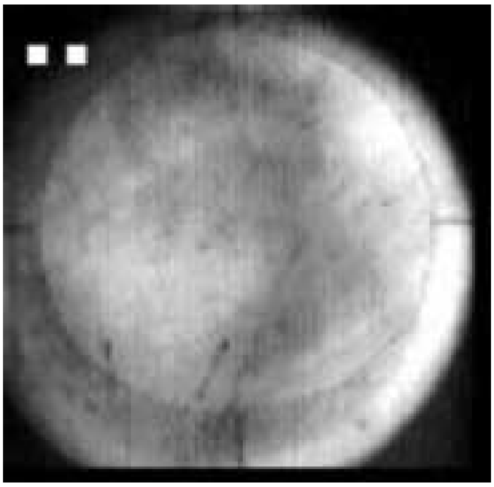

Figure 7.48: Basic View by the Camera

Event #	01	02	03	04	05	06	07	08	09	10	11
N_p [TP]	0	0	0	3,8	3,8	0,8	1,0	2,1	2,1	3,0	2,74

Table 7.12: Experiment 3.1 - Events

7.10.3 Results

Overview of Events

In table 7.12 the single experiment runs (events) are summarized. N_p gives the proton beam intensity (number of protons) in TP (Tera Protons = 10^{12} Protons).

Region of Interaction

It is possible to estimate the complete region of interaction of the proton beam with the mercury jet. As the the destroyed jet travels past the viewing wndow of the camera, the complete action can be estimated only to a certain level. Furthermore it is possible to estimate, wether the shock wave is travelling back inside the jet towards the nozzle.

Velocities

There are several groups of velocoties,which can be measured. These split up in maximum speeds of droplets and bulk, measured at the very beginning, so shortly after proton impact and measured after a relatively large time delay, where they might have slowed down by fricition. The different groups of velocities are allocated to classes 1 - 4.

Classes
class 1: drops at very beginning
class 2: bulk at very beginning
class3: drops later
class4: bulk later

With Event 04 (figure 7.49) an example is showed with the different gropups, where the velocoities are measured ($t_0 < t_1 < t_2 < t_3$). There is indicated the

bulk expansion (red lines) and the drops (green points).

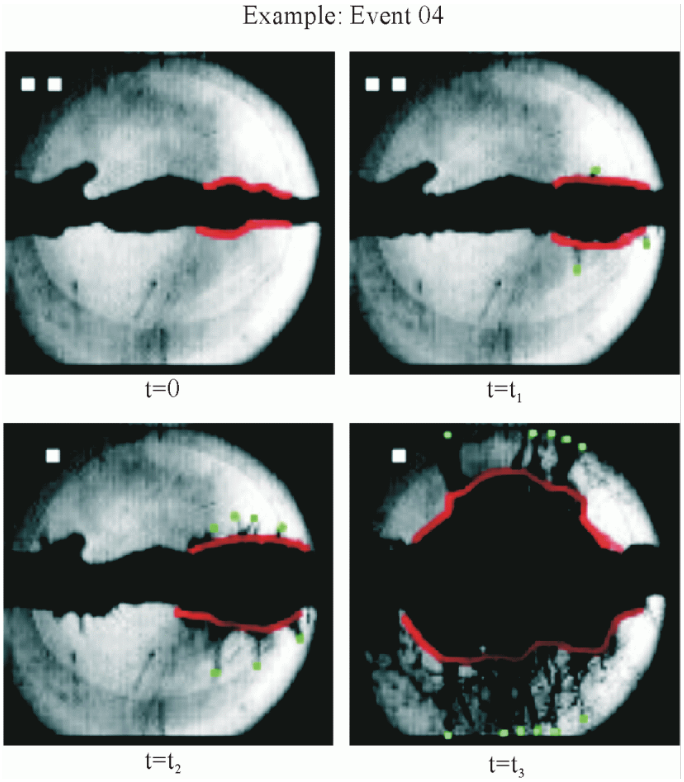

Figure 7.49: Experiment 3.1 - Example Pictures

For measuring the velocities only the highest ones were taken, as they can be assumed to be the ones flying perpendicular to the viewing direction.

The measured quantities are velocity (class 1-4), interaction area and offset of the droplet time (start-end).

Event 06

Event 006 and 007 are very similar, not only from the number of protons per bunch. The disruption of the jet is almost negligible. The main part (99%) stays on the initial trajectory (initial width of jet 1,3 cm). Only a few threads are ejected from the jet and decay quickly into droplets (see figure 7.50). The first move of the mercury surface due to the proton impact is seen at the same time as in all other events, of course with the given time resolution of the camera.

The measured velocities are 8,5; 16,8; 5; 9,1 and 6,1$\frac{m}{s}$. They are all of the first type. There are no effects of class 2, 3 and 4 to see. Most reasonable velocity is about 8m s. This is learned from a very gerous measurement. The length of the affected area is approx. 4,5cm along the mercury jet (offset -1,1cm).

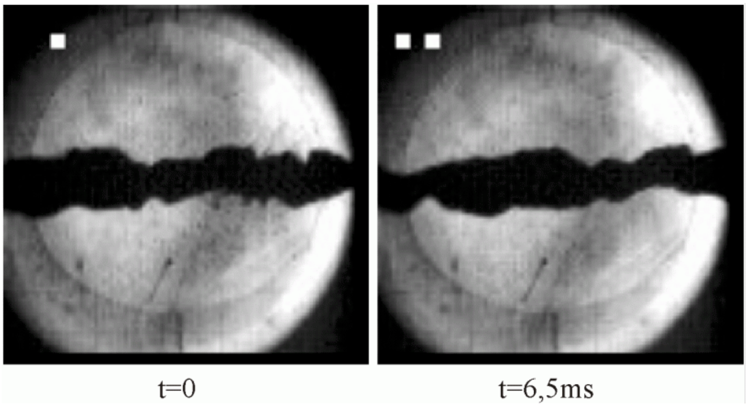

Figure 7.50: Experiment 3.1; Event 06: Mercury Jet after t=0 and t=6,5ms after Proton Beam Impact at 0,8 TP

Event 07

Most resenable velocity is about $8\frac{m}{s}$.

The length of the affected area is approx. 4,7cm along the mercury jet (offset 1,3 cm).

Event 08

class 1: 14,9; 12,5; 9,6; 8,7; 11,5; $4{,}7\frac{m}{s}$

class 2: $2{,}6\frac{m}{s}$

class 3: $0{,}5\frac{m}{s}$

class 4: 4,5; $4{,}9\frac{m}{s}$

The length of the affected area is approx. 5,6cm along the mercury jet (offset 2,6cm).

From this movie it could be learned, that the possible travelling wave does not affect the following jet.

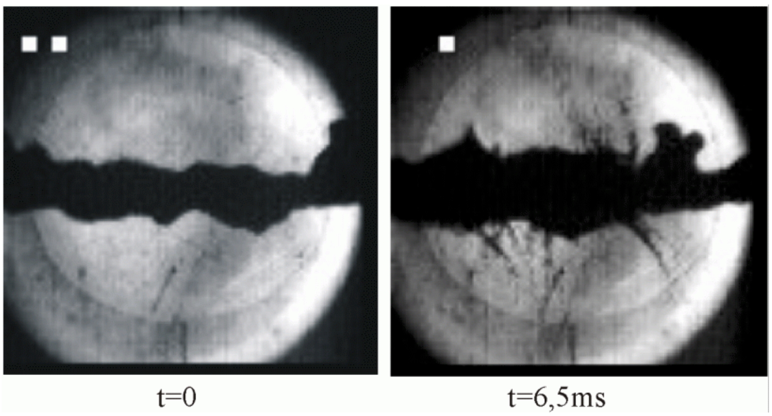

Figure 7.51: Experiment 3.1; Event 08: Mercury Jet after t=0 and t=6,5ms after Proton Beam Impact at 2,1 TP

Event 09

initial width 0,8 -1,3cm of mercury jet.

class 1: 15,4; 10,3; 17,5; 11,3; 12,2; 13,8; 17,8; 12,7$\frac{m}{s}$

class 2: 1,9; 1,2$\frac{m}{s}$

class 3: 2,3$\frac{m}{s}$

The length of the affected area is approx. 11,1cm along the mercury jet (offset 1,7cm).

Ii looks like that the explosion direction tends to be alsways perpen-dicular to the surface.

In this movie one can very good verify, where the beam line have been.

Event 10

initial width 1,3cm of mercury jet.

class 1: 5,9; 5,7$\frac{m}{s}$

class 3: 1,2$\frac{m}{s}$

The length of the affected area is approx. 5,1cm along the mercury jet (offset 3,5cm).

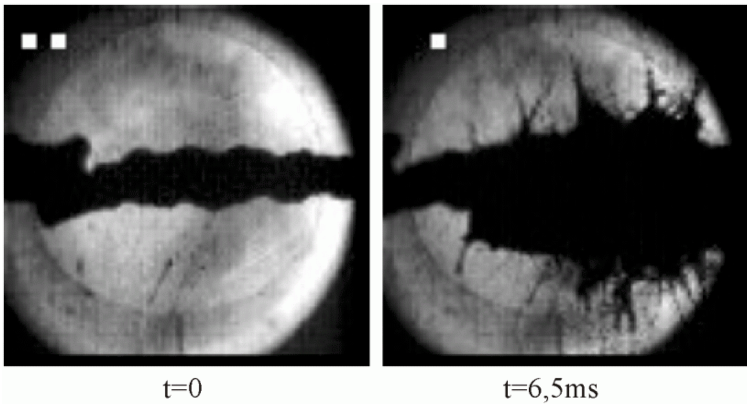

Figure 7.52: Experiment 3.1; Event 10: Mercury Jet after t=0 and t=6,5ms after Proton Beam Impact at 3 TP

Event 11

initial width 0,8 -1,3cm of mercury jet.

class 1: 7,0; 16,1; 19,6; 11,.9; 8,4; 10,6$\frac{m}{s}$

class 2: 6,4$\frac{m}{s}$

class 3: 7,7$\frac{m}{s}$

class 4: 2,8; 1,2$\frac{m}{s}$

Hard to measure as the interaction point is in front of the visible area.

The length of the affected area is approx. 8,9cm along the mercury jet. In this video it looks like if there is possibly a pressure wave travelling back.

Event 004

initial width 0,6 -1,5 cm of mercury jet.

class 1: 20,0; 12,3; 12,2$\frac{m}{s}$

class 2: 4,7; 10,8$\frac{m}{s}$

class 3: 21,3; 10,5$\frac{m}{s}$

class 4: 2,1$\frac{m}{s}$

The length of the affected area is approx. 8,3cm along the mercury jet (offset 2,1cm; here it looks also like if there is possibly a pressure wave travelling back).

It seems that thinner (0,6 -0,7cm) parts of the jet are more affected than thicker (1,5 cm) parts.

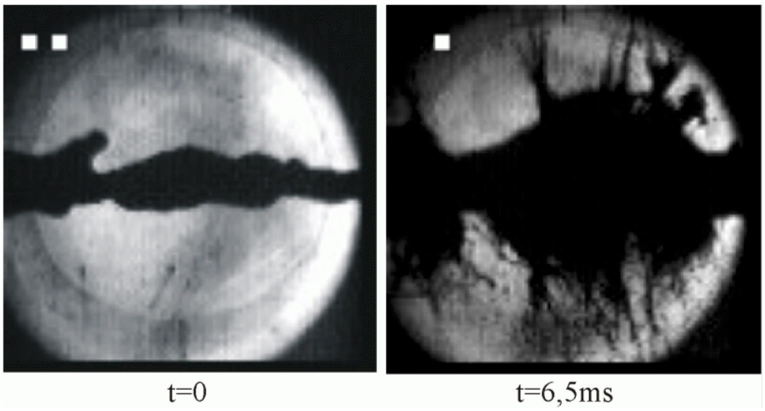

Figure 7.53: Experiment 3.1; Event 04: Mercury Jet after t=0 and t=6,5ms after Proton Beam Impact at 3,8 TP

Event 005

initial width 0,9 -1,4cm of mercury jet.

class 1: 47,0; 22,7; 24,0; 19,0; 10,1; 15,9; 20,1$\frac{m}{s}$
class 2: 6,9$\frac{m}{s}$
class 3: 5,5; 3,9; 4,5; 2,2$\frac{m}{s}$
class 4: 3,0$\frac{m}{s}$

The length of the affected area is more than 10cm along the mercury jet (offset bigger than 5 cm). The interaction length is not to determine as there are also parts exploding in the non visible area.

Summary

The graphs in figure 7.54 give the measured velocities versus the proton beam energy for the four classes. The measured maximal velocities seem to raise with the proton beam energy with a nearly linear propagation (exception class 4). The droplets reach a velocity of about 25$\frac{m}{s}$ at a beam intesity of 3,8 TP. The bulk expansion velocity reaches about 12$\frac{m}{s}$.

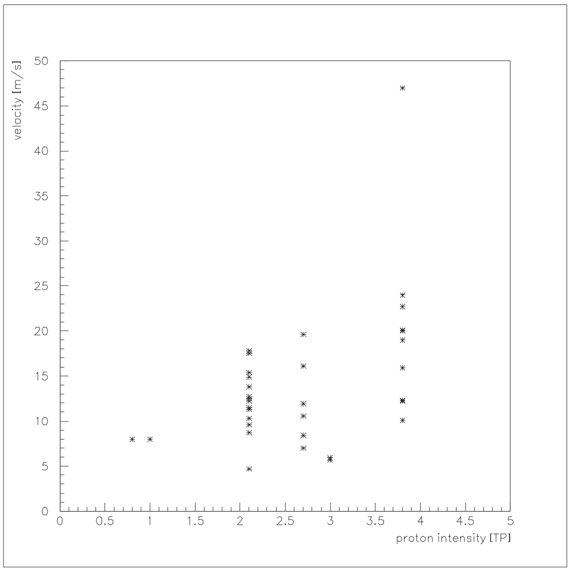

Class 1

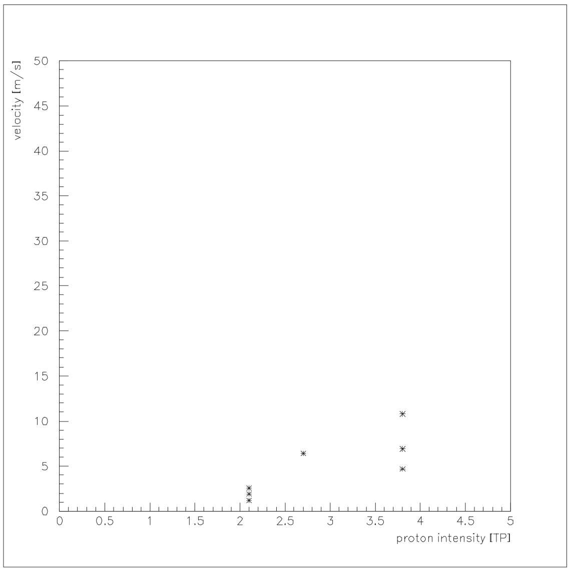

Class 2

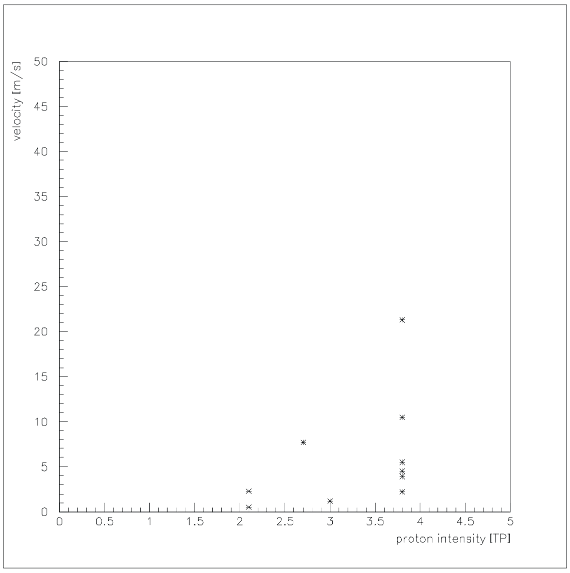

Class 3

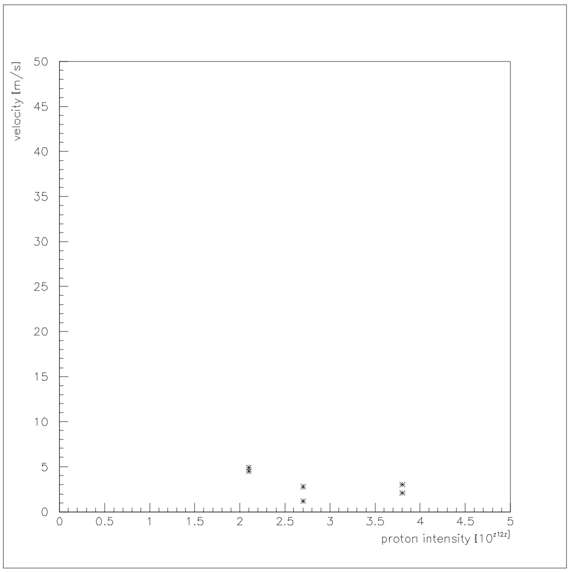

Class 4

Figure 7.54: Experiment 3.1 - Velocities vs. Proton Beam Energy

Figure 7.55 gives the interaction (destruction) length versus the proton beam energy. As the offset increases with higher energies, one could assume that a pressure wave propagates in the backward direction. But it is hard to say whether this effect is due to a pressure wave or initial disruption of the jet. The overall destruction length also increases slightly with increasing energy due to higher forces in longitudinal direction of the jet.

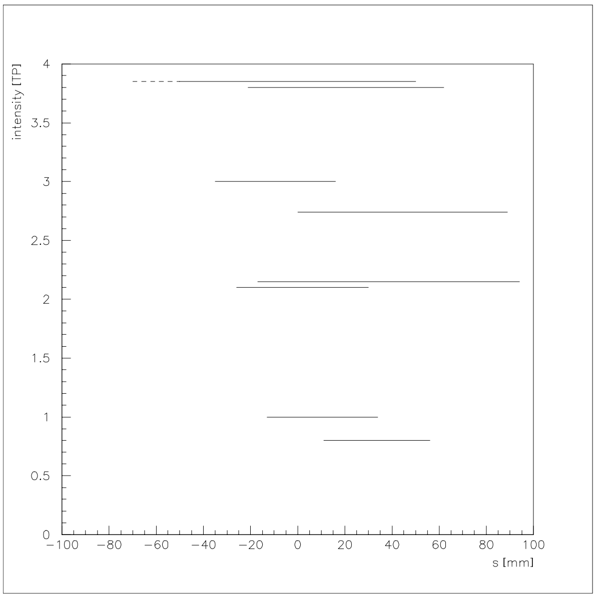

Figure 7.55: Experiment 3.1 - Interaction Length vs. Proton Beam Energy

7.11 Summary of Results

7.11.1 Effect of Magnetic Field

- The mercury jet is accelerated by the magnetic field.
- Instabilities on the surface of the jet are damped.
- The diameter of the jet is increased due to a concentration of droplets along the jet (side effect of the damping of the instabilites).

Consequences

The magnetic field seems to have no massive negative effect on the mercury jet. The acceleration of the jet probably will have to be took in account for the jet timing in the final neutrino factory target design.

7.11.2 Effect of Proton Beam Impact

In one sentence: The effect of the proton beam impact is not negligible. The energy (heat) deposition causes a rupture of the jet. Since the results of the experiment show that it is possible, that a pressure wave propagates downwards towards the nozzle, it seems almost unfeasible to realize a continuous jet which will be bombarded with repeated proton beam pulses. But the rupture of the jet will not affect following pulsed jet sections. What could be a problem is the collection of the mercury droplets which are catapulted away. To provide a collection device and to protect the surrounding solenoid or magnetic horn, the target will have to be contained in a confinement. But this confinement would stop a certain amount of secondary particles produced by the target. So the design of the target station will be a very challenging issue. Possible sollutions could be to make the confinement out of a material which stops only a few particles of to integrate the confinement into the solenoid or horn.

Chapter 8

Summary

The task of the present work was the investigation of effects of interaction with high magnetic fields and proton beam impact on liquid metals (in particular mercury). The application of such liquid metals should be a pion production target for a neutrino factory.

Such a neutrino factory is very desired by nuclear physisists in order to enable further exploration of the properties of neutrinos. A pion production target emits secondary particles when it is hit by a high energy proton beam. These particles (among others mainly pions) are then collected, directed into one direction and focused by an intense magnetic field. That is why the target (mercury) has to withstand the conditions of the energy deposition by the proton beam and the high magnetic field. Conventional targets, which are in operation today in the nuclear research centres, exist of solid materials like carbon or different metals. A further difference between the neutrino factory target and existing targets is the much higher energy load on the mercury induced by the proton beam.

Such a target has never existed before, so there is no experience in using liquid metals as a pion production target. It is assumed that a liquid target material will react completely different than a solid one, because the induced energy will cause pressure waves which could rupture the liquid and as a liquid metal, which conducts electricity, will be used also the magnetic field could influence the liquid. The liquid metal most likely will be provided by a pulsed jet. So there are several issues to be worked on.

There have allready been made some calculations to simulate the reaction of the liquid metal. The results show very interesting aspects of the behaviour of a liquid metal under such conditions. But some simulations yield results which differ from each other. Others are very uncertain due to simulation codes and methods which are not yet proven.

The description of the problems above results in the tasks which have been worked out. The main part consists of the preparation and the performance of several experiments. These experiments are one of the most important part of the Neutrino Factory Target Design project. The outcome of these experiments should prove the theoretical studies and show the feasibility of a liquid metal pion production target.

First a basic knowledge about the context of the project (basic nuclear physics) was gained. A very important issue was to obtain experience in handling mercury including studying the properties of mercury, work out saftey procedures for all further work with mercury and set up a mercury laboratory. Then the already existing simulations have been studied and summed up. Basic concepts for the experiments were developed and the required equipment and material were supplied. The experiments involved the following: Two different types of experiments, one for the proton beam experiment and one for the magnetic field experiment, were planed. For the proton beam experiment one setup to put some mercury at rest (in a thimble) in the line of a proton beam and one setup to produce a mercury jet and put this jet in the line of a proton beam were built. The magnetic field experiments also required two setups, to shoot a mercury jet into a solenoid with horizontal and one with a vertical bore. Detailed sketches and plans of all required parts for the experiment setups were made and the production of the parts was initiated and supervised. A major sub-task was to build an apparatus to provide a mercury jet. This apparatus was made using a piston pump (which equals a pressure tranmitter, which converts the pressure of compressed air into a 16 times higher pressure on the mercury) to force the mercury through a nozzle which in turn produces the mercury jet. The reaction of the mercury to the proton beam impact and the behaviour of the mercury jet in a magnetic field were observed by taking high speed videos. A special high speed CCD camera connected to a PC was used. Valuating the captured high speed video clips results in parameters like size and velocity of droplets escaping from the jet or even a impression what happens. The high speed video clips of the events were valuated using a software or by manual picture analysis. After the completion of the experiment setups, the experiments were performed successfully. Attending some of the experiments, collecting the data from the experiment results, valuating and summarizing them was among the tasks carried out as well as assessing the validity of the simulations and the consequences of the results for the final target design.

The experiments showed that the impacts on the mercury are within what was predicted by the simulations. The effects are very intense. But the extend of the influences are not that high that a neutrino factory based on a liquid metal target would be absolutely unfeasible. As it is forseen to operate the final target station with a pulsed mercury jet, the disruption of a jet segment by the proton beam impact will not affect the following jet segment.

There are further issues to be addressed in the ongoing R&D program. Among these are to develop an optimized nozzle design to produce more stable mercury jets, how to treat the irradiated mercury or to develop a setup to realize a pulsed mercury jet up to 75 Hz. In summary the present study represents a successful initial step which will be followed by the next steps towards a liquid metal target station and the overall goal, a neutrino factory.

Bibliography

[1] CERN Homepage, http://www.cern.ch

[2] http://pubweb.bnl.gov/people/gallardo/collaborationlist.ps

[3] http://www.physik.uni-erlangen.de/Didaktik/Grundl_d_TPh/SM_Et/SM_ET_01.html

[4] http://www.physik.uni-erlangen.de/Didaktik/Grundl_d_TPh/SM_Et/SM_ET_02.html

[5] http://na47sun05.cern.ch/target/fundamentalparticles.html

[6] http://www.physik.uni-erlangen.de/Didaktik/Grundl_d_TPh/SM_Et/SM_ET_Lep1.html

[7] http://wwwlapp.in2p3.fr/neutrinos/ankes.html

[8] Physics Review 105, 1413 (1957)

[9] C.M. Ankenbrandt et al., Status of Muon Collider Research and Development and Future Plans, Phys. Rev. ST Accel. Beams 2, 08001 (August 1992).

[10] B. Autin, A. Blondel, J. Ellis (Eds.), Prospective Study of Muon Storage Rings at CERN, CERN 99- 02, ECFA 99-197 (April 1999).

[11] S. Geer, Phys. Rev. D57, 6989 (1998).

[12] S. Geer and H. Schellman (editors) "Physics at a Neutrino Factory", Report to the Fermilab Directorate, FERMILAB-FN-692 (April 2000).

[13] N. Holtkamp and D. Finley (editors), A feasibility Study of a Neutrino Source Based on a Muon Storage Ring, FERMILAB-PUB-00-108-E.

[14] A. M. Sessler, Neutrino Factories: The Facility (Lawrence Berkeley National Laboratory, August 2000).

[15] H. Haseroth (for the Neutrino Factory Working Group), Status and Plans for a Neutrno Factory at CERN, CERN/PS 2000-026(PP).

[16] MUCOOL Notes http://www-mucool.fnal.gov/notes/notes.html

[17] P. Thieberger, Estimated perturbations of the axial motion of a liquid-metal jet entering a strong magnetic field (BNL, November 2000)

[18] http://www.cap.bnl.gov/mumu/studyii/talks/lebedev.pdf

[19] P. Sievers and P. Pugnat, Response of Solid and Liquid Targets to High Power Proton Beams for Neutrino Factories, CERN-NuFACT Note 035

[20] N. Hotekamp and D. Finley, A Feasibility Study of a Neutrino Source Based on a Muon Storage Ring (2000).

[21] J. Allesi at al., An R&D Programe for Targetry and Capture at a Muon-Collider Source – A Proposal to the BNL AGS Division (1998).

[22] G.S. Bauer, ESS Liquid Metal Target Studies, ESS 95-33-T (Oct. 1995).

[23] G.S. Bauer, Mercury as a Target Material for Pulsed (Fast) Spallation Neutron Sources, ICANS-XIII, PSI-Proceedings 95-02 (Oct. 1995), p. 547.

[24] B.R. Appleton and G.S. Bauer, Proc. Int. Workshop on the Technology and Thermal Hydraulics of Heavy Liquid Metals (Hg, Pb, Bi and Their Eutectics), (Schruns, Austria, Mar.1996), ORNL CONF-9603171 (June 1996).

[25] T.A. Broome, High Power Targets for Spallation Sources Proc. EPAC96 (Sitges, Spain, 1996), p. 267; http://www.cern.ch/accelconf/e96/PAPERS/ORALS/TUY04A.PDF

[26] T.A. Gabriel et al., The National Spallation Neutron Source Target Station: A General Overview, Proc. PAC97 (Vancouver, 1997), p. 86; http://www.triumf.ca/pac97/papers/pdf/2B012.PDF

[27] Target Systems, Chap. 5 of the National Spallation Neutron Source Conceptual Design Report (NSNS/CDR-2, May 1997); http://www.ornl.gov/~nsns/CDRDocuments/CDRSections/Sect5.pdf

[28] J.R. Haines, Comparison of Liquid and Solid Targets for Pulsed Spallation Neutron Sources, ORNL report NSNS/TSR0009 (July 1997).

[29] J.A. Hassberger, Flowing Liquid Lithium Target, in[48], p. 12.

[30] R.J. Stefanski, A Study in Target Design, in [48], p. 41.

[31] Feasibility Study into the Development of a Liquid Metal Pulsed Current Target for ACOL, Report No. C2365/F, Contract No: R/785.985/PS/AA (Cambridge Consultants Ltd., Cambridge, U.K., 1985).

[32] Z. Tang and K. Anderson, Shock Waves in p Target Fermilab/TN-1763 (Nov. 1991).

[33] K. Skala and G.S. Bauer, On the Pressure Wave Problem in Liquid Metal Targets, ICANS-XIII, PSI-Proceedings 95-02 (Oct. 1995).

[34] D.A. Wilson, J.W. Hoyt and J.W. McKane, Measurement of tensile strength of liquids by an explosion technique, Nature 253 , 723 (1975).

[35] R.P. Taleyarkhan, S.H. Kim and J.R. Haines, Modelling & Analysis of AGS Thermal Shock Experiment, ORNL report.

[36] R.P. Taleyarkhan, F. Moraga and C.D. West, Experimental Determination of Cavitation Thresholds in Liquid Water and Mercury, Proc. 2nd Int. Topical Meeting on Accel. Applications, AccApp'98, (Gatlinburg, TN, Sept. 1998); ORNL report.

[37] R.P. Taleyarkhan et al., Results of Thermal-Shock Modeling & Analyses for the National Spallation Neutron Source, inProc. Topical Meeting on Nuclear Applications of Accelerator Technology, (Albuquerque, NM, Nov. 1997), p. 293.

[38] L. Ni and G. Bauer, Dynamic Stress of a Liquid Metal Target Container under Pulsed Heating, PSI report (1998); http://puhep1.princeton.edu/mumu/target/bauer/1.html

[39] J.R. Haines, A simple Figure of Merit for Comparison of Thermal Shock Capabilities of Candidate Target MAterials, ORNL Report NSNS/TSR5 (Mar. 3, 1997).

[40] D.H. Trevena, Cavitation and Tension in Liquids (Adam Hilger, Bristol, U.K., 1987).

[41] F.R. Young, Cavitation (McGraw-Hill, New York, 1989).

[42] T.G. Leighton, The Acoustic Bubble (Academic Press, San Diego, 1994).

[43] A. Kovacs, Estimating the Full-Scale Tensile, Flexular and Compressive Strength of First-Year Ice, CRREL Report 96-6 (Sept. 1996), Fig. 9; http://www.crrel.usa.ce.army.mil/techpub/CRREL Reports web/reports/CR96 11.pdf

[44] L. Briggs, Limiting Negative Pressure of Water, J. Appl. Phys. 21 , 721 (1950).

[45] J. Lettry et al., Experience with ISOLDE Molten Metal Targets at the CERN-PS Booster, in Proceedings of ICANS-XIII (1995); http://puhep1.princeton.edu/mumu/target/

[46] G.I. Silvestrov, Liquid Metal Jet Targets for Intense High Energy Beams, Budker Institute preprint (Aug. 1998); http://puhep1.princeton.edu/mumu/silvestrov/jet silvestrov.pdf

[47] R.N. Lyon (ed.), Liquid Metals Handbook, 2nd ed., NAVEXOS-P.733 (June 1952, revised 1954); Liquid Metals, inReactor Handbook, 2nd ed., C.R. Tipton, Jr., (ed.), Interscience, New York, 1960), p. 994.

[48] C. Lu and K.T. McDonald, Low-Melting-Temperature Metals for Possible Use as Primary Targets at a Muon Collider Source, Princeton/ /97-3 (1998); http://puhep1.princeton.edu/mumu/mumu-97-3.ps

[49] R. Weggel, Behavior of Conducting Solid or Liquid Jet Moving in Magnetic Field: 1) Paraxial, 2) Transverse, 3) Oblique, CAP-220-MUON-98R (1998).

[50] J. Walker and W.H. Wells, Drag Force on a Conducting Spherical Drop in a Nonuniform Magnetic Field, ORNL/TN-6976 (Sept. 1979).

[51] Lewis, R.J. 1993. Hawley's Condensed Chemical Dictionary. 12th ed. New York: Van Nostrand Reinhold Co.

[52] Rom, W.N. ed. 1992. Environmental & Occupational Medicine. 2nd ed. Boston: Little Brown and Company.

Appendix A

Content Appendix

A.1 1. HAZOP Study

A.2 2. Operating Instruction Jet Test Setup

CERN/TIS/GS/TM/2001-01

EUROPEAN ORGANIZATION FOR NUCLEAR RESEARCH

HAZOP STUDY OF MERCURY IN MAGNETIC FIELD EXPERIMENT

J. D. Gulley, C. W. Nuttall and D. Schaffarzick

CONTENTS

SUMMARY

In total 40 recommendations were made in the study. The results of the HAZOP study are shown in Section 4 of the report with a complete listing of the HAZOP minute sheets given in Appendix I. A description of the HAZOP technique can be found in Appendix II.

1. INTRODUCTION

This report discusses the conclusions of the Hazard and Operability (HAZOP) study of the Mercury in Magnetic Field Experiment. The original flow chart used for the HAZOP study is shown in Figure 1. The Flow Chart with the modifications resulting from the study is shown in Figure 2. These diagrams are only intended to show the flow of materials between the different items of equipment. They do not represent the geographical location of the different equipment in relation to each other. Other drawings showing details of the equipment used in the experiment are included in Appendix III. Appendix IV is an equipment schedule containing details of the experimental equipment whilst Appendix V gives further details on the Nordson piston pump and ball tip valve used in the experiment.

For the HAZOP study the process was divided up into sections (called nodes) which are then studied using the HAZOP technique. The nodes considered are listed in section 2.

Finally a material safety data sheet for mercury is given in Appendix VI.

2. SCOPE

The purpose of this study was to identify potential hazards or operability problems with the process that had not previously been recognised. The process was divided up into 5 nodes. These are listed below:

1. Mercury Reservoir
2. Mercury Reservoir to Experiment Chamber
3. Experiment Chamber
4. Argon gas purge line to Experiment Chamber
5. Compressed air system

3. DESCRIPTION OF EXPERIMENT

This experiment will be used to study the response of a mercury jet injected into a magnetic field. Measurements of the jet formation/deformation and timing of the jet will be made by using a high-speed video. In order to be able to "see" what happens inside the bore of the magnet, a fibrescope, which guides the pictures to the high-speed camera, will be used.

The main parts of the experimental setup are the NORDSON 25B piston-pump, the NORDSON A7A ball tip valve, an injection nozzle, an experiment chamber and a Mercury reservoir. The air driven pump sucks the mercury out of the Mercury reservoir and pressurizes it. On the high-pressure output line from the pump is a ball tip valve which when triggered (by compressed air) directs the jet through the nozzle into the experiment chamber. From there the mercury flows back into the reservoir by gravity.

The experiment chamber is designed to a high level of safety to prevent mercury escaping from the system. It is an airtight rectangular Plexiglas chamber surrounded by a Plexiglas tube that fits into the bore of a magnet. This tube is an additional protection if the inner chamber leaks. In principle it too is airtight, but there are two feedthroughs at mid-height through which the fibrescope and the light guides for illumination will be placed. These "holes" are closed by rubber with an "x-cut" to provide protection if the inner chamber leaks.

The rear side of the inner chamber, where the mercury jet hits the wall is shaped in such a way that the jet will be deflected and flow back into the reservoir as fast as possible.

There is a secondary housing containing all the plumbing as well as the flexible high-pressure hoses, the hose for the back flowing mercury from the experiment chamber and the trigger valve.

The experiment chamber will be flooded with argon to prevent oxidization of the mercury. For this purpose there is a connection point mounted to the experiment chamber. A flow control valve and flow indicator will be installed on the argon line.

Before performing the experiment with mercury, a bottle of argon will be connected and the experiment chamber will be flooded. The gas flows via the hose for the back flowing mercury to the mercury reservoir. There is an additional pipe connected to the reservoir, which leads out of the safety housing. This pipe can be used for evacuating the reservoir if the experiment chamber is located lower than the mercury reservoir to pump the mercury back into the reservoir. The air exits through this pipe, when the experiment chamber and the mercury reservoir are flooded with argon.

4. RESULTS OF HAZOP STUDY

The complete results of the HAZOP study are shown in Appendix I. In total 40 recommendations were made in the study. Those concerning the design of the experiment are shown in Table 4.1. Recommendations concerning maintenance and inspection/testing of equipment are shown in Table 4.2, whilst those regarding administrative safeguards (e.g. operating procedures) are given in Table 4.3. General safety recommendations are listed in Table 4.4.

Table 4.1 – Recommendations from HAZOP Study (Design)

RECOMMENDATION (and No.)	REF.
7. Consider having all lines in stainless steel.	Node 1, Page 2.
10. To reduce vibration in pump adversely affecting reservoir consider damping and use of flexible line between reservoir and pump.	Node 1, Page 2.
19. Consider connecting hose and box such that fan draws air from entire system. Remove line I. Opening to atmosphere on safety hose (sized to relieve possible supplied air). Check whether there is a need, based on the size of the fan, for either a safety bubbler or a hinged/flap valve on box such that air enters system if low pressure in box.	Node 1, Page 8.
23. Remove manual valve V3 from system.	Node 1, Page 8.
25. Ensure clean, dry, filtered compressed air is used.	Node 1, Page 8.
29. Choose a valve with a high reliability for V4.	Node 2, Page 13
32. Set Safety Relief Valve V7 to operate at a safe pressure below chamber design pressure.	Node 3, Page 15
37. To ensure redundancy, have pressure regulator S1 reduce the pressure to the safe operating pressure of the pump then regulator R2 will be used to adjust/reduce the pressure still further.	Node 5, Page 17
38. Set the operating pressure of Safety Relief Valve V6 to operate well below the maximum safe operating pressure of the pump is reached.	Node 5, Page 18

Table 4.2 – Recommendations from HAZOP Study
(Maintenance and inspection/testing of equipment)

RECOMMENDATION (and No.)	REF.
4. Ensure mercury detector is calibrated before start-up.	Node 1, Page 1.
5. All lines to be cleaned using non-degrading techniques.	Node 1, Page 2.
9. Mechanical support to be tested beforehand (for maximum weight of mercury than can be delivered).	Node 1, Page 2.
17. Inform Fire Brigade and carry out an inspection with Fire Prevention Section beforehand (for both experimental locations).	Node 1, Page 6.
18. Set Safety Relief Valve at a safe pressure below the design pressure of the reservoir. Test pressure of reservoir with Mechanical Section of TIS.	Node 1, Page 7.
22. Establish maintenance schedule for filters.	Node 1, Page 8.
24. Check with Mechanical Section/TIS whether reservoir can withstand vacuum. If it cannot install a vacuum breaker on reservoir.	Node 1, Page 9
27. Pressure test lines with Mechanical Section of TIS.	Node 2, Page 13
30. Ensure that pressure reducers and safety relief valves have been tested by TIS. Establish a maintenance schedule if necessary.	Node 2, Page 13

Table 4.3 – Recommendations from HAZOP Study (Administrative Safeguards)

RECOMMENDATION (and No.)	REF. (and Notes)
1. Ordering procedures to be established.	Node 1, Page 1.
2. Establish a filling procedure that mentions the need to maintain a watch of experiment during initial cycle and at intervals thereafter. Establish a logbook for recording comments.	Node 1, Page 1.
3. During filling switch mercury detector manually between box and hose to check for leaks (Filling Procedure).	Node 1, Page 1. See also Recommendation 21, which if adopted will affect this Recommendation.
5. Ensure good quality mercury is ordered.	Node 1, Page 1.
6. When experiment not in use set mercury detector to measure in ambient air.	Node 1, Page 2.
8. Experimental apparatus is never to be left unattended (include in operating procedures).	Node 1, Page 2.
11. Decontamination and Emergency procedures need to be established (Collect leaks or waste in non-metal containers).	Node 1, Page 3.
12. Operating Procedures to include a method for easily removing excess Mercury from system.	Node 1, Page 3.
13. An Emergency Shutdown procedure needs to be drafted.	Node 1, Page 4.
26. Include check in start-up procedure and after maintenance to ensure fan is connected the correct way around	Node 1, Page 10
28. Establish a troubleshooting checklist for this scenario, which may prevent the need to dismantle the apparatus.	Node 1, Page 13
31. Shut-Down procedure to state that compressed air pressure should be slowly reduced either: by use of pressure regulator and not by closing Valve V2; or by use of pressure regulator R1 and then closing valve V2.	Node 3, Page 14
33. Operator must continually monitor the image of the chamber on the screen (as a check that V4 is not failed open and chamber filling up).	Node 3, Page 15
34. It must be clear to the operator that shut-down in this instance must be very fast (see remark). Procedure must be prominently displayed.	Node 3, Page 15
39. Check valve V2 is open before start-up.	Node 5, Page 18
40. Establish a troubleshooting checklist for this scenario, which may prevent the need to dismantle the apparatus.	Node 5, Page 18

Table 4.4 – Recommendations from HAZOP Study (General Safety)

RECOMMENDATION (and No.)	REF.
14. Ensure a fire extinguisher is present.	Node 1, Page 5.
15. No smoking policy to be enforced. Place warning signs.	Node 1, Page 5.
16. Combustible materials in the vicinity of the experiment to be reduced to a minimum.	Node 1, Page 5.
35. Ensure safety relief valves are vented safely.	Node 4, Page 16.
36. Modify Flow Chart to show that C1 is a Flow Indicator, V5 is a Flow Controller.	Node 4, Page 16.

5. CONCLUSIONS

The main recommendations of the HAZOP study are summarized below.

1. For the design (Table 4.1), recommendations have been made regarding:

i.) Changes to the configuration of the containment hose and box;
ii.) Pressure regulators and safety relief of compressed air system; and
iii.) Mechanical design of equipment items.

2. The maintenance and testing of equipment items was determined to be critical and a number of recommendations were made (see Table 4.2).

3. Recommendations were made regarding the writing of procedures for ordering, filling/start-up, operating, shut-down, emergency shut-down and decontamination. Also troubleshooting checklists should be drawn-up. See Table 4.3.

4. Some general recommendations are also given in Table 4.4.

Operating Instructions Mercury Jet Setup

Contents

1. Purpose

This procedure describes the steps to prepare and operate the mercury jet setup for the mercury in magnetic field experiment

2. References

Mercury Material Safety Data Sheet MSDS Nr. M1599
International Chemical Safety Cards ICSC: 0056
Operating manual mercury vapor detector VM-3000
Operating manual Nordson 25B piston pump
Operating manual Nordson A7A spray gun

3. Precautions

All work must be carried out by persons, instructed and authorized to work with mercury.

4. Special Equipment

- Mercury vapor monitor
- Mercury spill collector or spill kit
- Protective gloves, safety glasses, light (disposable) breathing mask, respirator with mercury vapor filter, lab coat
- Funnel
- stainless steel or plastic tray

5. Prerequisites

- The setup has been tested by the mechanical section of TIS
- Make sure, the mercury vapor detector is working properly and calibrate it (see manual VM-3000).
- Inform TIS and fire brigade.
- The room temperature should not be above 20°C
- Remove all sources of fire and flammable materials from the vicinity.
- Place the mercury spill collector and breathing mask nearby.

6. Procedure Steps

<u>Note the section Procedures for Mercury Alarm</u>

Filling the Setup with Mercury

This procedure must only be done in the mercury laboratory (3-1-031). Wear protective clothing

1. Examine the setup (mercury pump, experiment chamber, connection lines) and look for any damages.
2. Place the mercury vapor detector nearby that you easily can read the display.
3. Switch on the fan.
4. Take two flasks (0.5l each) out of the mercury storage cupboard, put them in the fume cupboard and write the amount of mercury taken out in the list placed at the door of the mercury storage cupboard.
5. Remove the protective hose from its mount on the confinement box and then remove the Rilsan-tube for the backflowing mercury from the feedthrough fitting (the fitting in the center of the mount for the protective hose).
6. Put the funnel into the fitting and slowly pour 1l of mercury into the funnel.
7. Put the empty flasks into the tray in the fume cupboard. Remove the funnel and put it into the tray in the fume cupboard.
8. Install the Rilsan-tube again to the fitting and secure the security hose again.
9. Remove the cap from the T-piece at the tube for the air outlet of the confinement box and connect the inlet of the mercury vapor detector to the T-piece. Watch the display for about 30 seconds. If the display shows a level above 0.05 mg/m^3 → see section “Mercury Alarm”.
10. If the monitor doesn’t show any contamination inside the confinement box, disconnect the inlet of the mercury detector from the T-piece and close it with the cap again. Watch the display again, if there is any contamination in the ambient air. If the display shows a level above 0.05 g/m^3 → see section “Mercury Alarm”.

Startup Procedure

During the whole procedure do the steps 9 and 10 of the filling procedure

1. Examine the setup again.
2. Place the experiment chamber on a table (trolley) near the pump-box.
3. Plug in the plug for the power supply
4. Make sure that all pressure reducers are set to minimum pressure (knobs are in most counterclockwise position) and the shut off valve for the air motor of the piston pump is closed.

5. Flush the experiment chamber with Argon: Open the valve of the Argon bottle and set the first pressure reducer to 15 bar. Set the second pressure reducer to 50-100 mbar. Set the flow to about 2-5 l/min.
6. Connect the pressurized air supply
7. Set the pressure reducer for the trigger valve to 5 bar.
8. Trigger the mercury valve a few times and check if it operates properly.
9. Slowly open the shut off valve of the pump.
10. Manually trigger the valve with the switch and leave it open
11. Slowly turn the pressure reducer for the air motor clockwise until the piston starts to move.
12. Look if there is mercury escaping from the nozzle. If there is no mercury coming out → see section "Troubleshooting".
13. Slowly increase the pressure until about 2 bar. (Test procedure)
14. Decrease the pressure again (until the piston moves slowly) and wait until the piston reaches the uppermost position and the air valve of the air motor toggles (you can hear a loud "klick"). Then release the switch immediately.
15. Set the pressure reducer to 2 bar and then trigger the valve with the pulse generator (set to single pulse, 500 ms pulse width).
16. Repeat step 13 and 14 and increase the pressure by 0.5 bar each step until reaching 4 bar (maximal pressure).
17. Make sure that the valve is clothing properly and the mercury is flowing back out of the experiment chamber. If not → see section "Troubleshooting".
18. If the mercury is not flowing out of the experiment chamber and one would continue to pump continuously, the chamber could be filled within 10 seconds (assumed that the pump works continuously with maximum speed – 60 strokes per minute)!

Shut Down Procedure

CAUTION

If first the shut off valve of the air motor is closed and then the air pressure relieved by decreasing the pressure at the pressure reducer, then the pressure in the mercury system remains. This situation can cause serious injury when opening the pressure lines !!!

→ Always relieve the pressure from the mercury lines by

- triggering the mercury valve after closing the shut off valve or
- first relieve the air pressure and then close the shut off valve of the air motor.
- (it is recommended to trigger the valve anyway before opening a connection on the mercury pressure lines)

After relieving the pressure:

1. Set all air pressure reducers to 0 bar.
2. Remove the pressurized air supply.
3. Plug out the supply of electricity.

4. Set the pressure reducers of the Argon flushing to 0 bar, close the flow control valve and close the valve of the Argon bottle.
5. Remove the fan box from the filter and close both filter outlets with caps.

7. Procedures for Mercury Alarm

The maximum concentration of mercury in ambient air is 0.05 mg/m3 (average over 5 days, 8 hours each). The absolute maximum high level is 0.1 mg/m^3.

Mercury vapor detector shows a value between 0.05 and 0.1 mg/m^3 in ambient air

1. Wear disposable mask.
2. Tell all other people around to leave the area.
3. Stop the setup (see shut down procedure).
4. Try to locate the source of the contamination by using the detector as a sniffler.
5. If there is a leakage which can not be fixed immediately, check if the setup can be transported to the mercury lab without any risk.
6. If this is impossible, call the fire brigade and get suitable tools to fix the leak.
7. If there are mercury spills → see section "Mercury Spills".

Mercury vapor detector shows a value between 0.1 and 0.5 mg/m^3 in ambient air

1. Wear respirator with mercury vapor filter.
2. follow steps 2 –7 of previous procedures.

Mercury vapor detector shows a value above 0.5 mg/m^3 in ambient air

The respirator with the mercury vapor filter is designed for a contamination up to 0.5 mg/m^3

1. Wear respirator with mercury vapor filter.
2. Stop the setup (see shut down procedure).
3. Leave the area, call the fire brigade.
4. Be sure that nobody enters the area until the fire brigade arrives.

Mercury vapor detector shows a value above 0.05 mg/m^3 in confinement box

1. Stop the setup (see shut down procedure).
2. Make a measurements of the ambient air.
3. Close the air inlet at the confinement housing around the mercury valve with a cap. Remove the fan box and close the filter outlet with a cap.
4. Try to see, if there is a leak inside the security hose.
5. If possible (no visible leak), transport the setup to the mercury lab
6. follow instructions for leakages

8. Mercury Spills

For small spills, a mercury collector (mercury absorbing sponge) is available at the mercury lab.
The mercury collector consists of a sponge, which is glued to the lid of a plastic can.
To pick up small mercury spills:

1. Check the ambient air with the mercury vapor detector. See “Procedures for Mercury Alarm”, if a respirator must be worn.
2. Wear protective gloves.
3. Unscrew the lid of the can and slightly press the sponge against the surface where the mercury was spilled.
4. Check if there are any spills left. Mercury spills very often can be much smaller than a pinhead!
5. Remove the sponge from the lid and place it in a plastic bag. Label the bag and bring it to TIS.
6. Glue a new sponge onto the lid and screw the lid back onto the can.
7. Check the area where the mercury was spilled with the mercury vapor detector, if there is any contamination left.

If larger spills occur, the fire brigade must be called.
They have a mercury vacuum cleaner.

1. Make sure, that nobody enters the area.
2. Check the mercury level in the air. If there is a high level (>0.05 mg/m^3), a respirator must be worn.
3. Wait until the fire brigade arrives. Assist the firemen cleaning up the spill by monitoring the mercury level in the air.
4. Also check the mercury level at the outlet of the vacuum to be sure, that the mercury filter works properly.

9. Leakages

If there is a leak inside the confinement box (the mercury vapor detector detects mercury inside):

1. Stop the setup (see “Shut Down Procedure”).
2. Check the mercury vapor level in the ambient air.
3. If there is no mercury in the ambient air, transport the setup to the mercury lab.
4. Wear a breathing mask.
5. Lift the cover of the setup.
6. Continuously monitor the mercury vapor level.
7. Find the leakage and fix it.

8. If there is a larger amount of mercury in the confinement box, try to collect it with a pipette and fill it into a flask in the fume cupboard.
9. Collect smaller spills with the mercury collector (see “Mercury Spills”).
10. Lower the cover back onto the confinement box and tighten the screws.
11. Make a test run while monitoring the atmosphere inside the confinement box.

If there is a leak inside the security hose:

1. Stop the setup (see “Shut Down Procedure”).
2. Check the mercury vapor level in the ambient air.
3. If there is no mercury in the ambient air, transport the setup to the mercury lab.
4. Wear a breathing mask.
5. Remove the security hose from its mount to get access to the leakage.
6. Continuously monitor the mercury vapor level.
7. Fix the leakage.
8. If there is a larger amount of mercury on the cover plate of the confinement box, try to collect it with a pipette and fill it into a flask in the fume cupboard.
9. Collect smaller spills with the mercury collector (see “Mercury Spills).
10. Remount the security hose.
11.

If there is a leak inside the safety housing around the mercury valve:

1. Stop the setup (see “Shut Down Procedure”).
2. Check the mercury vapor level in the ambient air.
3. If there is no mercury in the ambient air, transport the setup to the mercury lab.
4. Wear a breathing mask.
5. Open the top lid of the safety housing.
6. Continuously monitor the mercury vapor level.
7. Fix the leakage.
8. If there is a larger amount of mercury inside the safety housing, try to collect it with a pipette and fill it into a flask in the fume cupboard.
9. Collect smaller spills with the mercury collector (see “Mercury Spills).
10. Put the top lid back again.
11. Make a test run while monitoring the atmosphere inside the confinement box, the security hose and the safety housing around the mercury valve.

If there is a leak at the experiment chamber:

1. Stop the setup (see “Shut Down Procedure”).
2. Check the mercury vapor level in the ambient air.
3. If there is no mercury in the ambient air, transport the setup to the mercury lab.
4. Wear a breathing mask.
5. Put a tray under the experiment chamber and its safety tube.
6. Remove the safety tube carefully.

7. Be sure that the mercury in the tube flows into the tray and put the experiment chamber in the tray.
8. Put the safety tube into the fume cupboard.
9. Probably there is no way to fix a leak at the experiment chamber easily. Decouple the chamber from all hoses and the nozzle.
10. Put it into a plastic bag and store it in the fume cupboard.
11. If there has to be built a new chamber, label the bag and give it to TIS.

10. Troubleshooting

No operation

1. Check the power and air supply.
2. Check all pressure reducers, if they are set correctly.
3. Is the pump shut off valve open?
4. Check the pressurized air plumbing.

The piston of the pump has moved a little bit, but there comes no mercury out of the nozzle, when triggering the mercury valve

1. Check the pressure reducer for the valve, if it is set correctly.
2. Check the power supply.
3. Check if the electro pneumatic valve operates properly.
4. Relief the air pressure by turning the pressure reducer for the pump counterclockwise.
5. Trigger the mercury valve a few times. Look at the rear end of the valve, if the little axle coming out of the valve housing is moving.
6. If the valve opens then, open the pressure reducer again and trigger the valve.
7. If the valve doesn't open, check the plumbing.
8. If you can not find any causes, transport the setup to the mercury lab, dismantle the valve and fix the bug.

The mercury is not flowing back out of the experiment chamber

1. Stop the setup immediately (see "Shut Down Procedure")!
2. Is the experiment chamber located higher than the mercury reservoir?
3. Carefully put the experiment chamber out of the magnet bore and hold lift it.
4. If then the mercury won't flow back, the setup has to be transported to the mercury lab.
5. Wear a breathing mask.
6. Continuously monitor the mercury vapor level.
7. Dismantle the connection line between the experiment chamber and the pump. Be sure that all eventual spilling mercury will be collected by a tray put under the point where you open a fitting.
8. Find the blockage and clean it properly.